



**DEPARTMENT OF  
MECHANICAL DESIGN**

NASA CR 135082

(NASA-CR-135082) ROLLER BEARING GEOMETRY  
DESIGN Final Report (Case Western Reserve  
Univ.) p HC A06/MF A01 CSCL 13I

N77-12403

Unclas  
G3/37 07980

**ROLLER BEARING GEOMETRY DESIGN**

BY

**MICHAEL SAVAGE AND BRUCE H. W. PINKSTON**

FOR

**NATIONAL AERONAUTICS AND SPACE ADMINISTRATION**

**NASA LEWIS RESEARCH CENTER**

**DAVID E. BREWE, PROJECT MANAGER**

**GRANT NSG 3077**



## Table of Contents

Forward	i
Summary	ii
Introduction	1
Stability Theory	4
Inner Race Stability	8
Outer Race Stability	10
Stable Roller Bearing Geometries	22
Stabilizing Torques	35
Contact Stresses and Deflections	50
Misalignment and Clearances	53
Compound Roller Bearing Geometry	60
Design Programs	63
Design Examples	73
Discussions of Results and Conclusions	101
Bibliography	106
Nomenclature	107
Distribution	109

Forward

This report describes the results of research conducted in the Mechanical Design Department of Case Western Reserve University under NASA Grant NSG 3077. The research was managed by David E. Brewe, Fluid System Components Division, NASA Lewis Research Center. Thanks are also due to William J. Anderson and Herbert W. Scibbe for their interest and suggestions throughout the work.

### Summary

The rollers in a rolling element roller bearing tend to skew as they roll around the inner race of the bearing. This tendency is a disadvantage of the bearing. High speed turbine bearings have a length to diameter ratio of close to one. With this ratio and small clearances between race shoulders and the rollers, a restoring moment is provided at the edges of the roller ends which restrains the roller from skewing. The cage also provides some resistance to the roller skewing through its contact with the roller.

The development of a new high speed, lightly loaded cylindrical roller bearing is the goal of this work. A kinematic and kinetic study is presented for the effects of cylindrical roller bearing contact geometry on the tendency of the rollers to become skewed. New roller race geometries are identified which will significantly reduce this skewing tendency. The end use application pertains to high speed turbine bearings which carry a light radial load but which must operate at increasingly higher speeds.

Twelve basic bearing modification designs are identified and modeled in this report. Four of these have single transverse convex curvature in their rollers while eight have rollers which have compound transverse curvature made up of a central cylindrical band surrounded by symmetric bands with slope and transverse curvature.

The bearing designs are modeled for restoring torque per unit axial displacement, contact stress capacity and contact area including dynamic loading, misalignment sensitivity and roller proportion. Design programs are available which size the single transverse curvature roller designs for a series of roller slopes and load separations and which design the compound roller bearings for a series of slopes and transverse radii of curvature. The compound rollers are proportioned to have equal contact stresses and minimum size. Designed examples are also given.

## Introduction

The rollers in a rolling element roller bearing tend to skew as they roll around the inner race of the bearing. This tendency is a disadvantage of the bearing. Thus needle bearings are normally used in low speed and high shaft alignment situations [1,2]\*. Higher speeds have resulted in caged roller bearings with shoulders on one of the races to guide the rollers. High speed turbine bearings have a length to diameter ratio of close to one. With this ratio and small clearances between race shoulders and the rollers, a restoring moment is provided at the edges of the roller ends which restrains the roller from skewing. The cage also provides some resistance to the roller skewing through its contact with the roller.

This roller skewing is primarily caused by a dynamic roller imbalance which can be appreciable at the high roller speeds inherent in operation at 2,000,000 DN.

The skewing of rolling elements is a problem which is not restricted to roller bearings. The skewing of flat belts on their pulleys was a problem encountered a century ago which was solved by crowning the pulleys to make the belts crawl up to the center of the pulleys [3]. The solution was based on the elastic nature of the belts in that the restoring moment was due to a tensile gradient in the belt tension across its width. In the centerless grinding process the rolling axis of the workpiece and the grinding wheel are deliberately skewed to each other to cause the workpiece to feed through the grinder [4]. Indeed this is a major problem in needle bearings in that a shaft slope at the bearings tends to push the needles out of the bearing. This is also a problem in traction drives [5,6] where large thrust forces

\* Numbers in brackets denote references in the bibliography.

are required to hold the rolling cylinders in place. The magnitudes of these forces have been studied in the case of a high speed, lightly-loaded cylindrical roller bearing [7]. The effects of shaft misalignment on the roller load distribution has also been studied [8]. Finally the wheel-rail interaction of railroad car wheel-sets with the rails has plagued designers for a long time [9,10,11]. The wheel-set is a rigid rolling cylinder on the rails which comprise a race of infinite radius. Flanges are needed on the wheels to provide the significant side forces required to accelerate the cars through the various turns in the road. However, it has been found that the slope of the flanges significantly affects the rolling of the wheels on the rails. Wheels which have a cone apex outside the body of the train are used in order to prevent the wheels from skewing as the train travels along the track. These cones produce a kinematic resistance to skewing which the reverse cones with the flange on the outside would not provide.

A recent investigation by the first author [6] has quantified a kinematic criterion for the axial stability of external contact rollers in dry free-rolling cylindrical contact. The axial instability of a roller is a direct consequence of its skewing. Thus the problem of axial stability and roller skewing are inter-related strongly. This analysis indicated that the introduction of axially symmetric shapes on the rollers and one race will provide a kinematic correcting mechanism for roller skewing.

The development of a new high speed, lightly loaded cylindrical roller bearing is the goal of this work. A kinematic and kinetic study is presented for the effects of cylindrical roller bearing contact geometry on the tendency of the rollers to become skewed. New roller race geometries are identified which will significantly reduce this skewing tendency. The end use application pertains to high speed turbine bearings which carry a light radial load but

which must operate at increasingly higher speeds.

A kinematic stability criterion is investigated and defined. It is applied to determine the basic bearing geometries which provide kinematic stabilization through one race while allowing free axial motion at the other. These bearings all have one straight race and one contoured race. Two levels of roller complexity are considered. The first is a simple roller with a single transverse convex curvature. There are four bearing geometries which use this roller. The second is a compound roller with a central band of constant radius. This radius is the largest radius of the roller. This central band is flanked by two symmetric bands with transverse curvature. The roller transverse curvature may be convex, straight or concave. Eight additional bearing geometries may employ these compound rollers. Models are also derived for the degree of kinematic stabilization available from a particular geometry, the basic capacity of a roller for that geometry at high speed and the sensitivity of the particular geometry to shaft slope or misalignment at the bearing.

Two basic design programs are presented. The first is for the bearing geometries which use the simple rollers. This program proportions the roller for a given length to diameter ratio, load spread factor and half cone angle. The program then analyzes the bearing for its contact stresses, restoring torque and misalignment sensitivity. The second program is for the compound roller geometries. This program proportions the roller load spread factor and length to diameter ratio to equalize and minimize the contact stresses. This program also analyzes its designed bearings for contact stress, restoring torque and bearing geometry. Design examples are given to illustrate the use of these programs.

### Stability Theory

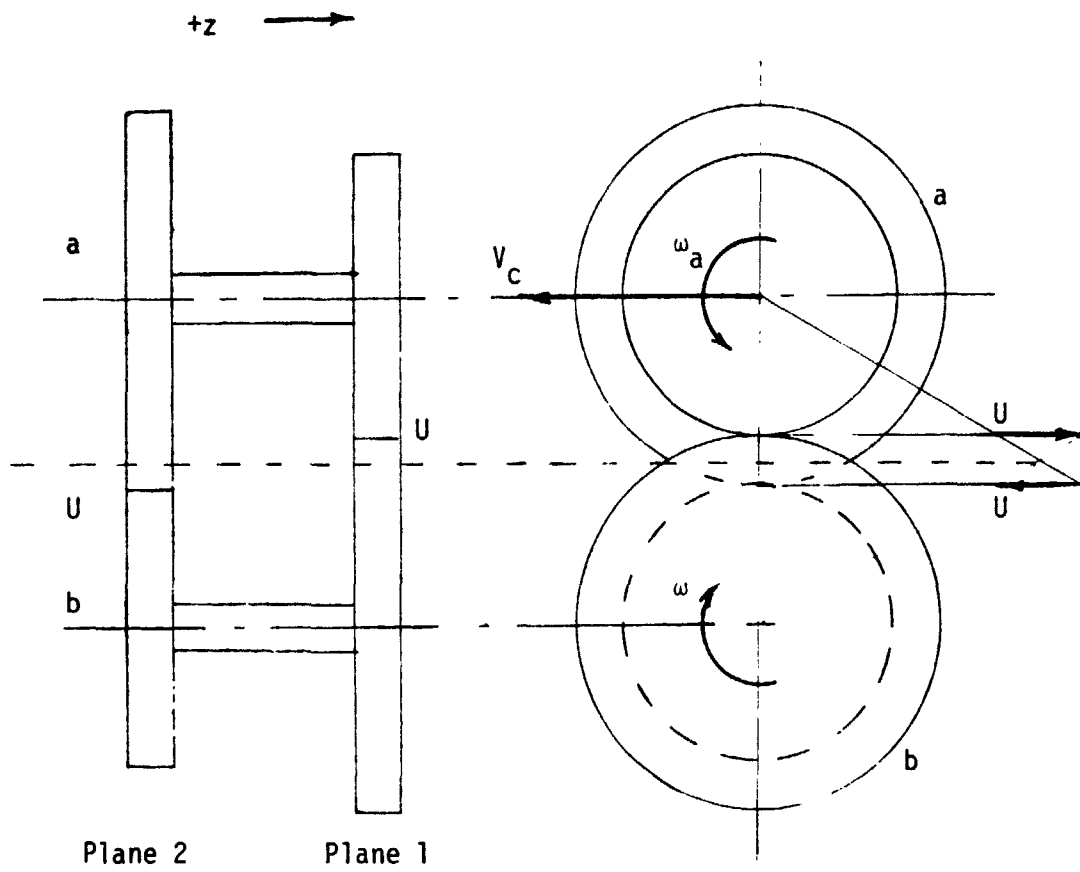
The basic model for rolling contact in a cylindrical roller bearing assumes that no skewing can take place since the axes of the rollers and races remain parallel. It further assumes that the races and the roller are perfect cylinders with constant radii along the length of their axes. Thus a single plane rolling model is used. This model is valid as long as the axes remain parallel.

In reality, the rolling surfaces are not uniform. The axes are not perfectly parallel. And roller contact occurs in more than one plane. The actual contact is thus not pure rolling but a complex combination of rolling and sliding across the face of the roller.

To establish the primary cause of skewing, this contact is modeled in two planes instead of the single plane of the basic roller model. This two plane model allows for rolling and sliding at the individual planes and a resultant generation of a skewing torque due to variations in rolling geometry from one plane to the other.

In this model consider roller a to be the rolling element, roller b to be the inner race and roller c to be the outer race of the bearing. The races rotate about fixed axes with no axial motion. Plane 1 is at the small end of the rolling element roller a. For equal and opposite slip in the two planes, the radius at which true rolling would occur is the average of the two rolling radii of roller a.

Figure 1 illustrates the rolling contact of the rolling element with the inner race. As shown in the velocity drawing, roller b slips ahead of roller a at the contact point in plane 1 while the relative velocity is reversed in



Roller - Inner Race Skewing

Figure 1

plane 2 and roller a slips ahead of roller b. These two skidding velocities produce a counterclockwise tractive couple on roller a which tends to push its plane 1 into the paper and pull its plane 2 out of the paper. This skewing turns the relative velocity of the center of roller a with respect to roller b slightly towards plane 1. The axial component of this velocity is thus an axial motion of roller a on roller b. If this motion decreases the ratio  $r_{1b}/r_{1a}$  and increases the ratio  $r_{2b}/r_{2a}$ , the skidding velocities will be reduced and even reversed when  $r_{1a}$  and  $r_{1b}$  pass the mean value. Assuming this antisymmetric behavior, the total stability or tendency to self correct without external forces can be measured by the inequality

$$\frac{\partial}{\partial z} \left( \frac{r_{1b}}{r_{1a}} \right) < 0 \quad (1)$$

where  $z$  measures the axial motion of roller a and is positive for motion toward plane 1 [6].

In a similar fashion, figure 2 illustrates the rolling contact of the rolling element with the outer race. As shown in the velocity drawing, roller c slips ahead of roller a in plane 1 and slips behind roller a in plane 2. The sliding tendency is not as great in this case since both centers of rotation are on the same side of the pitch point. However, it is still there and in the same direction as in the previous case. For the same direction of rotation of the race c in this case as that of the race b in the previous case, the angular velocity of the roller a reverses but the relative velocity of its center with respect to the race is also out of the paper. Thus a similar counterclockwise tractive torque produces the same skewing and axial motion toward plane 1 - the small end of the roller. If this motion decreases the ratio  $r_{1c}/r_{1a}$  and increases the ratio  $r_{2c}/r_{2a}$  the skidding velocities will be



reduced as before. An equivalent stability criterion can thus be stated as

$$\frac{\partial}{\partial z} \left( \frac{r_{1c}}{r_{1a}} \right) < 0 \quad (2)$$

### Inner Race Stability

The stability or self correcting action of the roller with the inner race is determined by applying the criterion of equation 1 to the possible transverse profiles for the roller and inner race. These profiles must be axially symmetric about the center plane of the roller and inner race. They must also afford only one contact point between the roller and race on each side of this center plane. The geometric combinations that satisfy this are:

- 1) convex - convex
- 2) convex - straight, and
- 3) convex - concave.

In these three cases, the rolling element may be either the first or second item. A fourth combination must be included which does not possess two definite contact points in order to include present bearings. That is:

- 4) straight - straight.

Prior to this study in "Kinematic Stability of Roller Pairs in Free Rolling Contact" by M. Savage and S. H. Loewenthal [6], this kinematic stability of two rollers was studied. In this study  $\rho$  refers to the roller with the apex of its cone of transverse geometry outside the roller for a positive slope of transverse curvature. The radii of transverse curvature for these rollers are denoted by  $\rho$  where  $\rho$  is positive for convex curvature and negative for concave curvature. Table 1 summarizes the stability conditions for rollers in free rolling contact where both rolling surfaces are on the outside of their respective cylinders. This contact is of external - external rollers.

Geometry	e - outside apex	d - outside apex
d - e		
convex - convex	$\frac{r_{1e}}{r_{1d}} < \frac{\rho_e}{\rho_d}$	$\frac{r_{1e}}{r_{1d}} > \frac{\rho_e}{\rho_d}$
convex - straight	yes	no
convex - concave	yes	no
straight - straight	$\frac{r_{1e}}{r_{1d}} < 1$	$\frac{r_{1e}}{r_{1d}} > 1$

Axial Stability of External - External Rollers

Table 1

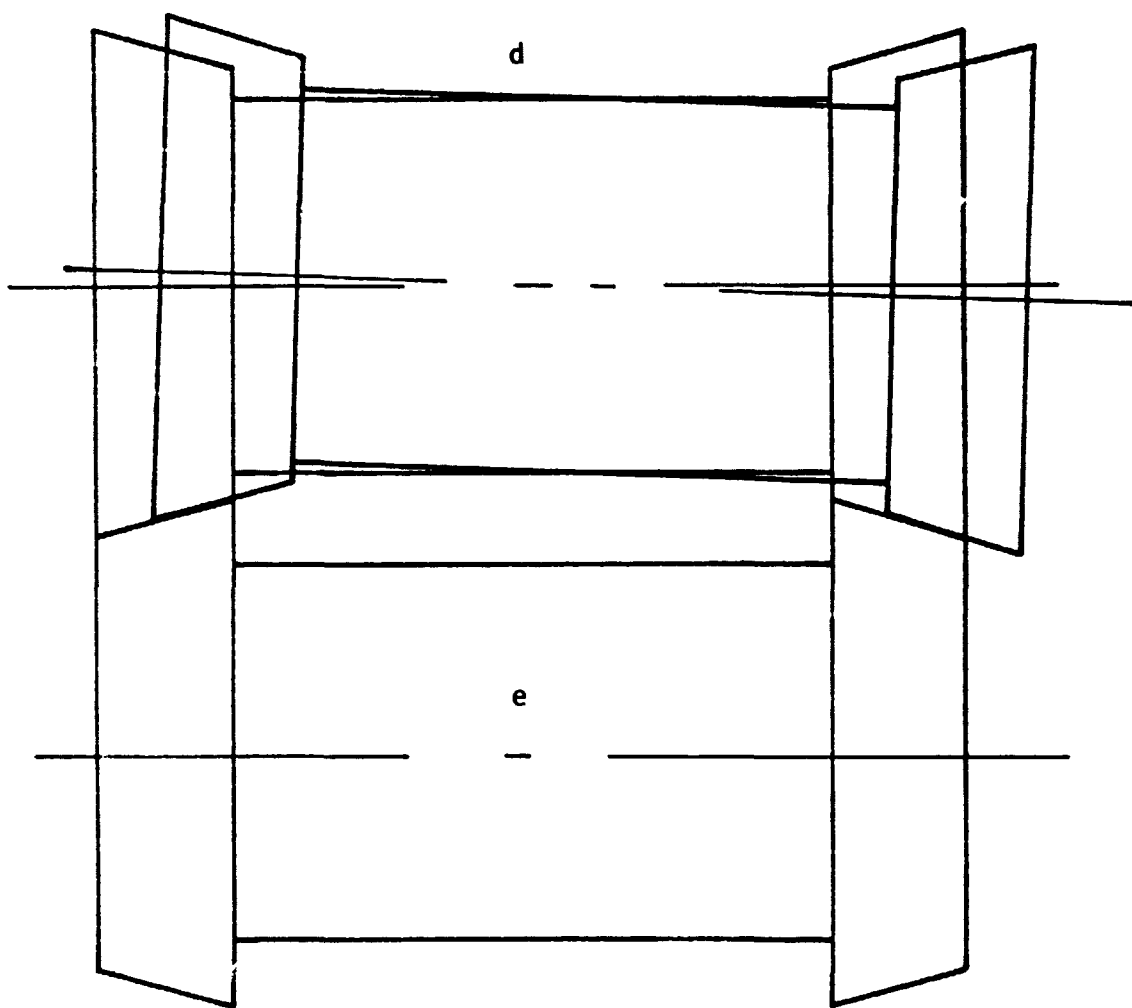
The results for straight - straight rollers were derived with the assumption that the contact point stays at the center of the overlapped region of straight cones. The validity of this assumption was questioned in the present study. As the roller shifts axially its axis tilts slightly in the plane of the two axes. This motion should cause the straight - straight geometry to contact at the edges of the contact surfaces. Thus one of the contacting radii would remain constant in each plane.

The geometry shown in Figure 3 shifts the surfaces of roller d onto the right edges of roller e. Since the two fixed radii of roller e in planes 1 and 2 are unequal, the compensating effects of equalizing rolling radii cannot occur. The same would be true if the roles were reversed and the surfaces of roller e rode across the edges of roller d. Thus if the assumption of central contact is invalid and edge contact occurs, straight sided rollers are at best neutrally stable in the non-tapered condition and are unstable in any tapered situation.

Table 2 shows these results in a form more easily applied to the bearing design problem at hand. In this expanded table, roller a is the rolling element and roller b is the inner race of the bearing. The cone angle of transverse curvature,  $\alpha$ , is considered positive if the cone radius of roller a is outside of the roller as is the case for roller e in figure 3.

#### Outer Race Stability

In a similar fashion, the stability of the roller with the outer race is determined by applying the criteria of equation 2 to the transverse profiles. These profiles must be axially symmetric about the center plane of the roller and outer race. They must also afford only one contact point between the roller and race on each side of this center plane. Each combination must



Straight Roller Cornering

Figure 3

a roller curvature	b inner race curvature	+α	-α
convex	convex	$\frac{r_{1a}}{r_{1b}} < \frac{\rho_a}{\rho_b}$	$\frac{r_{1a}}{r_{1b}} > \frac{\rho_a}{\rho_b}$
convex	straight	no	yes
convex	concave	no	yes
straight	convex	yes	no
straight	straight	$\frac{r_{1a}}{r_{1b}} < 1$	$\frac{r_{1a}}{r_{1b}} > 1$
concave	convex	yes	no

Roller - Inner Race Stability Conditions

Table 2

be considered separately. Listing the roller transverse curvature first and the outer race transverse curvature second, these contact combinations are:

- 1) convex - convex
- 2) convex - straight
- 3) convex - concave
- 4) straight - convex
- 5) straight - straight, and
- 6) concave - convex.

These cases are treated with the following nomenclature. The slope of the transverse curvature is identified by the angle  $\alpha$  which is positive for external cone apexes on roller a. The radius of transverse curvature,  $\rho$ , is positive for convex and negative for concave surfaces. The rolling radius,  $r$ , and radius to the center of transverse curvature,  $R$ , are both positive when directed from the center of roller rotation toward the contact point and negative when opposite. A positive  $dz$  identifies motion of roller a towards plane 1 as before. The center distance of transverse curvature is

$$C = \rho_a + \rho_c \quad (3)$$

Figure 4 shows the geometry of the first case, convex - convex. The slope angle,  $\alpha$ , is related to the axial position of roller a by

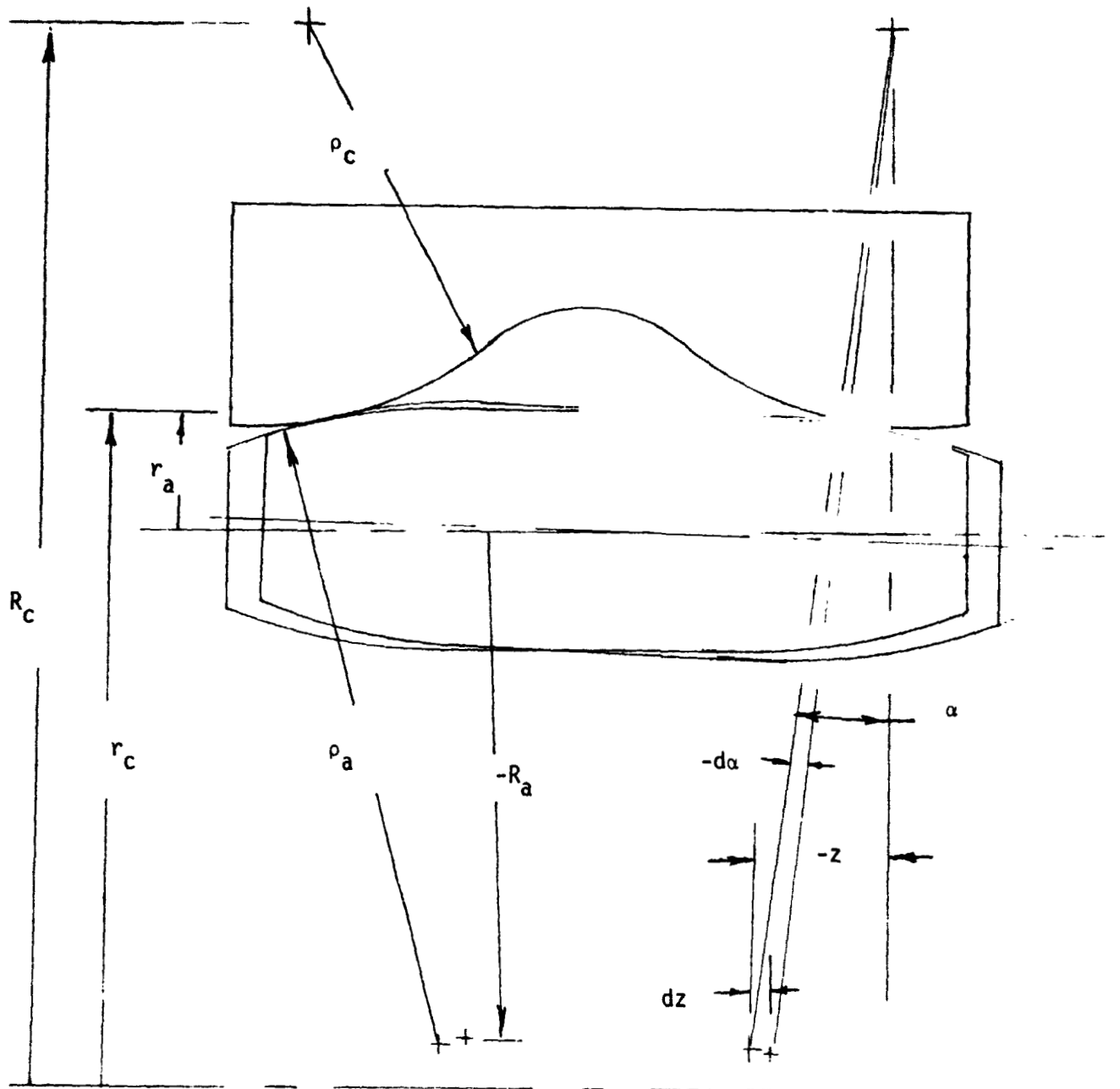
$$\sin \alpha = \frac{-z}{C} \quad (4)$$

In plane 1 the two rolling radii are given by:

$$r_{1a} = R_a + \rho_a \cos \alpha \quad (5)$$

and

$$r_{1c} = R_c - \rho_c \cos \alpha \quad (6)$$



Convex - Convex Outer Race Contact Geometry

Figure 4

Thus

$$\frac{r_{1c}}{r_{1a}} = \frac{R_c - \rho_c \cos \alpha}{R_a + \rho_a \cos \alpha} \quad (7)$$

and assuming that the radial shift of the roller axis is negligible compared to the axial roller shift

$$\frac{\partial}{\partial z} \left( \frac{r_{1c}}{r_{1a}} \right) = - (r_{1a} \rho_c + r_{1c} \rho_a) \frac{\tan \alpha}{C r_{1a}^2} \quad (8)$$

Since every length in this geometry is positive, this case is determined solely by the sign of the slope angle,

$$- \frac{(r_{1a} \rho_c + r_{1c} \rho_a) \tan \alpha}{C r_{1a}^2} < 0 \quad (9)$$

for positive  $\alpha$  values or slopes as drawn in Figure 4.

Figure 5 shows the geometry for the second case, convex - straight. In this case the slope angle is constant and the rolling radii are given by:

$$r_{1a} = R_a + \rho_a \cos \alpha \quad (10)$$

$$r_{1c} = r_{0c} - z \tan \alpha \quad (11)$$

where  $z$  has a value of zero in the initial position. A second difference of the straight cone cases from the others is that  $z$  is referenced at the contact point directly and not at a center of transverse curvature off the surface. The quantity  $r_{0c}$  is the rolling radius of the outer race in plane 1 in the initial position. Thus

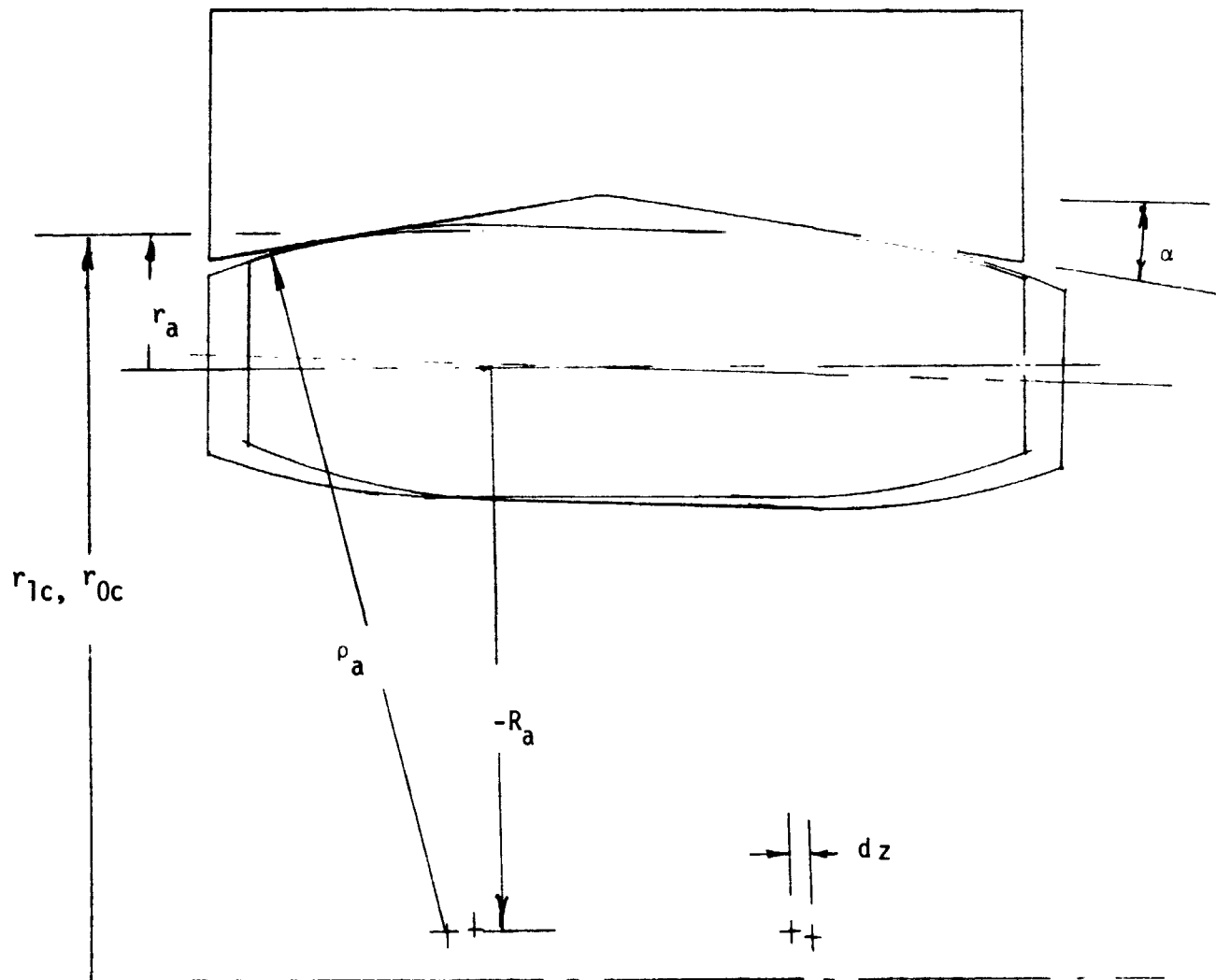
$$\frac{r_{1c}}{r_{1a}} = \frac{r_{0c} - z \tan \alpha}{R_a + \rho_a \cos \alpha} \quad (12)$$

and

$$\frac{\partial}{\partial z} \left( \frac{r_{1c}}{r_{1a}} \right) = - \frac{\tan \alpha}{r_a} \quad (13)$$

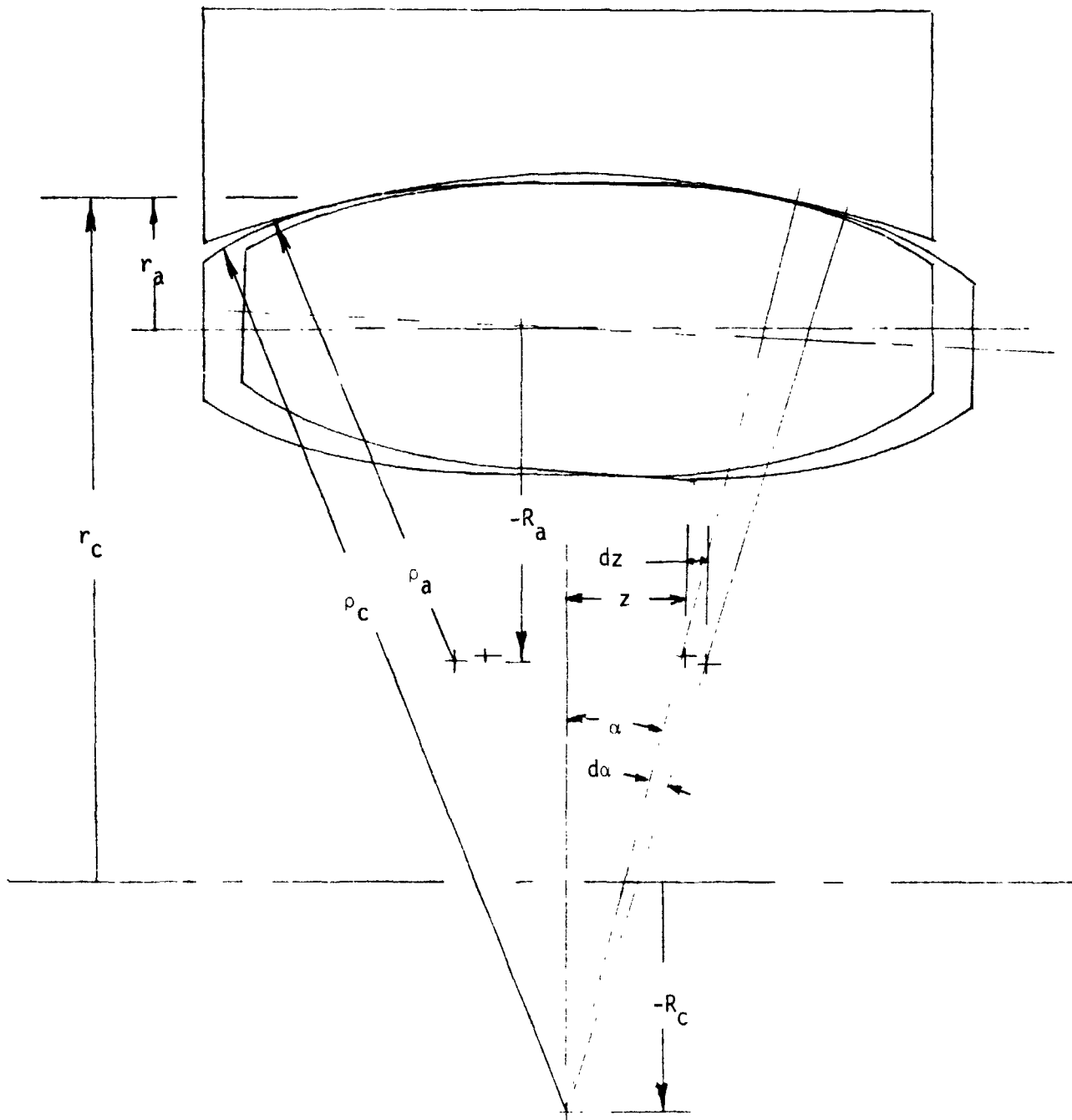
Once again this is controlled by the sign of the angle  $\alpha$ , so stability is obtained with a positive angle  $\alpha$  as shown in Figure 5:

$$- \frac{\tan \alpha}{r_a} < 0 \quad (14)$$



Convex - Straight Outer Race Contact Geometry

Figure 5



Convex - Concave Outer Race Contact Geometry

Figure 6

Figure 6 shows the geometry for the third case, convex - concave. The slope angle,  $\alpha$ , is defined by equation 4 and the two rolling radii are given by equations 5 and 6. Thus the analysis of this case is the same as that for the convex - convex case. However, since  $\rho_c$  is negative, the stability conclusions to be drawn from equation 9 change slightly. Since  $|\rho_c|$  must be greater than  $\rho_a$ ,  $C$  is negative and

$$(r_{1a}\rho_c + r_{1c}\rho_a) \tan \alpha < 0 \quad (15)$$

Thus two possible stable conditions result.

$$\frac{r_{1c}}{r_{1a}} < \left| \frac{\rho_c}{\rho_a} \right| \text{ and } \alpha > 0 \quad (16)$$

or

$$\frac{r_{1c}}{r_{1a}} > \frac{\rho_c}{\rho_a} \text{ and } \alpha < 0 \quad (17)$$

In either case the two factors offset each other so the stability is not as great as that of the first two cases.

Figure 7 shows the geometry for the fourth case, straight - convex. As in the second case, the slope angle  $\alpha$  is a constant. The rolling radii are given by:

$$r_{1a} = r_{0a} + z \tan \alpha \quad (18)$$

and

$$r_{1c} = R_c - \rho_c \cos \alpha \quad (19)$$

Thus

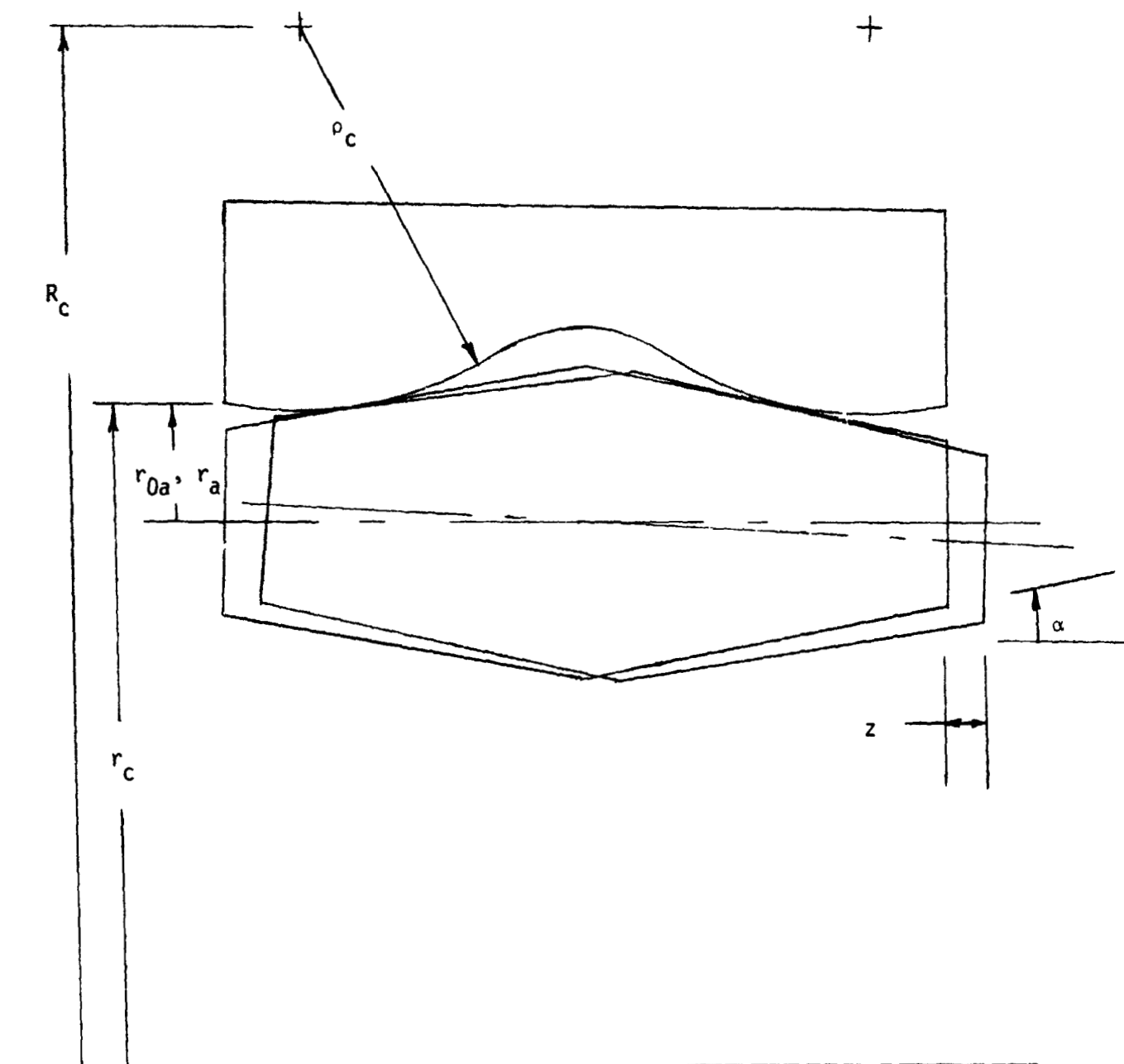
$$\frac{r_{1c}}{r_{1a}} = \frac{R_c - \rho_c \cos \alpha}{r_{0a} + z \tan \alpha} \quad (20)$$

and

$$\frac{\partial}{\partial z} \left( \frac{r_{1c}}{r_{1a}} \right) = - \frac{r_c \tan \alpha}{r_a^2} \quad (21)$$

Since  $r_c$  is always positive then stability is once again determined primarily by the sign of the slope angle  $\alpha$ .

REPRODUCIBILITY OF THE  
ORIGINAL PAGE IS POOR



Straight - Convex Outer Race Contact Geometry

Figure 7

$$-\frac{r_c \tan \alpha}{r_a^2} < 0 \quad (22)$$

for positive values of  $\alpha$  and is not true for negative values.

Figure 8 shows the geometry for the fifth case, straight - straight. This case differs from the other five in that kinematically defined contact points do not exist. If it is assumed that the contact point remains in the center of the contact region and that the contact pressure remains nearly uniform then the rolling radii can be expressed as

$$r_{1a} = r_{0a} + \frac{z}{2} \tan \alpha \quad (23)$$

and

$$r_{1c} = r_{0c} - \frac{z}{2} \tan \alpha \quad (24)$$

Where the slope angle  $\alpha$  is a constant and the two radii  $r_{0a}$  and  $r_{0c}$  are the initial rolling radii in plane 1.

The ratio is thus

$$\frac{r_{1c}}{r_{1a}} = \frac{r_{0c} - \frac{z}{2} \tan \alpha}{r_{0a} + \frac{z}{2} \tan \alpha} \quad (25)$$

and its derivative with respect to  $z$  is

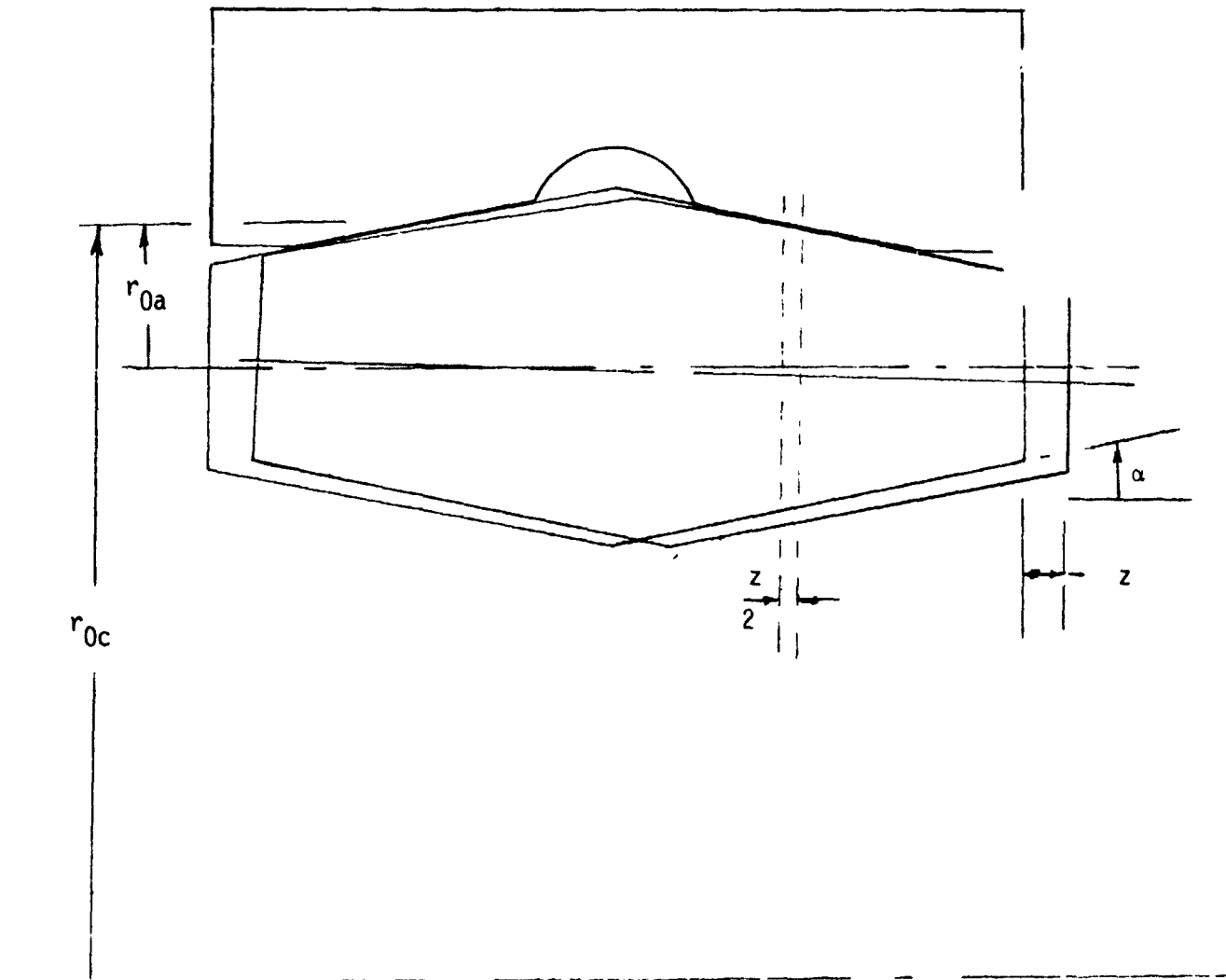
$$\frac{\partial}{\partial z} \left( \frac{r_{1c}}{r_{1a}} \right) = \frac{-(r_{1c} + r_{1a}) \tan \alpha}{2(r_{1a})^2} \quad (26)$$

Stability is thus defined by

$$-\frac{(r_{1c} + r_{1a}) \tan \alpha}{2r_{1a}^2} < 0 \quad (27)$$

which is satisfied for positive  $\alpha$  and not satisfied for negative  $\alpha$  values.

If it is assumed that the contact points shift to the right hand edge of roller c's surfaces then roller a will continue to roll to the right without correction since a fixed imbalance will exist between the rolling radii  $r_{1c}$  and  $r_{2c}$  of the outer ring.



Straight - Straight Outer Race Contact. Geometry

Figure 8

If it is assumed that the contact points shift to the left hand edges of roller a, then the imbalance will be between the rolling radii  $r_{1a}$  and  $r_{2a}$  of the roller. This imbalance will shift the roller to the left until contact on these edges is no longer possible at which time the roller might be shifted back to the right by the aforementioned outer ring edge rolling contact.

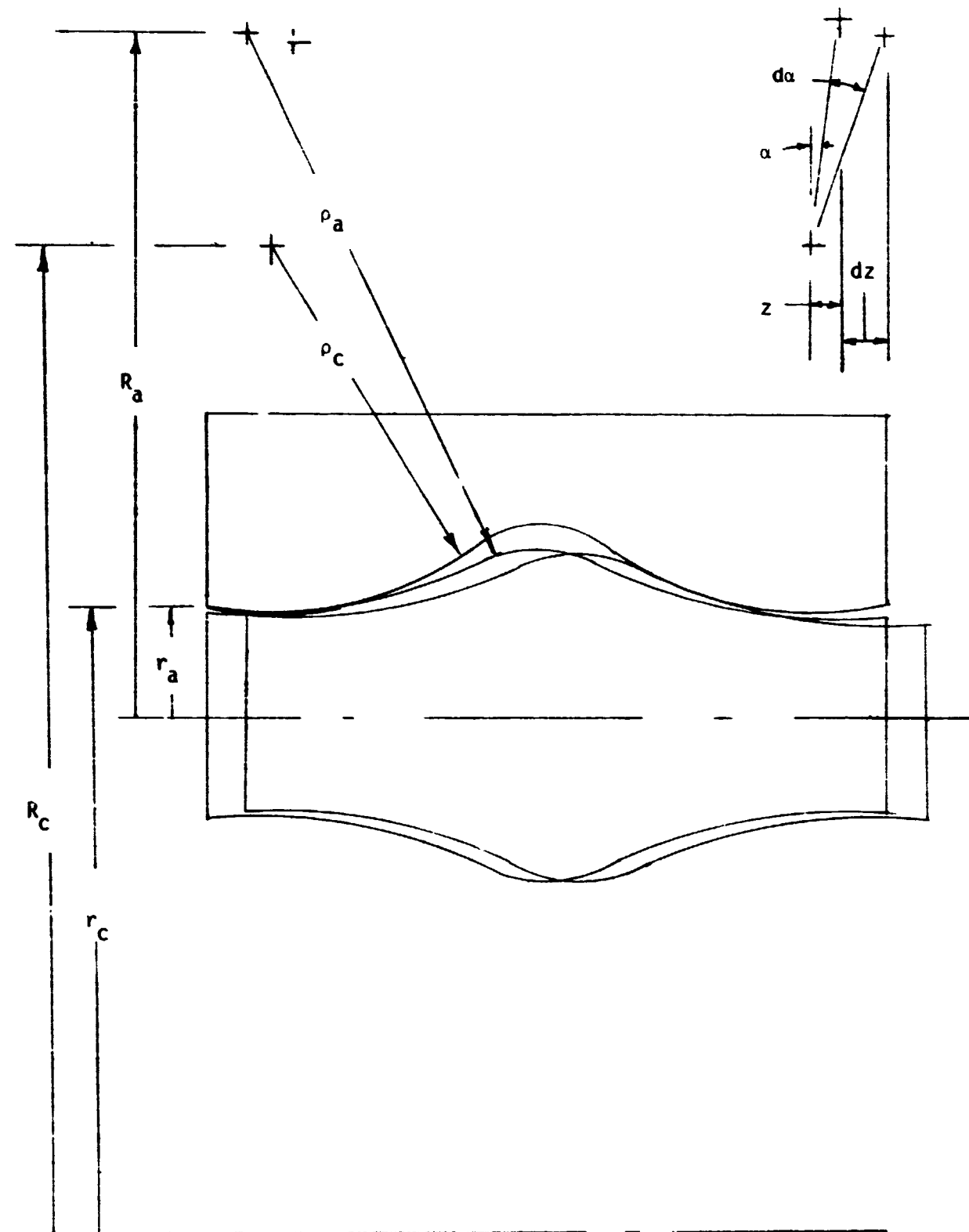
In any case, if edge rolling contact occurs on the straight cases, instabilities at least to the point of limit cycle oscillations will occur.

Figure 9 shows the geometry for the sixth and final case, concave-convex. As in the third case, the first analysis applies with the awareness of a sign change. The radius of transverse curvature of the roller,  $\rho_a$ , is negative and greater in magnitude than the radius of transverse curvature of the outer race,  $\rho_c$ . This makes  $C$  negative and results in the condition of equation 15 for stability. Since  $r_{1c}$  is greater than  $r_{1a}$ , the second term is much larger than the first. Since this term is negative, stability is determined by the sign of the slope angle  $\alpha$ . A positive value indicates stability while a negative value indicates instability.

Table 3 is a summary of the stability conditions for the six cases of roller-outer race contact, assuming mid-point contact for the straight sided rollers.

### Stable Roller Bearing Geometries

A roller bearing must allow free axial motion of the supported shaft with respect to the housing. To do this, one race rolling surface must be straight or parallel to the shaft centerline. The roller must have a single rolling band as its largest radius to contact that race rolling surface. To minimize the restriction to shaft slope or misalignment, this rolling band should be located in the center of the roller. Two levels of roller complexity are considered in this work: (1) a single convex transverse curvature with zero



Concave - Convex Outer Race Contact Geometry

Figure 9

roller curvature	outer race curvature	+α	-α
convex	convex	yes	no
convex	straight	yes	no
convex	concave	$\frac{r_{1c}}{r_{1a}} < \left  \frac{\rho_c}{\rho_a} \right $	$\frac{r_{1c}}{r_{1a}} > \left  \frac{\rho_c}{\rho_a} \right $
straight	convex	yes	no
straight	straight	yes	no
concave	convex	yes	no

Roller - Outer Race Stability Conditions

Table 3

REPRODUCIBILITY OF THE  
ORIGINAL PAGE IS POOR

slope at the center as shown in Figure 10, and (2) a compound transverse slope composed of a central cylinder with the largest rolling radius flanked by two symmetric transverse curvatures which have tangent cones with apexes outside the roller center as shown in Figure 14. In both roller configurations, the roller cone angle,  $\alpha$ , must be positive.

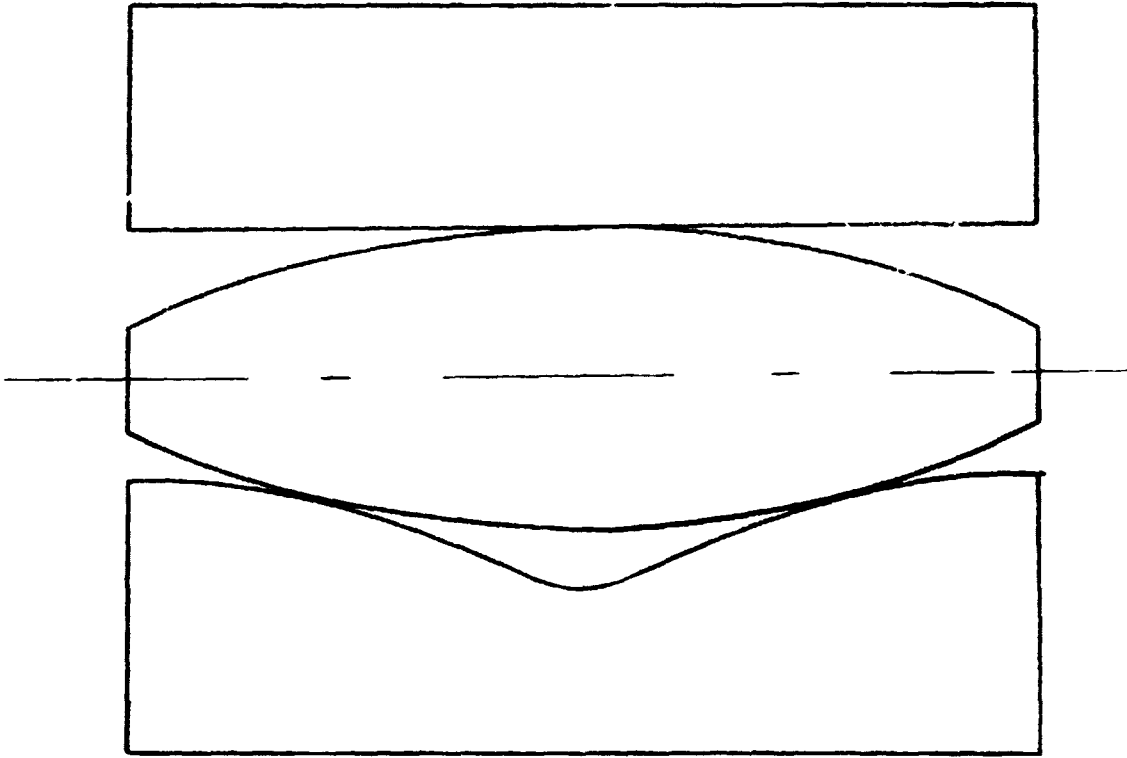
Table 4 lists the twelve possible stable bearing configurations which these restrictions allow. The type of transverse curvature on the coned surfaces is listed in the table. The straight cylindrical race is noted by the dash under inner or outer race curvature for each bearing in the table. For the four bearings for which the stability is listed as conditional, the radii of transverse curvatures must satisfy an inequality for the geometry to be stable. Geometries which require straight cones to contact straight cones are considered unstable due to the cornering effects of their contact.

These twelve bearings with simple and compound rollers which provide kinematic stabilization are illustrated in Figures 10 through 17. Figures 10 through 13 show the basic restoring geometry of both the four simple roller bearings and the first four compound roller bearings. Each Figure represents the geometry of a simple roller bearing and a compound roller bearing. Figures 14 through 17 show the basic restoring geometry of the last four compound roller bearings which have no simple roller counterpart. The first four bearings represent the only possible stable combination of a convex roller with either an inner or an outer contoured race surface. The final eight bearings of table 4 extend this class of stable bearings by introducing the first level of compound roller curvature. They represent the only stable bearings with symmetric single curvature restoring surfaces. It is important to note that for each of these geometries, the roller is contained by both the inner and outer races with three contact points in the transverse plane. Thus its position will be well defined and solid contact at each point is assured. The

roller type	roller curvature	inner race curvature	outer race curvature	stability
simple	convex	convex	-	conditional
		-	convex	stable
		-	straight	stable
		-	concave	conditional
compound	convex	convex	-	conditional
		-	convex	stable
		-	straight	stable
		-	concave	conditional
	straight	convex	-	stable
		-	convex	stable
	concave	convex	-	stable
		-	convex	stable

Stable Bearings

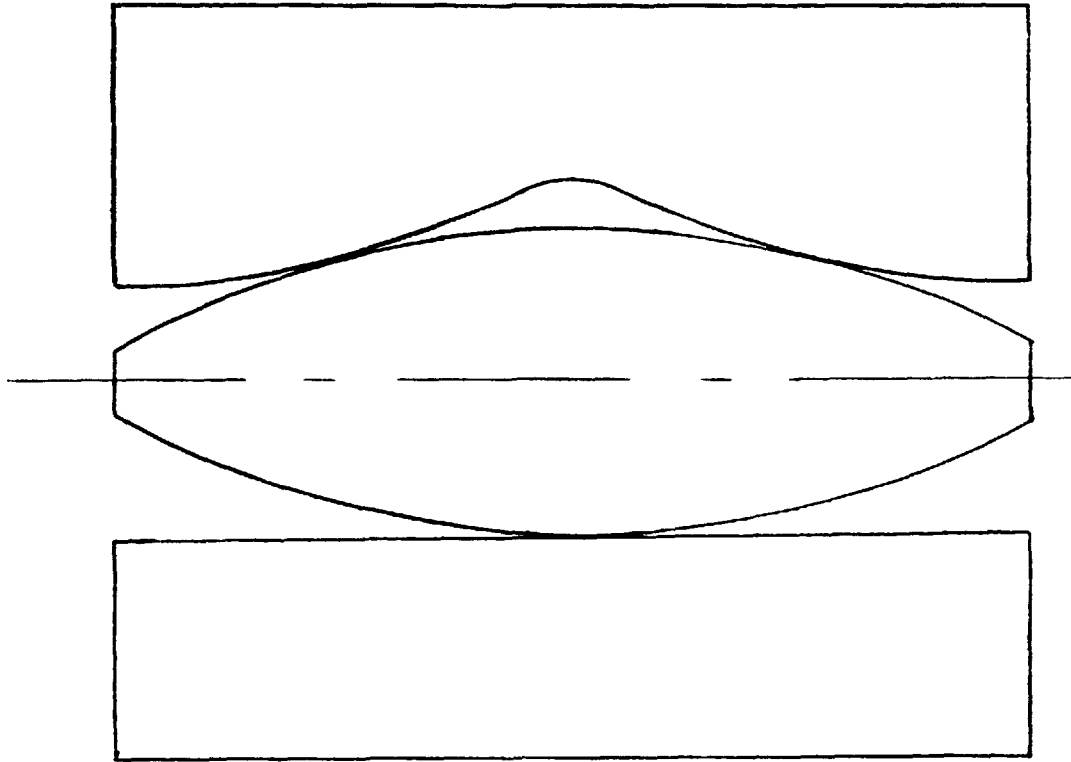
Table 4



---

Stable Convex - Convex - Neutral Bearing

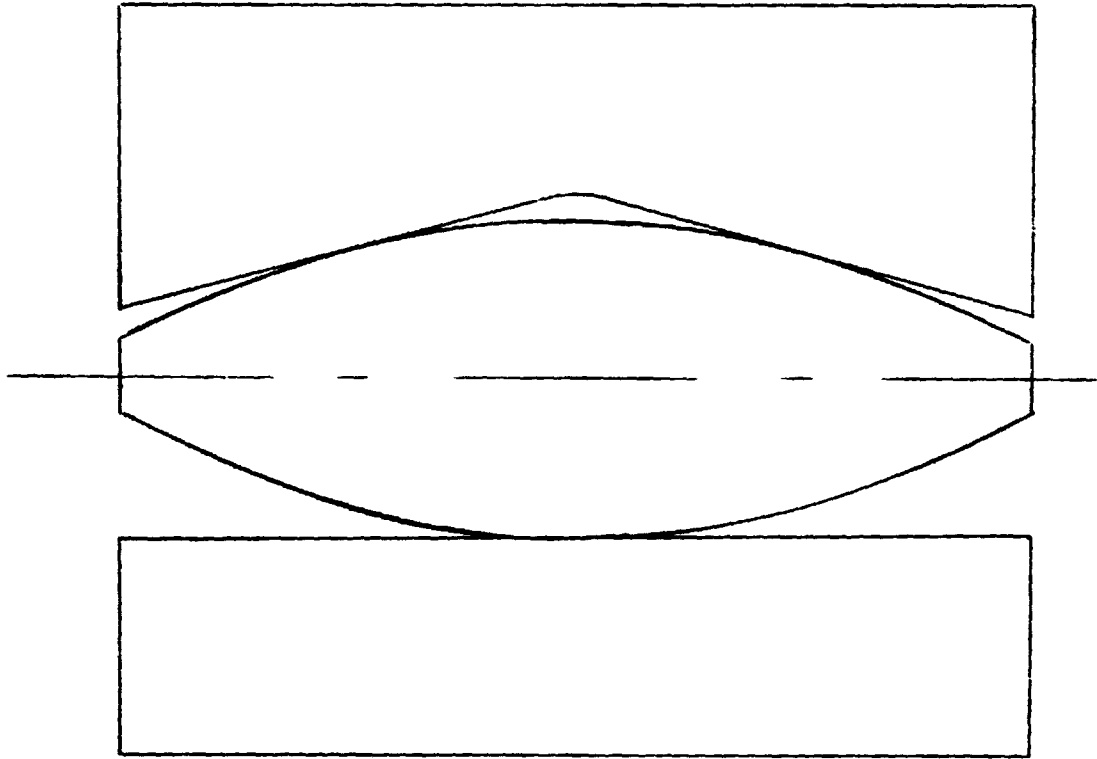
Figure 10



---

Stable Convex - Neutral - Convex Bearing

Figure 11

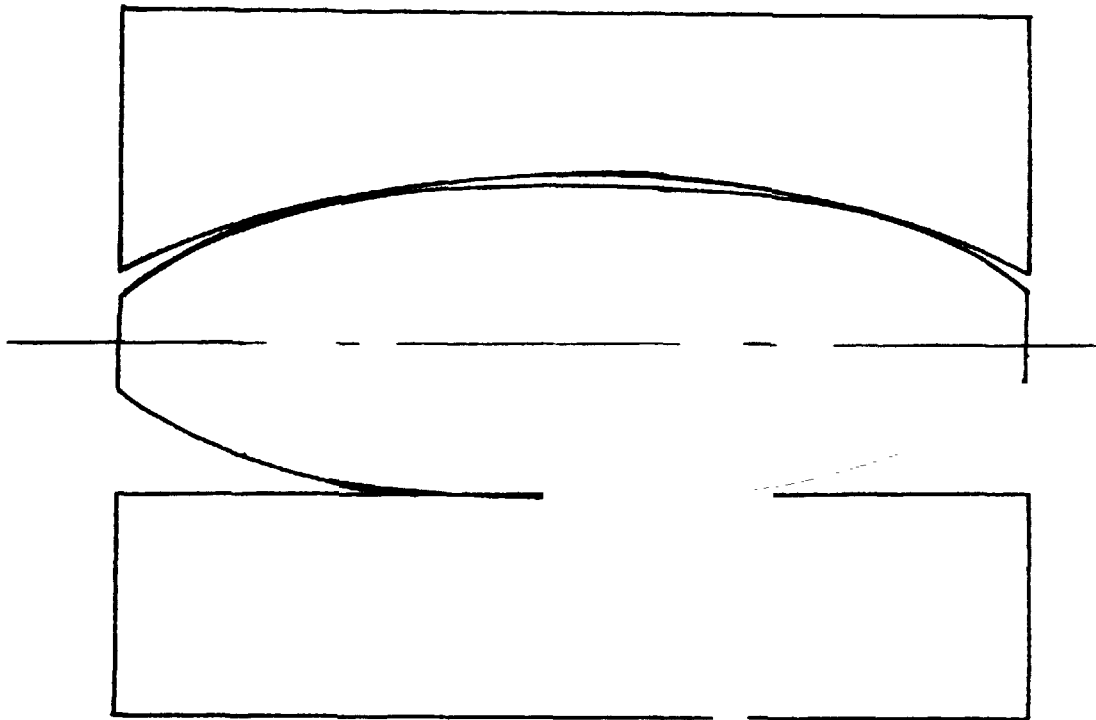


---

Stable Convex - Neutral - Straight Bearing

Figure 12

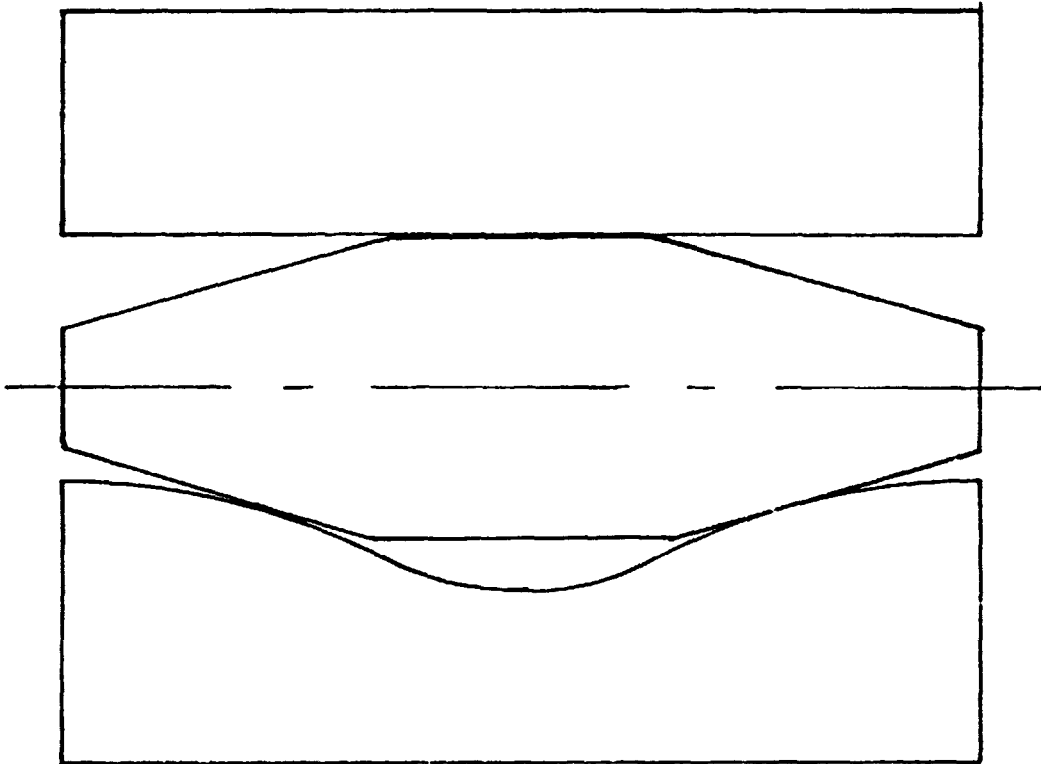
REPRODUCIBILITY OF THE ORIGINAL PAGE IS POOR



---

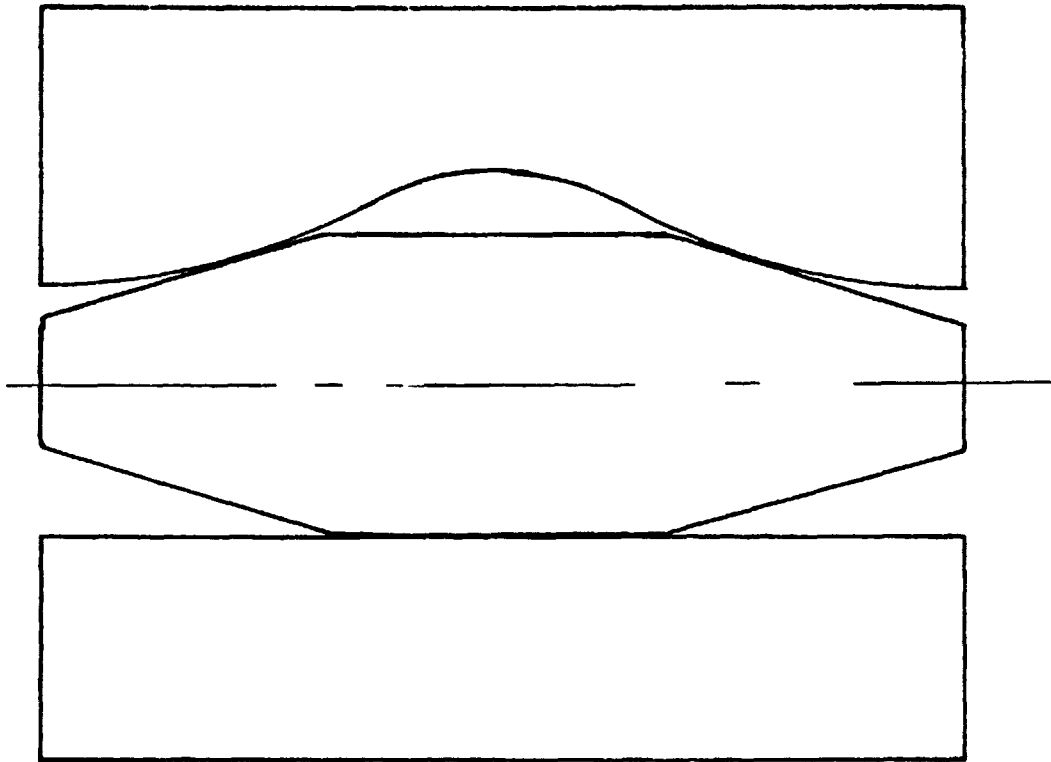
Stable Convex - Neutral - Concave Bearing

Figure 13



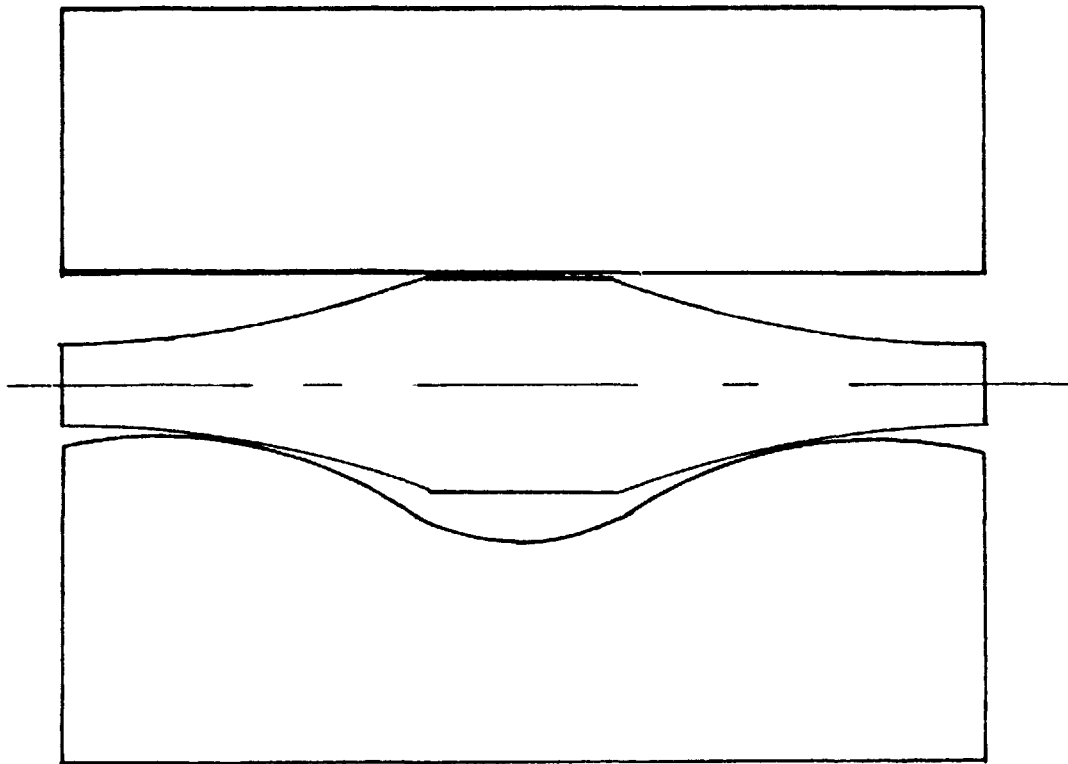
Stable Straight - Convex - Neutral Bearing

Figure 14



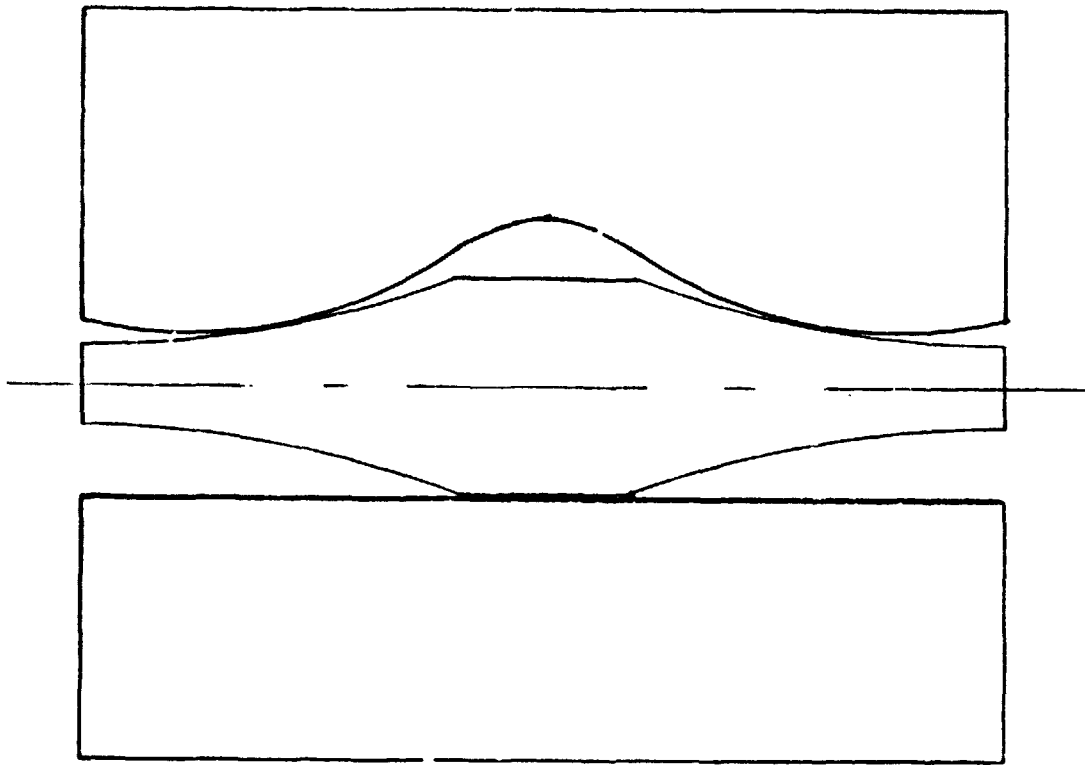
Stable Straight - Neutral - Convex Bearing

Figure 15



Stable - Concave - Convex - Neutral Bearing

Figure 16



---

Stable Concave - Neutral - Convex Bearing

Figure 17

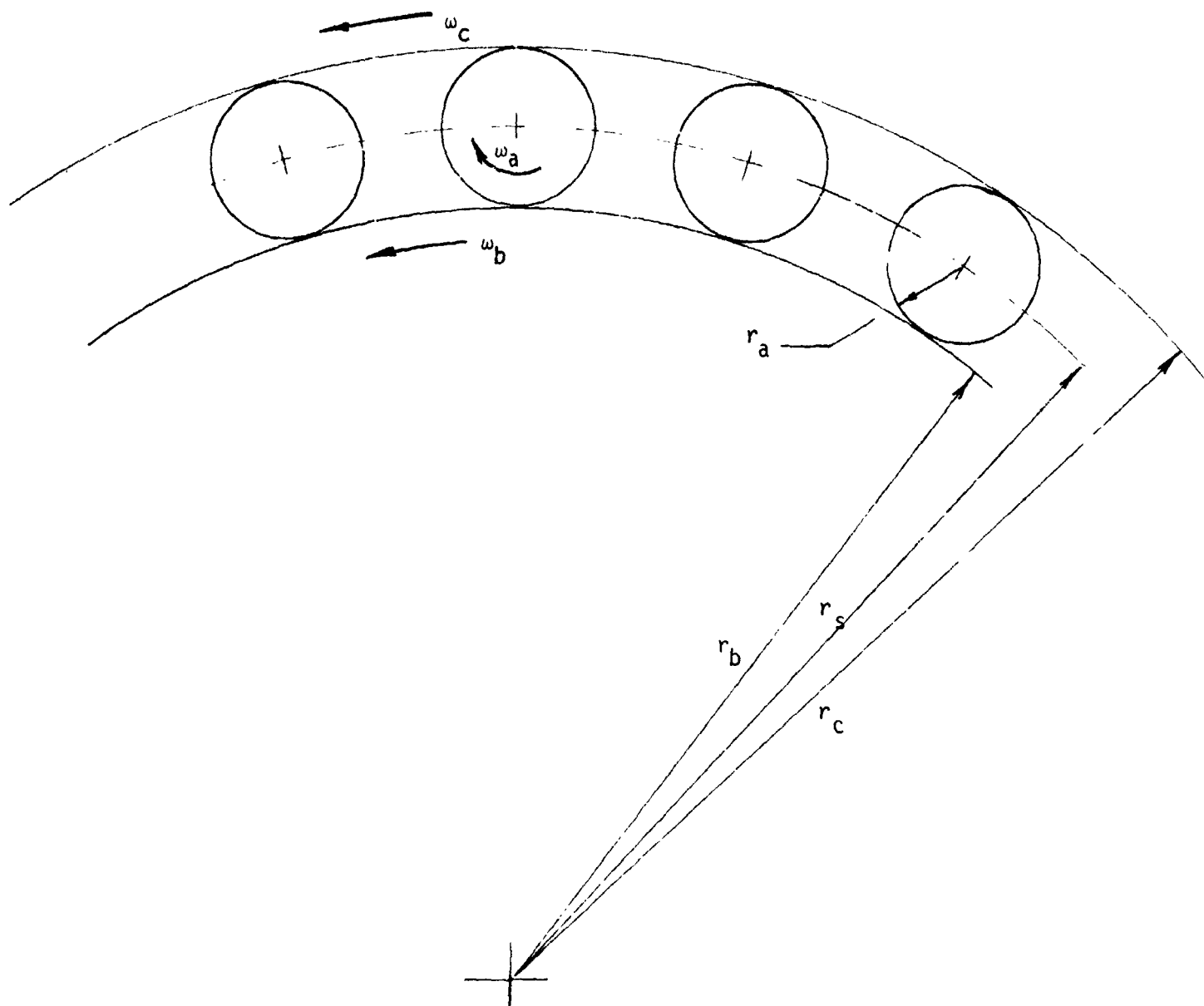
next level of roller complexity is variable radii of transverse curvature. This geometry is considered beyond the scope of the present work and will not be considered here. However, it should be investigated as the bearing designs are refined.

### Stabilizing Torques

The transverse geometry of the bearings works to skew the rollers slightly and walk them to a neutral position where the rolling action in the two contact planes is identical. This skewing is caused by small slip velocities at the contact points which act as a couple. This slip velocity couple is transformed into a torque by the tractive properties of the bearing lubricant [12].

The restoring torque of the bearing geometries which have their stabilizing contour on the inner race should be compared to the restoring torque of the other bearing geometries which have their stabilizing contours on the outer race - at the same operating conditions. The conditions chosen are that of a fixed outer race and rotating inner race. Since the velocity analysis is conducted relative to the cage with the rollers in place, the angular velocity of each race should be written as a function of the shaft speed expressed in RPM, in the operating case.

Figure 18 illustrates this planetary action. Let  $N$  be the speed of the shaft in the operating situation.  $\omega_s$  be the speed of the cage,  $\omega_a$  be the speed of the roller,  $\omega_b$  be the speed of the inner race, and  $\omega_c$  be the speed of the outer race. Subscript F denotes the frame, also all starred radii represent the nominal rolling radii of the respective elements. As shown on the instant center velocity diagram, Figure 19, the coincident point relative velocity between the inner race and the rollers at the contact point with the



REPRODUCIBILITY OF THE ORIGINAL PAGE IS POOR

Planetary Action

Figure 18



outer race, is twice that at the roller center. Thus:

$$\omega_b r_c - \omega_c r_c = 2[\omega_b r_s - \omega_s r_s] \quad (28)$$

or the angular velocity of the inner race relative to the cage is:

$$\omega_{b/s} = 1/2 \omega_{b/c} (r_c/r_s) \quad (29)$$

$$\omega_{b/s} = 1/2 [\omega_{b/F} - \omega_{c/F}] [1 + r_a/r_s] \quad (30)$$

Thus the fixed cage inner race speed becomes

$$\omega_b = \frac{\pi}{60} [1 + r_a^*/(r_a^* + r_b^*)] N \quad (31)$$

in terms of shaft RPM.

Similarly, the coincident point relative velocity between the outer race and the roller at the contact point with the inner race is twice this relative velocity at the roller center. These velocities are also indicated in the instant center diagram. Thus:

$$\omega_c r_b - \omega_b r_b = 2 [\omega_c r_s - \omega_s r_s] \quad (32)$$

or the angular velocity of the outer race relative to the cage is:

$$\omega_{c/s} = 1/2 \omega_{c/b} [r_b/r_s] \quad (33)$$

or

$$\omega_{c/s} = 1/2 [\omega_{c/F} - \omega_{b/F}] [1 - r_a^*/(r_a^* + r_b^*)] \quad (34)$$

and the fixed cage outer race speed becomes:

$$\omega_c = \frac{-\pi}{60} [1 - r_a^*/(r_a^* + r_b^*)] N \quad (35)$$

in terms of the shaft RPM.

The restoring torque may now be modeled as a function of: these race speeds relative to the cage; the slip or creep velocity,  $U$ , of the rolling pair; the true normal load,  $P$ ; a coefficient,  $K$ ; and the roller length between the contact points,  $Q\ell$ . In general terms this expression is:

$$T = (KPQ\lambda) U \quad (36)$$

Here  $Q$  is the percentage of the total bearing length between the contact points. The only factor in this equation which varies with the different geometries is the slip velocity,  $U$ . There are eight cases to consider since the contacting geometries of the first four compound rollers are the same as those of the simple rollers.

The first case to consider is that of a convex roller on a convex inner race. In this case, the slip velocity is the difference between the pitch point's velocity of the roller and of the inner race. Thus:

$$U = r_b \omega_b - r_a \omega_a \quad (37)$$

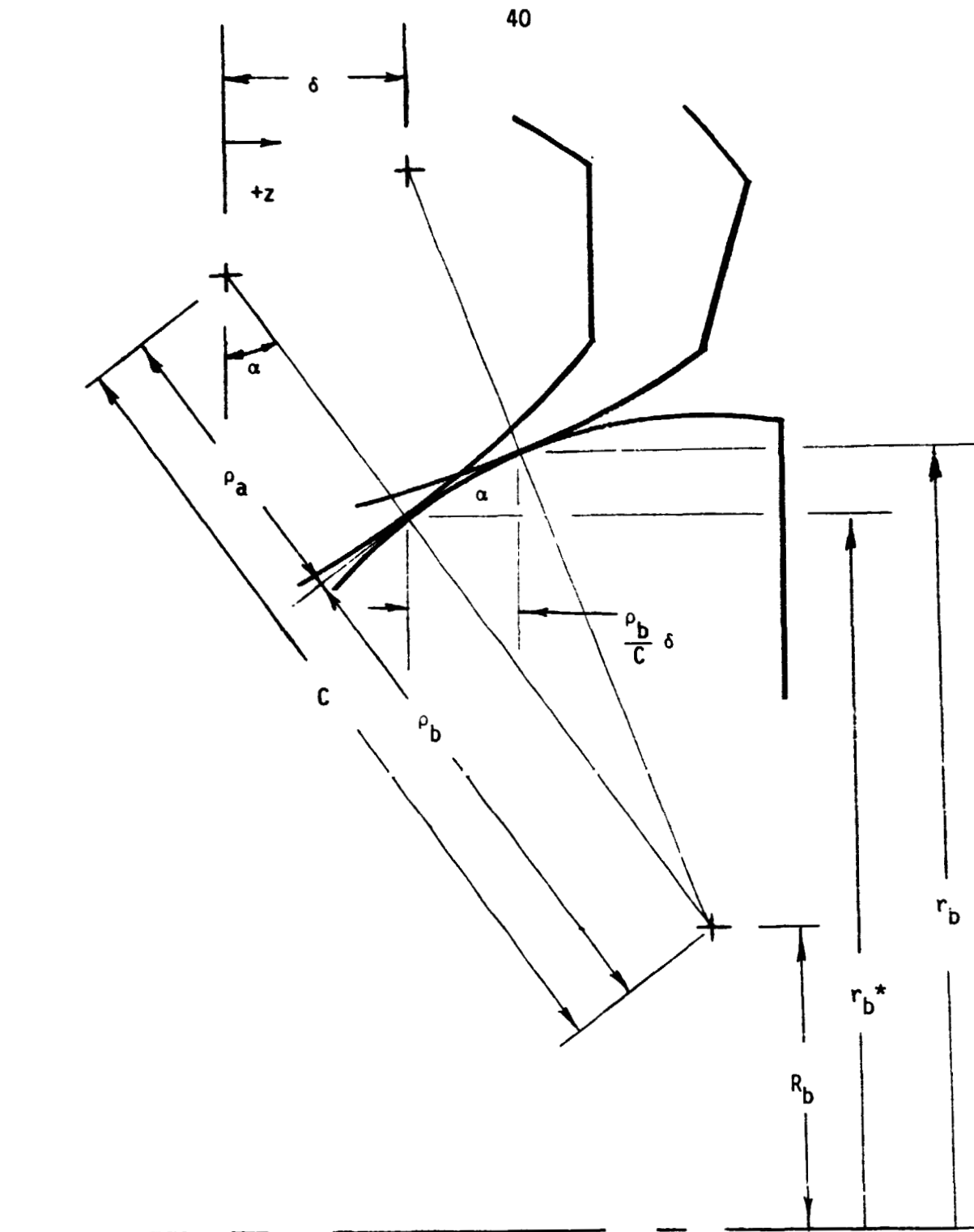
This slip couple is shown in Figure 1. A positive value for  $U$  and thus for  $T$  will serve to increase the skew and axial motion in the  $+z$  direction. Thus for a restoring torque,  $U$  must be negative for a displacement of roller  $a$  in the  $+z$  direction. From the condition of stability given in equation 1, the ratio of  $r_a$  to  $r_b$  must grow from equilibrium. Thus a negative value for a restoring torque is produced by a stable geometry.

The geometry of a finite shift in axial position from that of true cylindrical rolling is shown in Figure 20 for this case. The true rolling radii are considered those at the initial position and are superscripted with a star. In terms of the inner race angular velocity, the roller angular velocity is given by:

$$\omega_a = \frac{r_b^*}{r_a^*} \omega_b \quad (38)$$

the slip velocity is thus:

$$U = \left( r_b - r_a \left( \frac{r_b^*}{r_a^*} \right) \right) \omega_b \quad (39)$$



Disturbed Rolling Geometry  
for Convex-Convex-Neutral Geometry

Figure 20

$$U = \left( \frac{r_a^* r_b - r_a r_b^*}{r_a^*} \right) \omega_b \quad (40)$$

In terms of the axial shift,  $\delta$ , the actual rolling radii becomes:

$$r_b = r_b^* + \frac{\rho_b}{C} \delta \tan \alpha \quad (41)$$

and

$$r_a = r_a^* + \frac{\rho_a}{C} \delta \tan \alpha \quad (42)$$

Thus the slip velocity becomes:

$$U = \frac{\left[ r_a^* \frac{\rho_b}{C} \delta \tan \alpha - r_b^* \frac{\rho_a}{C} \delta \tan \alpha \right]}{r_a^*} \omega_b \quad (43)$$

or in terms of the fixed radii to the centers of transverse curvature:

$$U = \frac{[R_a^{\rho_b} - R_b^{\rho_a}]}{r_a^*} \frac{\delta}{C} \omega_b \tan \alpha \quad (44)$$

and the restoring torque per unit axial displacement in terms of the actual shaft speed becomes:

$$T/\delta = -KRQ \frac{[R_a^{\rho_b} - R_b^{\rho_a}]}{r_a^*} \frac{\tan \alpha}{C} \left[ 1 + \frac{r_a^*}{r_a^* + r_b^*} \right] \frac{\pi N}{60} \quad (45)$$

The negative sign is included to make the restoring torque positive for a stable configuration.

In the next three cases, two through four, the restoring torque is generated by contact of the roller with the outer race. The slip velocity for contact with the outer race is:

$$U = \omega_c r_c - \omega_a r_a \quad (46)$$

This slip couple is shown in Figure 2. Given positive values for  $\omega_c$  and  $\omega_a$ , positive values for  $U$  and  $T/\delta$  will cause an increase in the skew, thus negative values here also indicate stability. This is also consistent with

the outer race stability criterion which states that  $r_{1a}$  must grow faster than  $r_{1c}$  for a positive displacement of the roller. The geometry of a finite shift of the roller in this case is given in Figure 21. As before, the starred quantities refer to the nominal rolling radii. Thus

$$\omega_a = \frac{r_c^*}{r_a^*} \omega_c \quad (47)$$

and the slip velocity becomes:

$$U = \frac{(r_c r_a^* - r_c^* r_a)}{r_a^*} \omega_c \quad (48)$$

For the second case - a convex roller in contact with a convex outer race or a convex-neutral-convex geometry, the actual rolling radii in terms of the axial shift,  $\delta$ , becomes:

$$r_c = r_c^* - \frac{\rho_c}{C} \delta \tan \alpha \quad (49)$$

$$r_a = r_a^* + \frac{\rho_a}{C} \delta \tan \alpha \quad (50)$$

Thus:

$$U = \frac{-[r_a^* \frac{\rho_c}{C} \delta \tan \alpha + r_c^* \frac{\rho_a}{C} \delta \tan \alpha]}{r_a^*} \omega_c \quad (51)$$

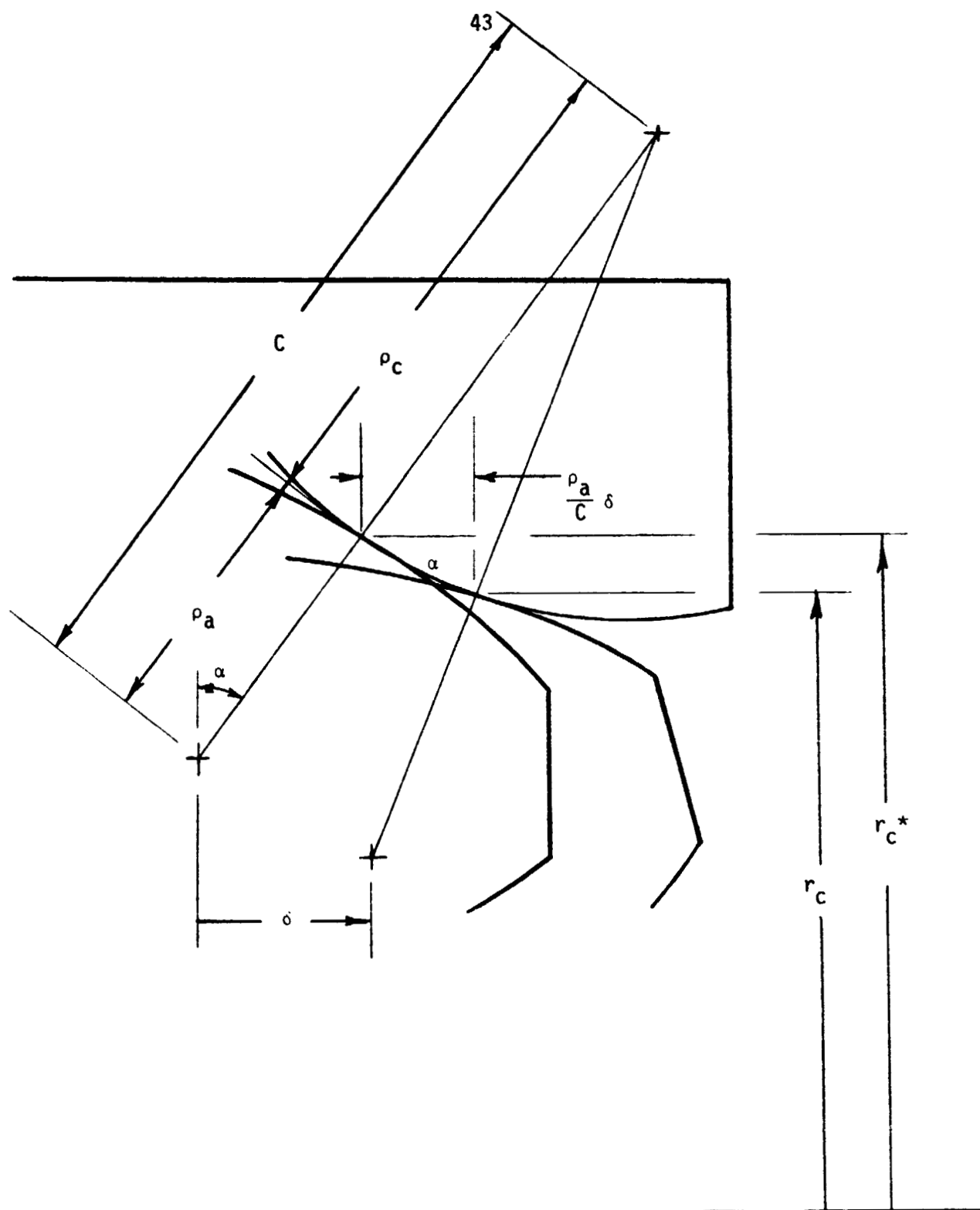
or

$$U = \frac{-[R_a \rho_c + R_c \rho_a]}{r_a^*} \frac{\delta}{C} \omega_c \tan \alpha \quad (52)$$

Thus the restoring torque per unit axial displacement in terms of the actual shaft speed becomes:

$$T/\delta = KPQ \ell \frac{[R_a \rho_c + R_c \rho_a]}{r_a^*} \frac{\tan \alpha}{C} \left[ 1 - \frac{r_a^*}{r_a^* + r_b^*} \right] \frac{\pi N}{60} \quad (53)$$

The positive values in this expression are due to the fact that  $\omega_c$  is



Disturbed Rolling Geometry  
for Convex-Neutral-Convex Geometry

Figure 21

negative, so a positive value for the equation indicates a stable geometry.

The third case is that of a convex roller in contact with a straight sided cone at the outer race. This convex-neutral-straight geometry differs from the second case only in the expressions for the actual rolling radii as a function of axial roller shift. In this case  $C$  is infinite and the shape of the contact does not change. Thus the roller's radius is constant and the radius to the straight cone is given by:

$$r_c = r_c^* - \delta \tan \alpha \quad (54)$$

Equation 48 still holds, so the slip velocity becomes:

$$U = - \delta \tan \alpha \omega_c \quad (55)$$

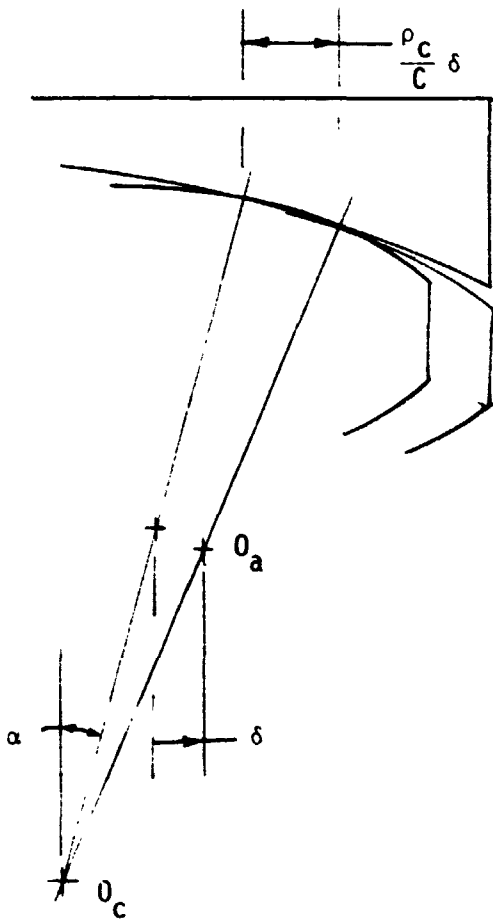
The restoring torque per unit displacement is:

$$T/\delta = KPQl (\tan \alpha) \left[ 1 - \frac{r_a^*}{r_a^* + r_b^*} \right] \frac{\pi N}{60} \quad (56)$$

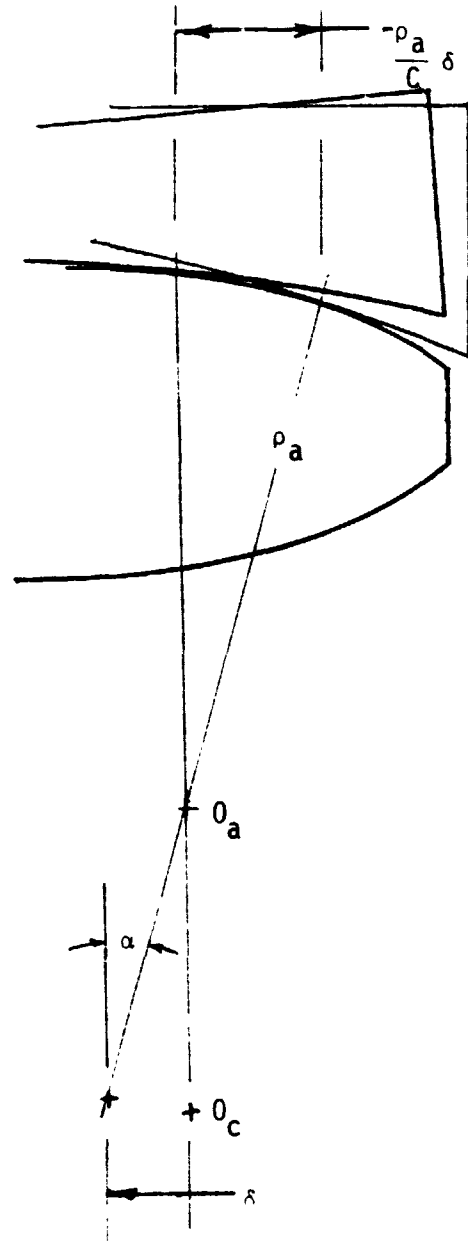
The fourth case is that of a convex roller with a concave outer race. For this convex-neutral-concave geometry, the only possible difference from the second case of convex-neutral-convex geometry is the expressions for the displaced rolling radii. However, the fact that  $\rho_c$  and the center distance,  $C$ , are both negative makes equations 49 and 50 valid for this case also. Figure 22 illustrates this for both equations. Thus equation 53 is also valid for this geometry.

These formulas are valid for the simple roller geometries as well as the first four cases of compound roller geometry which have the same correcting race curvatures. The last four cases, five through eight, require more attention.

Cases five and six have straight cones on the roller. Thus the contacting race rolling radii remain constant and the roller rolling radii change directly with the displacement. For the straight-convex-neutral geometry, the



a) Relative to Outer Race



b) Relative to Roller

Disturbed Rolling Geometry for  
Convex - Neutral - Concave Bearing

Figure 22

slip velocity is given by equation 40, and the actual rolling radii are:

$$r_b = r_b^* \quad (57)$$

$$r_a = r_a^* + \delta \tan \alpha \quad (58)$$

Equation 40 thus becomes:

$$U = \frac{-r_b^*}{r_a^*} \delta \tan \alpha \omega_b \quad (59)$$

and the restoring torque per unit displacement is:

$$T/\delta = +KPQ\ell \frac{r_b^*}{r_a^*} \tan \alpha \left[ 1 + \frac{r_a^*}{r_a^* + r_b^*} \right] \frac{\pi N}{60} \quad (60)$$

Once again this equation has had its sign changed to produce a positive restoring torque for a stable configuration.

The sixth case with a straight cone on its roller is the straight-neutral-convex geometry which has the convex transverse contour on the outside race. For this case, equation 48 describes the slip velocity and the actual rolling radii are given by

$$r_c = r_c^* \quad (61)$$

and

$$r_a = r_a^* + \delta \tan \alpha \quad (62)$$

Equation 48 thus becomes

$$U = -\delta \frac{r_c^*}{r_a^*} \tan \alpha \omega_c \quad (63)$$

and the restoring torque per unit displacement is:

$$T/\delta = KPQ\ell \frac{r_c^*}{r_a^*} \tan \alpha \left[ 1 - \frac{r_a^*}{r_a^* + r_b^*} \right] \frac{\pi N}{60} \quad (64)$$

The final two cases, seven and eight, have concave transverse curvature on the roller. For the seventh case, the roller contacts the inner race and thus the case is of a concave - convex - neutral

geometry. This geometry is shown in Figure 23 in its displaced position. Once again the slip velocity is given by equation 40 and the displaced rolling radii are given by equations 41 and 42 where  $\rho_a$  and the center distance are negative due to the concave surface. Thus equation 45 holds for this case.

The eighth case is that of a concave roller on a convex outer race. This is the concave-neutral-convex geometry. As in the concave-convex-neutral case, the analysis is identical as that for the convex-neutral-convex case with the sole exception of the signs of  $\rho_a$  and the resulting center distance, C. Thus equation 53 describes the restoring torque per unit displacement for the concave-neutral-convex geometry.

These restoring torque per unit displacement equations are all positive for stable geometries. They are summarized in table 5 for the eight different contacting geometries. In these equations,  $Q\ell$  is the actual distance between the tractive forces at the contact centers and P is the normal force on the contact. If the contacts are with the inner race, then P is only a function of the external force per roller,  $P_o$ , and the cone angle,  $\alpha$ :

$$P_b = \frac{P_o}{2 \cos \alpha} \quad (65)$$

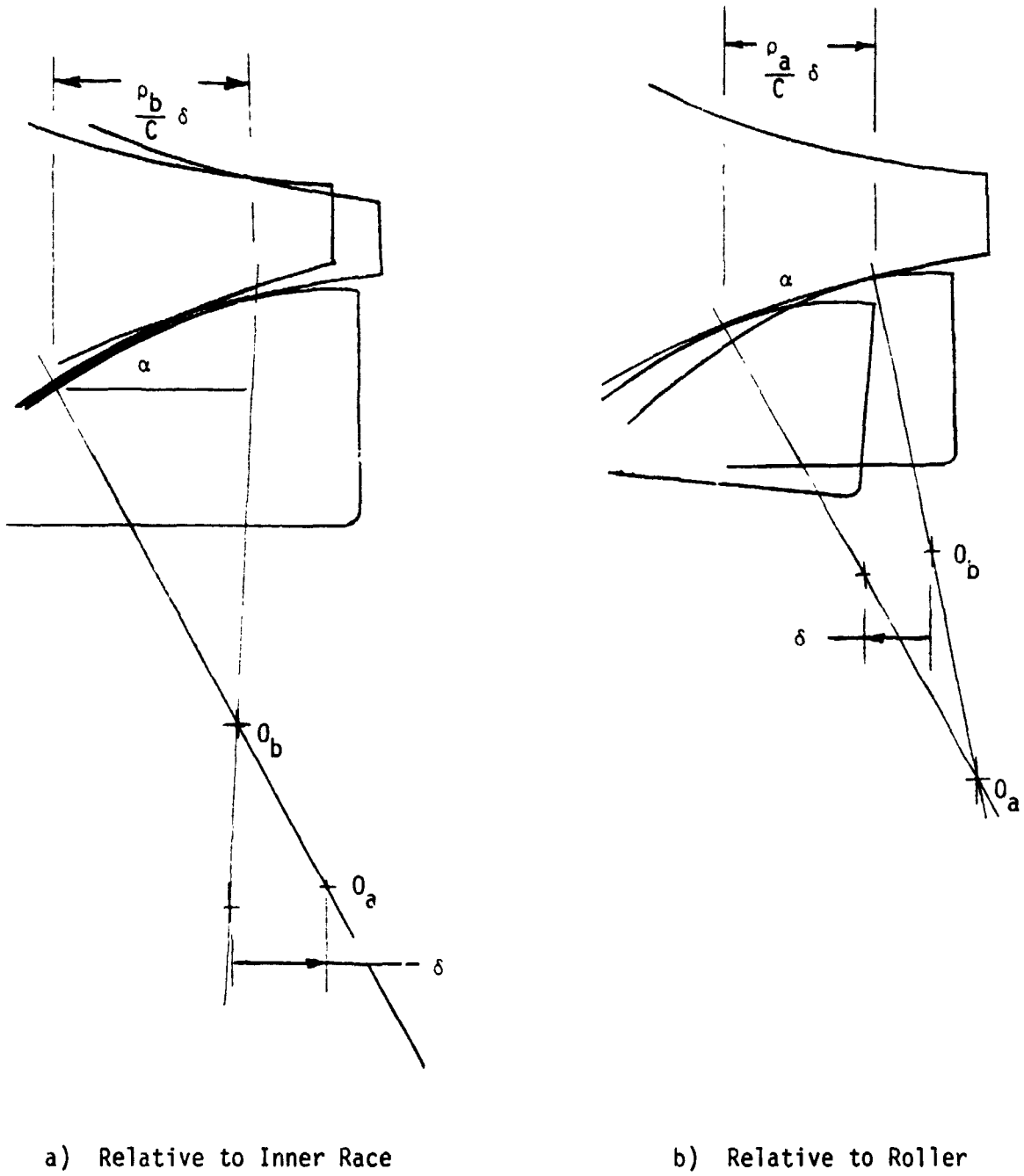
If the contacts are with the outer race then the dynamic force of the roller must be included

$$P_c = \frac{P_o + \frac{W}{g} (\pi r_a^{*2} \ell) (r_b^* + r_a^*) \omega_s^2}{2 \cos \alpha} \quad (66)$$

or

$$P_c = \frac{P_o + \frac{W}{g} (\pi r_a^{*2} \ell) (r_a^* + r_b^*) \left[ \left( 1 - \frac{r_a^*}{r_a^* + r_b^*} \right) \frac{\pi N}{60} \right]^2}{2 \cos \alpha} \quad (67)$$

Finally the coefficient, K, is a function of the traction coefficient for high speed rolling of lubricated steel surfaces. This tractive coefficient has



Disturbed Rolling Geometry for  
Concave - Convex - Neutral Bearing

Figure 23

roller curvature	inner race curvature	outer race curvature	coefficient of $KPQ \tan \alpha \left( \frac{\pi N}{60} \right)$
convex	convex	-	$-\frac{[R_{a^{\rho}b} - R_{b^{\rho}a}]}{r_a^* C} \left[ 1 + \frac{r_a^*}{r_a^* + r_b^*} \right]$
convex	-	convex	$\frac{[R_{a^{\rho}c} + R_{c^{\rho}a}]}{r_a^* C} \left[ 1 - \frac{r_a^*}{r_a^* + r_b^*} \right]$
convex	-	straight	$\left[ 1 - \frac{r_a^*}{r_a^* + r_b^*} \right]$
convex	-	concave	$\frac{[R_{a^{\rho}c} + R_{c^{\rho}a}]}{r_a^* C} \left[ 1 - \frac{r_a^*}{r_a^* + r_b^*} \right]$
straight	convex	-	$\frac{r_b^*}{r_a^*} \left[ 1 + \frac{r_a^*}{r_a^* + r_b^*} \right]$
straight	-	convex	$\frac{r_c^*}{r_a^*} \left[ 1 - \frac{r_a^*}{r_a^* + r_b^*} \right]$
concave	convex	-	$-\frac{[R_{a^{\rho}b} - R_{b^{\rho}a}]}{r_a^* C} \left[ 1 + \frac{r_a^*}{r_a^* + r_b^*} \right]$
concave	-	convex	$\frac{[R_{a^{\rho}c} + R_{c^{\rho}a}]}{r_a^* C} \left[ 1 - \frac{r_a^*}{r_a^* + r_b^*} \right]$

Restoring Torque Equations

Table 5

been measured by Hewko [12] for these conditions. The tractive coefficient can be obtained from equation 36 as:

$$f = \frac{T}{PQ\ell} = K U \quad (68)$$

Thus the coefficient K has units of seconds per inch and can be obtained from data of tractive coefficient versus creep or percent slip. For a 35 mm bearing turning at 60,000 RPM, the pitch point velocity of the roller surface with respect to the cage is slightly less than 3,000 inches per second or 15,000 feet per minute. From Hewko's data, for a 1% creep or a slip velocity of three inches per second, one should expect a traction coefficient of 0.03 at a Hertzian contact pressure of 180,000 psi. To be conservative, a traction coefficient of one half this value is assumed at this slip velocity due to the possible differences between cylindrical and spherical contact. From equation 68 the coefficient K which would produce this tractive coefficient at this slip velocity is 0.005 seconds per inch.

### Contact Stresses and Deflections

The loads of equation 65 or 67 act on two of the three contact points of the roller. If the corrective geometry is on the inner race, then the two contact points on that race see  $P_b$  as a normal load. If the corrective geometry is on the outer race the  $P_c$  acts normal to both contact points. The third contact point is with the straight race. If the corrective geometry is on the inner race then this outer contact force is:

$$P = P_0 + \frac{W}{g} (\pi r_a^{*2} \ell) (r_a^* + r_b^*) \left[ \left( 1 - \frac{r_a^*}{r_a^* + r_b^*} \right) \frac{\pi N}{60} \right]^2 \quad (69)$$

If the corrective geometry is on the outer race, then the contact force with the straight inner race is merely  $P_0$ , the applied radial load to the roller.

For the simple roller geometry, the contact stress and deflection analysis can be modeled as a three dimensional double curvature Hertzian contact. This model is appropriate for all three contacts. The formulation of the solution to this problem is taken from Seely and Smith [13]. The solution is given in terms of the principal radii of curvature of the surfaces -  $R_1$  and  $R_2$  which are the smallest radii of curvature of the two bodies in absolute value and  $R_1'$  and  $R_2'$  which are the largest radii of curvature of the two bodies in absolute value at the contact point. In our case, the smallest radii are the rolling radii times the cosine of the cone angle,  $\alpha$ , and the largest are the transverse radii. Two constants are defined in terms of these radii:

$$A = 1/2 \left( \frac{1}{R_1} + \frac{1}{R_2} \right) \quad (70)$$

and

$$B = 1/2 \left( \frac{1}{R_1'} + \frac{1}{R_2'} \right) \quad (71)$$

In terms of these constants, three coefficients are determined from charts. To simplify these calculations, the three coefficients are expressed in terms of these constants as:

$$K = 0.7826 \left( \frac{B}{A} \right)^{-0.5707} \quad (72)$$

$$\nu_\delta = 2.827 \left( \frac{B}{A} \right)^{-0.4557} \quad (73)$$

and

$$C_5 = 0.7212 \left( \frac{B}{A} \right)^{-0.1893} \quad (74)$$

Due to this curve fitting, the three coefficients are felt to be representative for values of  $B/A$  greater than 10. For steel on steel contact, the stresses and deflections are given by

$$\sigma_{\max} = \frac{-b}{\Delta} \quad (75)$$

where

$$b = c_b \sqrt[3]{P \Delta} \quad (76)$$

$$a = b/K \quad (77)$$

$$\delta = -c_\delta \frac{P}{\pi} \left( \frac{A+B}{\sigma_{\max}} \right) \quad (78)$$

and

$$\Delta = \frac{2}{A+B} \left( \frac{1-\mu^2}{E} \right) \quad (79)$$

In these equations,  $\sigma_{\max}$  is the maximum contact pressure,  $b$  is the contact half width in the circumference direction,  $a$  is the contact half width in the transverse direction and  $\delta$  is the amount of approach of the two contacting bodies under the action of the load. The quantity  $\Delta$  is an intermediate constant dependant on the surface curvature and elastic properties of modulus,  $E$ , and Poisson's ratio,  $\mu$ . In the calculations  $E$  is taken as  $29.5 \times 10^6$  psi and  $\mu$  is 0.285.

A subroutine called Hertz has been written to calculate those quantities for the contact points for which at least one surface has double curvature. This is true for all contact points for the simple rollers but only for the two contact points with the corrective geometry race for the compound rollers. In that case, cylindrical contact exists with the straight race. Although both the race and the roller are stiffened at the ends of the contact region by unloaded material outside the contact region, a simple two dimensional Hertz model is used to calculate the stress and deflection at this contact [14].

The model is:

$$b = \sqrt{\frac{8 (R_1 R_2) P}{\pi (R_1 + R_2) t} \left( \frac{1-\mu^2}{E} \right)} \quad (80)$$

$$\sigma_{\max} = - \frac{2P}{\pi tb} \quad (81)$$

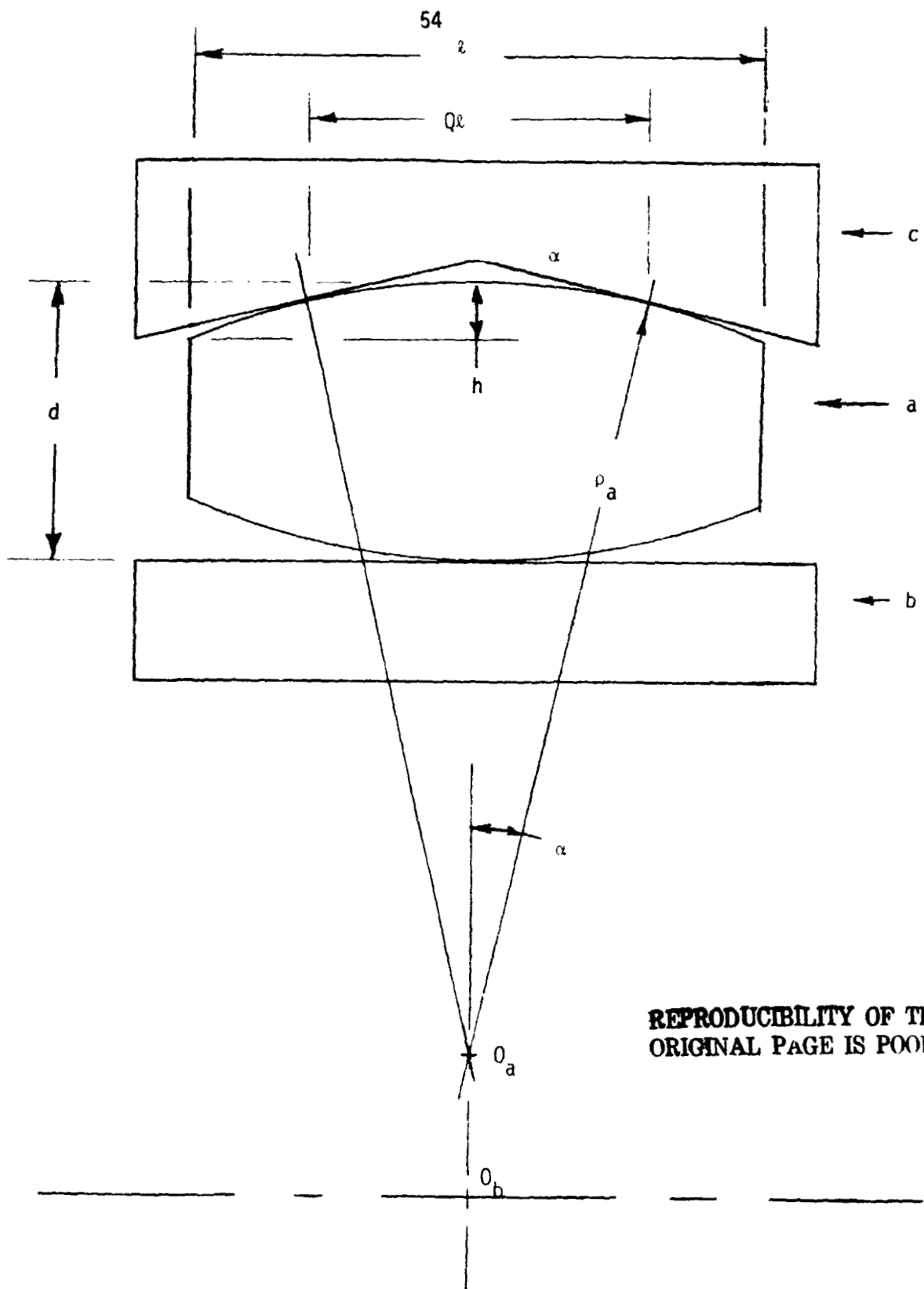
$$\delta = 4 \left( \frac{1 - \nu^2}{E} \right) \frac{P}{\pi t} \left[ \ln \left( \frac{2}{b} \right) + \frac{1}{2} \right] \quad (82)$$

All the variables carry the same meaning as in the proceeding case where the only additional variable,  $t$ , is the length of contact in the transverse direction. For a concave outer race, its rolling radius is taken as negative. The formulas are programmed in subroutine CYL for use in estimating the contact stress at the contact of the compound roller with the straight race. The straight portion of the roller may have a slight crown to alleviate the edge stresses and make this two dimensional uniform model more realistic.

#### Misalignments and Clearances

In evaluating the relative merits of different designs, a third factor should be considered in addition to the stabilizing torque and load capacity. That factor is the sensitivity of the bearing to shaft misalignment in the form of a slope at the bearing. Due to the double contact with the contoured race and the single contact with the straight race, the roller's position in the loaded region can be determined as a function of the shaft slope. For the simple convex rollers, the radius of transverse curvature of the roller surface is directly related to the half cone angle,  $\alpha$ , the roller length,  $\ell$ , and the percentage of roller length between the two contact points. As can be seen from Figure 24,

$$\rho_a = \frac{Q\ell}{2} \sin \alpha \quad (83)$$



Simple Convex Roller Geometry

Figure 24

The roller can turn about the center of this transverse curvature with respect to the contoured race. Thus, as the shaft deflects under load and assumes a slope at the bearing center, the roller will also tilt. When the contoured race is the outer race as shown in Figure 24, both the shaft and the roller will tilt the same amount. The difference between the minimum distance from the shaft center to the roller bottom and the radius of the inner race is derived from Figure 25 as:

$$CLR = (\rho_a - 2r_a - r_b) (1 - \cos \gamma) \quad (84)$$

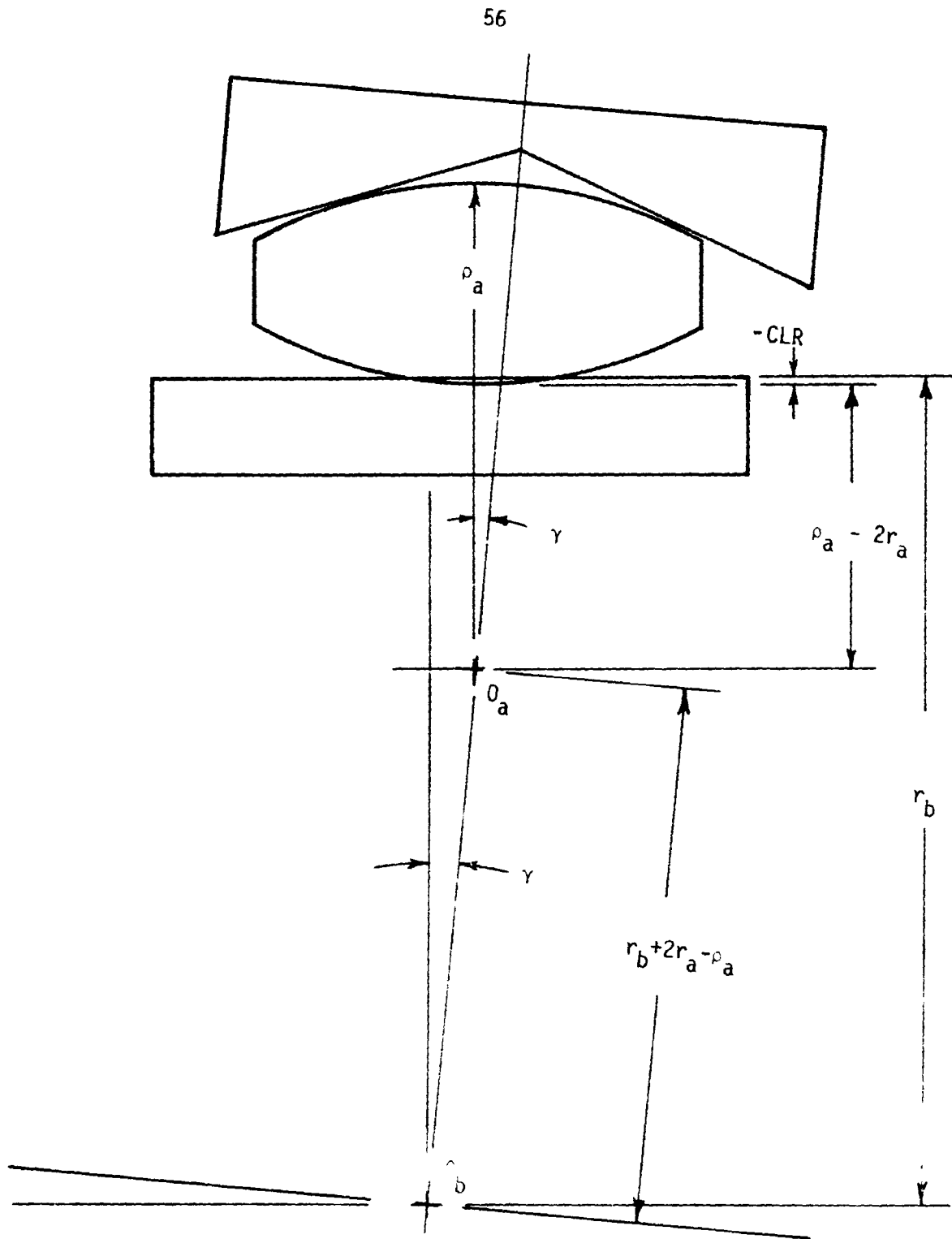
where  $\gamma$  is the angle of tilt or misalignment of the shaft. Note that if  $\rho_a$  is greater than  $r_b + 2r_a$ , the center of transverse curvature will be below the shaft centerline and the clearance will be positive. This would indicate that no large edge loading would be impressed on the rollers in the load region and that the shaft would deflect in the bearing through a distance equal to CLR to take up this slack. If CLR were negative then this center of curvature would be above the shaft centerline and the bearing would pick up additional radial loading to cause deformations equal to CLR. High negative values of CLR for expected shaft misalignments should therefore be avoided.

If the corrective geometry is on the inner race as shown in Figure 10, the roller will remain parallel to the outer race. Thus a clearance will be obtained as a function of shaft slope  $\gamma$  as shown in Figure 26:

$$CLR = (\rho_a + r_b) (1 - \cos \gamma) \quad (85)$$

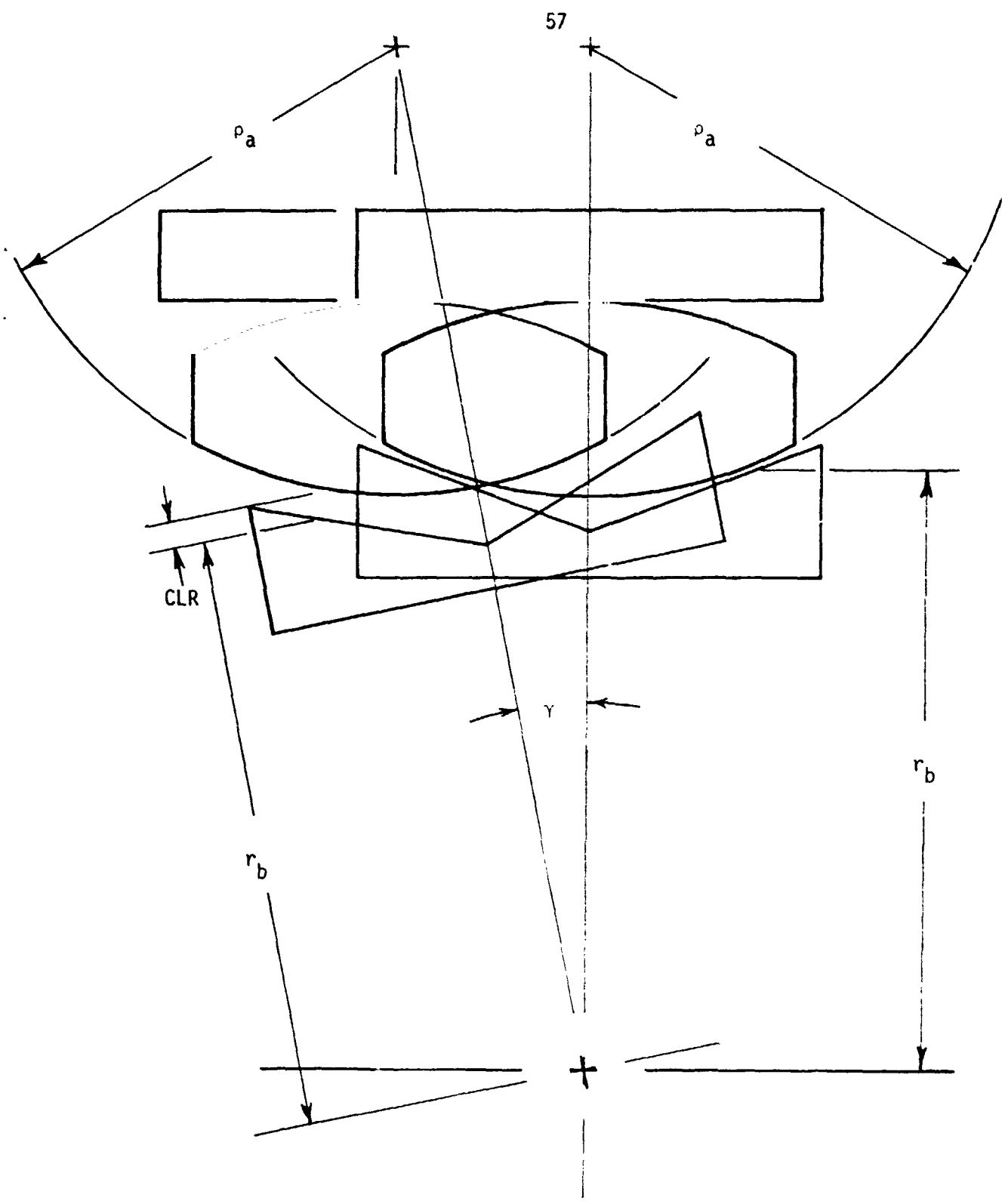
This clearance will always be positive and thus will result in a radial displacement of the shaft in the bearing.

A quantity of interest in comparing various bearings is the drop of the roller. This quantity is the difference in radius of the roller from the maximum value at the center to the minimum value at the outside. The higher the drop, the more the roller is trapped between the two contact points with



Shaft Slope Geometry

Figure 25



Shaft Slope Geometry

Figure 26

the corrective geometry race. Thus this race acts as a race with shoulders if the drop is sufficiently high. For the simple rollers with a single radius of transverse curvature this drop is:

$$h = \rho_a \left( 1 - \cos \left[ \sin^{-1} \frac{\ell}{2\rho_a} \right] \right) \quad (86)$$

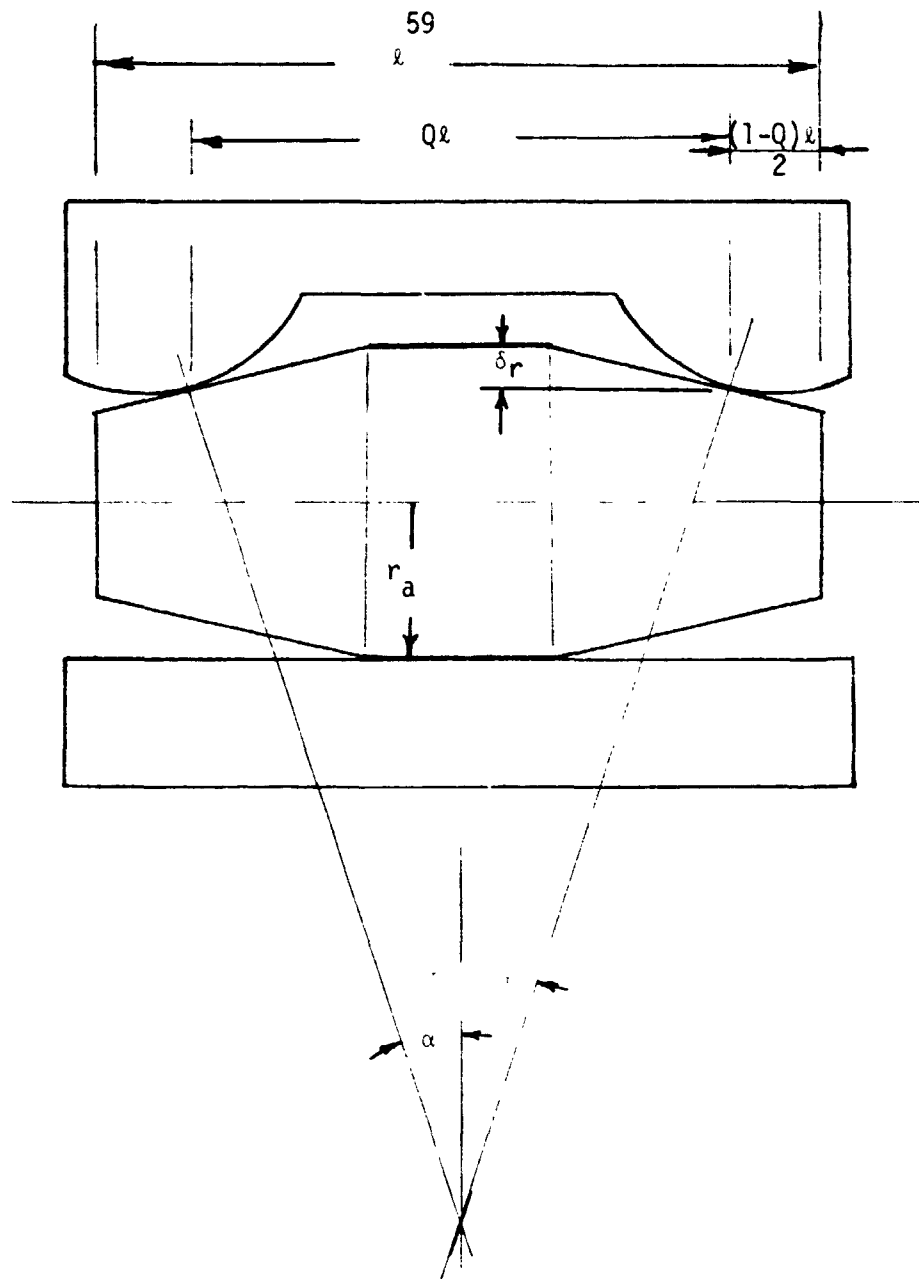
as can be seen in Figure 24.

For the compound rollers, as illustrated in Figure 27, the roller is not able to rotate about a center of transverse curvature because this center does not exist. The intersection of the two contact normals to the restoring geometry defines a center about which the roller could rotate. But since the center of curvature of the roller surface is greater than the distance from this center to the contact point, a rotation of the roller is possible only with extreme compressive loading and deflection at one of the contact points. Thus the compound rollers are held parallel to the race with the corrective geometry and any shaft misalignment will produce edge loading on the straight portion of the roller. Since this width is fairly small in comparison to the total roller length, one would expect lower sensitivity to edge loading than in a standard roller. An exact comparison would be difficult, however. The straight section of the roller should be crowned, as straight rollers are, to reduce this edge loading.

The compound roller geometry is proportioned so that the nominal contact points lie in the center of the outer contoured regions. Thus  $Q$  must be somewhere between 0.5 and 1.0 for three surface bands to exist. Also the length of each outside band is given by:

$$\ell_o = (1 - Q) \ell \quad (87)$$

The drop of each roller can thus be determined in terms of  $Q$ ,  $\ell$ ,  $r_a$ ,  $\rho_a$ , and  $\alpha$ . For the straight roller this is:



Compound Straight Roller

Figure 27

$$h = (1 - Q) \ell \tan \alpha \quad (88)$$

Figure 28 shows a compound convex roller with the appropriate geometry for calculating its drop.

$$\sin \alpha_1 = \sin \alpha - \frac{(1 - Q) \ell}{2 \rho_a} \quad (89)$$

$$\sin \alpha_2 = \sin \alpha + \frac{(1 - Q) \ell}{2 \rho_a} \quad (90)$$

and

$$h = \rho_a (\cos \alpha_1 - \cos \alpha_2) \quad (91)$$

Figure 29 shows a compound concave roller with its appropriate geometry for calculating the drop. Noting that  $\rho_a$  is negative in this case, the drop can be calculated from equations 89 through 91 using the appropriate negative value for  $\rho_a$ .

### Compound Roller Bearing Geometry

In the development of the equations for the bearing cage velocities, the contact stress levels and the restoring torques of the bearings, it has been assumed that the nominal rolling radii of the rollers and races are close enough to the actual radii to be used in all calculations. Due to the small roller drops in the simple roller designs, this assumption is valid for these four bearing configurations. However, as noted in equation 88 and 91, the drop for the compound rollers of the last eight bearing configurations can be significant due to the fact that the contour transverse slope need not be zero at the center of the bearing for these configurations.

Thus the calculation of these quantities should include the effect of this roller drop for the eight compound roller configurations. For these bearings,

one race rolls at its nominal radius with the full roller radius. This is the straight race which rolls on the center portion of the compound roller. The second race, which is the contoured race, rolls on a reduced radius of the contoured portion of the roller. The reduction in roller radius for a straight roller can be seen in figure 27 and is given by:

$$\delta_r = \frac{(1 - Q)l}{2} \tan \alpha \quad (92)$$

The reduction in roller radius at the contact center of the contoured band of convex or concave curvature rollers is illustrated in figures 28 and 29 and can be expressed as:

$$\delta_r = \rho_a (\cos \alpha_1 - \cos \alpha) \quad (93)$$

For the bearings with a straight outer race, the inner race radius increases by  $\delta_r$  and the roller becomes a compound roller with a rolling radius of  $r_a - \delta_r$  with the inner race and a rolling radius of  $r_a$  with the outer race which has a rolling radius of  $r_c$ . For these bearings, the cage velocity becomes:

$$\omega_s = \frac{r_a (r_b + \delta_r)}{(2r_a - \delta_r)(r_a + r_b)} \left[ \frac{\pi N}{30} \right] \quad (94)$$

for the calculation of the roller dynamic load. The Hertz stress calculation for the double curvature contacts uses

$$R_1 = (r_a - \delta_r) \cos \alpha \quad (95)$$

and

$$R_2 = (r_b + \delta_r) \cos \alpha \quad (96)$$

as the two minimum radii of surface curvature. Finally the restoring torque is multiplied by the factor

$$\frac{2 r_a (r_b + \delta_r)}{(2r_a - \delta_r) r_b} \quad (97)$$

for the straight - convex - neutral case, (5), with a straight roller. In the other two configurations with a contoured inner race, (1 and 7), this restoring torque modification factor becomes:

$$\frac{2 r_a}{2r_a - \delta_r} \quad (98)$$

For the bearings with a straight inner race, the outer race radius decreases by  $\delta_r$  and the roller becomes a compound roller with a rolling radius  $r_a - \delta_r$  with the outer race and a rolling radius of  $r_a$  with the inner race which has a rolling radius of  $r_b$ . For these bearings, the cage velocity becomes:

$$\omega_s = \frac{(r_a - \delta_r) r_b}{(2r_a - \delta_r)(r_a + r_b)} \left[ \frac{\pi N}{30} \right] \quad (99)$$

for the calculation of the roller dynamic load. The Hertz stress calculation for the double curvature contacts uses:

$$R_1 = (r_a - \delta_r) \cos \alpha \quad (100)$$

$$\text{and } R_2 = -(r_c - \delta_r) \cos \alpha \quad (101)$$

as the two minimum radii of surface curvature. The factors for altering the restoring torques from those calculated assuming a full radius roller are:

$$\frac{2r_a}{2r_a - \delta_r} \quad (102)$$

for the convex - neutral - convex case, (2), the convex - neutral - concave case (4) and the concave - neutral - convex case (8);

$$\frac{2(r_a - \delta_r)}{2r_a - \delta_r} \quad (103)$$

for the convex - neutral - straight case (3); and

$$\frac{2r_a (r_c - \delta_r)}{(2r_a - \delta_r) r_c} \quad (104)$$

for the straight - neutral - convex case (7). Multiplying the appropriate coefficient in table 5 by the corresponding factor (97, 98 and 102 through 104) yields restoring torques which reflect the roller geometry more closely than the torque expressions listed in table 5 which assume that the roller rolls on its full radius with both races.

### Design Programs

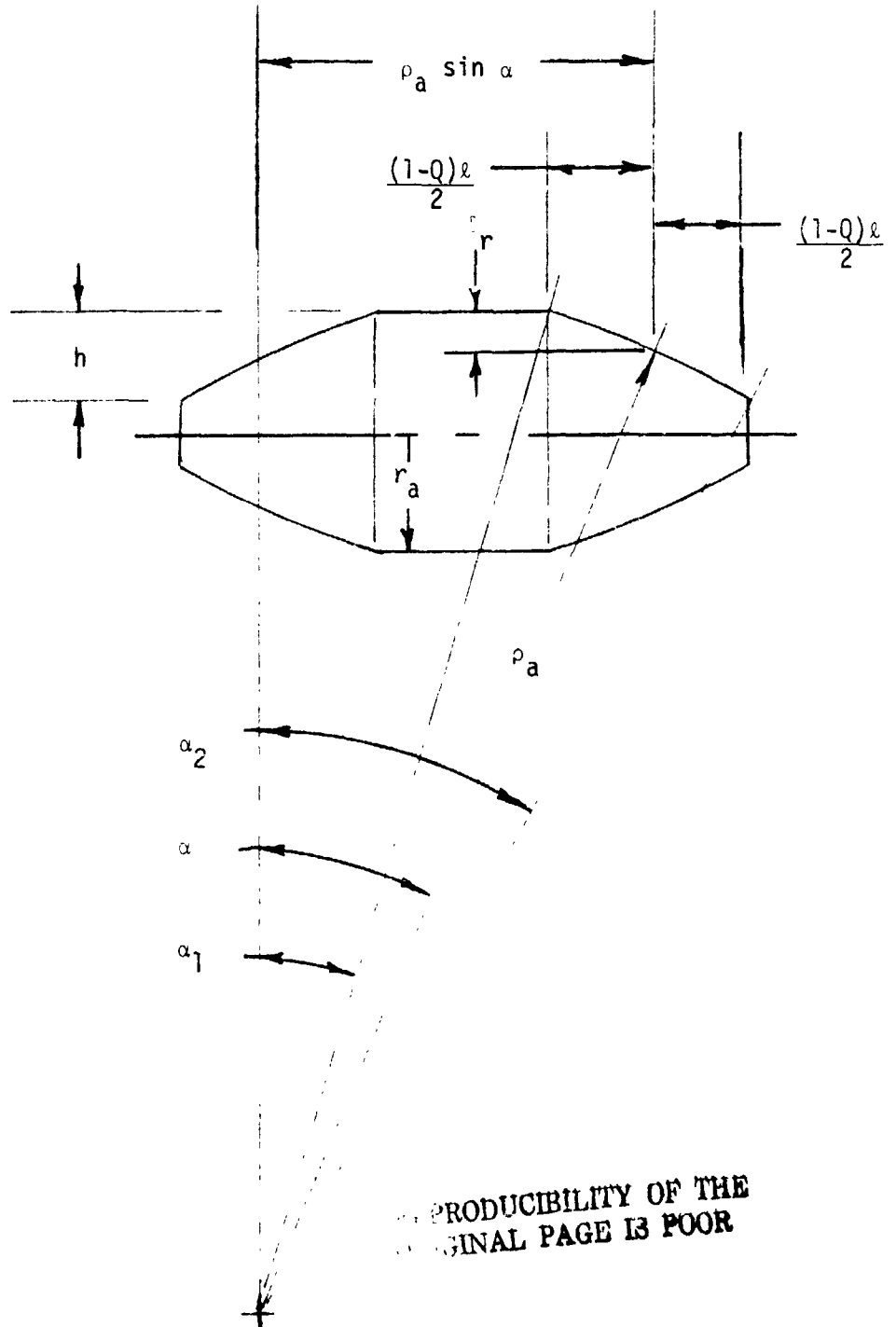
For all bearings, a given size normally has its outside diameter and inside diameter specified from the application and the bearing it is to replace. Thus the rolling radii of the races and the roller are considered input quantities to the design. Other quantities in this category are the shaft speed in RPM and the radial load of the bearing on a per roller basis.

For the four bearing geometries which use convex rollers with a single transverse curvature, this radius of transverse curvature is related directly to the half cone angle  $\alpha$  (equation 83) by the need to have zero slope at the center of the roller. Thus for each of these bearing geometries, one is free to specify the length to diameter ratio of the roller,  $l/d$ ; the load spread factor,  $Q$ ; and the half cone angle,  $\alpha$ , which are shown in Figure 24.

The first geometry listed is that of a convex roller with a convex inner race and a straight outer race as pictures in Figure 10. From table 2, the radius of transverse curvature of the inner race must satisfy the inequality

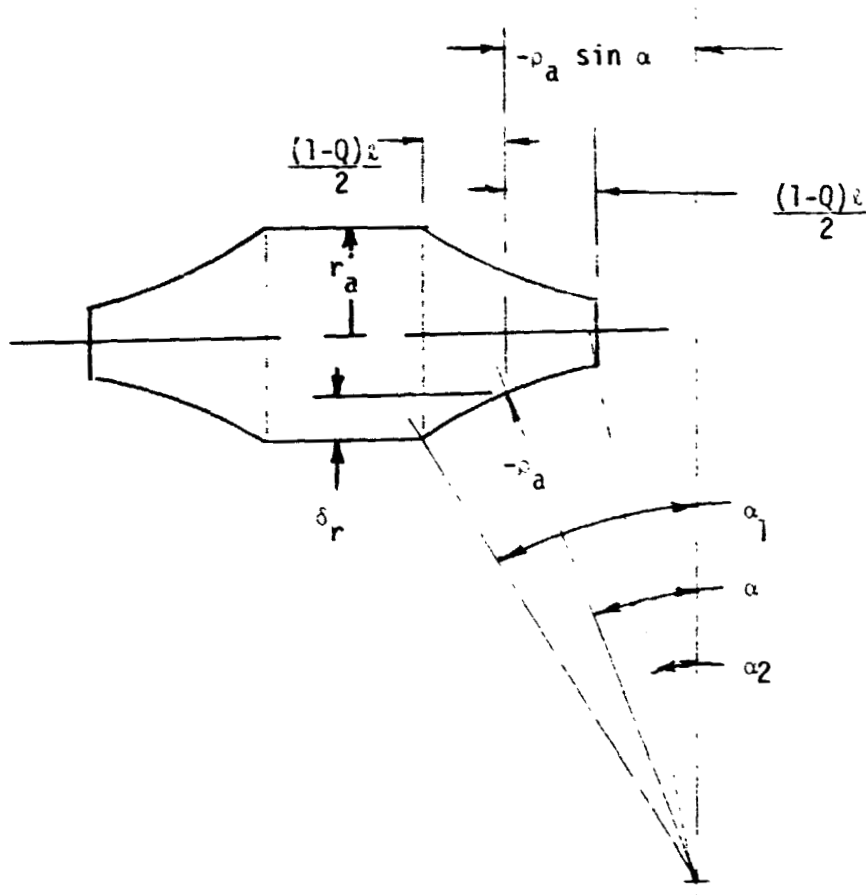
$$\rho_b < \rho_a \frac{r_b}{r_a} \quad \text{for } \alpha > 0 \quad (105)$$

for stability. If  $\rho_b$  equalled this limiting value then the restoring torque would be zero. This negates the entire purpose of the geometry. To look at some simple designs which are stable, the radius of transverse curvature for



Compound Convex Roller Drop

Figure 28



Compound Concave Roller Drop

Figure 29

the inner race is arbitrarily set at one-half this limiting value. If this geometry were of prime interest this factor could be varied to produce a series of designs. The present program sets the  $\lambda/d$  ratio and for three load spread factors sweeps a range of half cone angles and analyzes the resulting bearings.

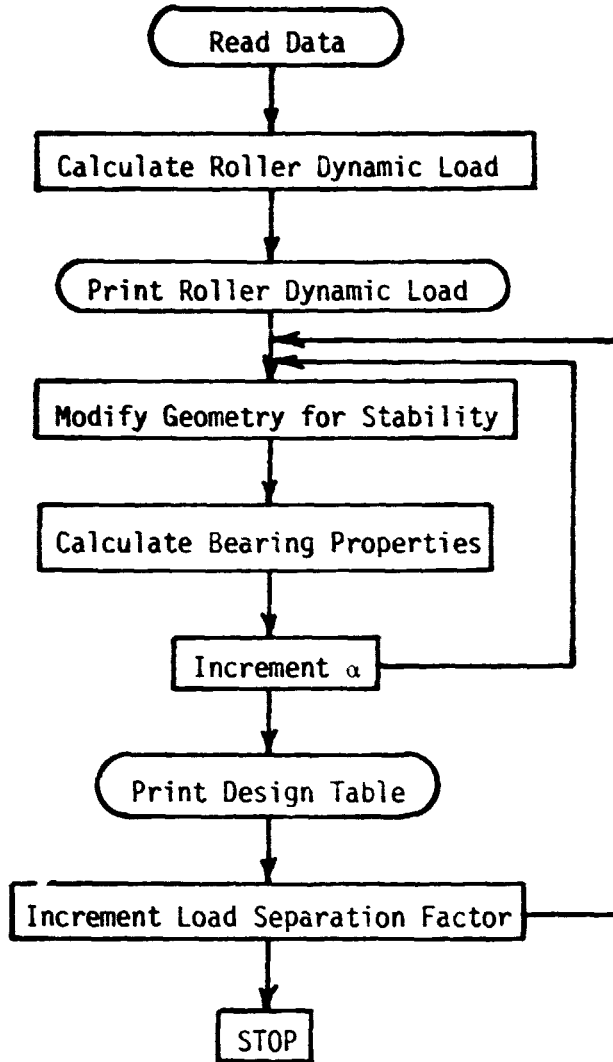
The program then prints out for each half cone angle and load spread factor a list of: the resulting radii of transverse curvature of the roller and inner race, the contact stress at the inner and outer contact points, the half widths of contact in the transverse direction, the restoring torque per inch of disturbance, the contact point deformations, the roller drop and the clearance caused by a one-quarter of a degree shaft misalignment. A perusal of the values in this list gives a fair evaluation of the expected performance of the designed bearing. Figure 30 is a flow chart for this program.

The second geometry listed is the convex-neutral-convex geometry which is stable for all combinations of transverse curvature. Thus several outer race radii of transverse curvature should be looked at. Three values were arbitrarily selected: one-half the radius of transverse curvature of the roller, the radius itself and two times the roller's radius of curvature. Thus this program produces three sets of output data - each containing three load separation factors for which five half cone angles are used.

The third geometry listed is that of convex-neutral-straight transverse surfaces. For this geometry, the transverse curvature of the outer race is zero and the stability is unconditional, so the designs are controlled by the three input factors and a single output is produced as in the first case.

The fourth geometry is that of convex-neutral-concave transverse surfaces. As in the case of the first geometry, the stability is conditional. For this case the radius of transverse curvature of the outer race is limited to be

$$\rho_c < -\rho_a \frac{r_c}{r_a} \quad (106)$$



Simple Roller Design Flow Chart

Figure 30

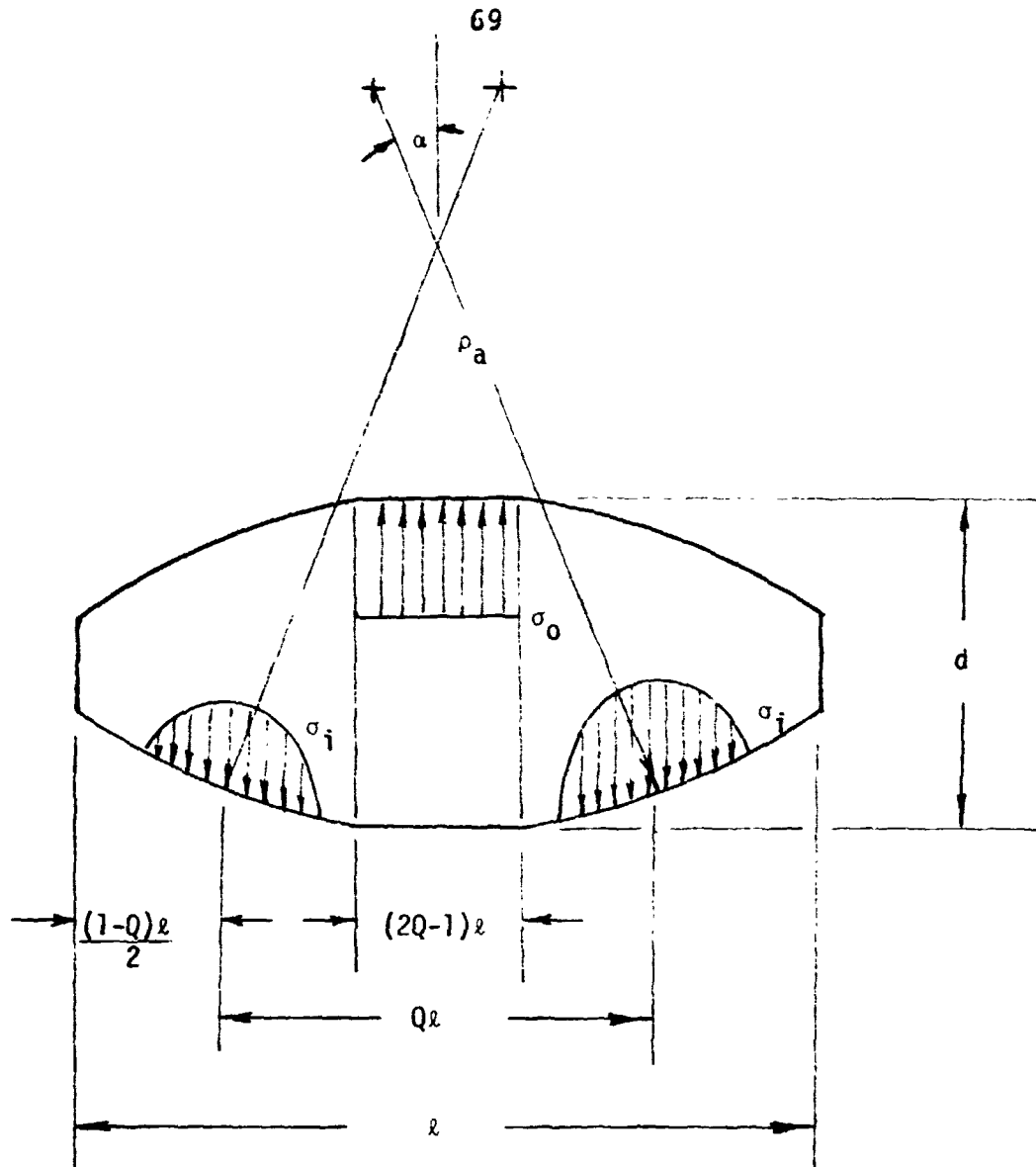
for stability. This expression comes from table 3 and forces the outer race to have a large negative radius of transverse curvature. For the purposes of the design program, a value equal to twice this limit is arbitrarily selected. This is done for the same reasons that the limiting value of  $\rho_b$  is halved in the first case - to insure stability and not compromise the load capacity excessively.

The above bearings all have rollers with a single radius of transverse curvature. This restricts the potential use of the restoring geometry concept by coupling the transverse radius of curvature to the half cone angle. As a result, the Hertzian stresses at the contacts with the inner and outer races are far from equal. In order to have more latitude in the design, the next level of roller complexity is also investigated in this report and design programs are developed for these eight bearing geometries as well. Figure 31 shows a roller of this type with convex curvature on its corrective geometry bands. The load separation factor,  $Q$ , and the length to diameter ratio of the roller are selected in the program to give the roller better load carrying balance. Thus for these design programs the inputs are the half cone angle,  $\alpha$ , and the radii of transverse curvature in addition to the fixed inputs of nominal rolling radii, roller load and shaft speed.

It is assumed that the restoring geometry contacts occur at the midpoints of the outer bands of the roller. Thus  $Q$  must be greater than one-half and less than unity and the width of the straight central band is:

$$t = (2Q - 1) \ell \quad (107)$$

In each program, for a given set of input data and roller length, the load separation factor is determined by a finite difference Newton Raphson iteration which makes the maximum Hertzian contact pressure at the central region,  $\sigma_0$ , differ from the maximum Hertzian contact pressure at the contoured contacts,

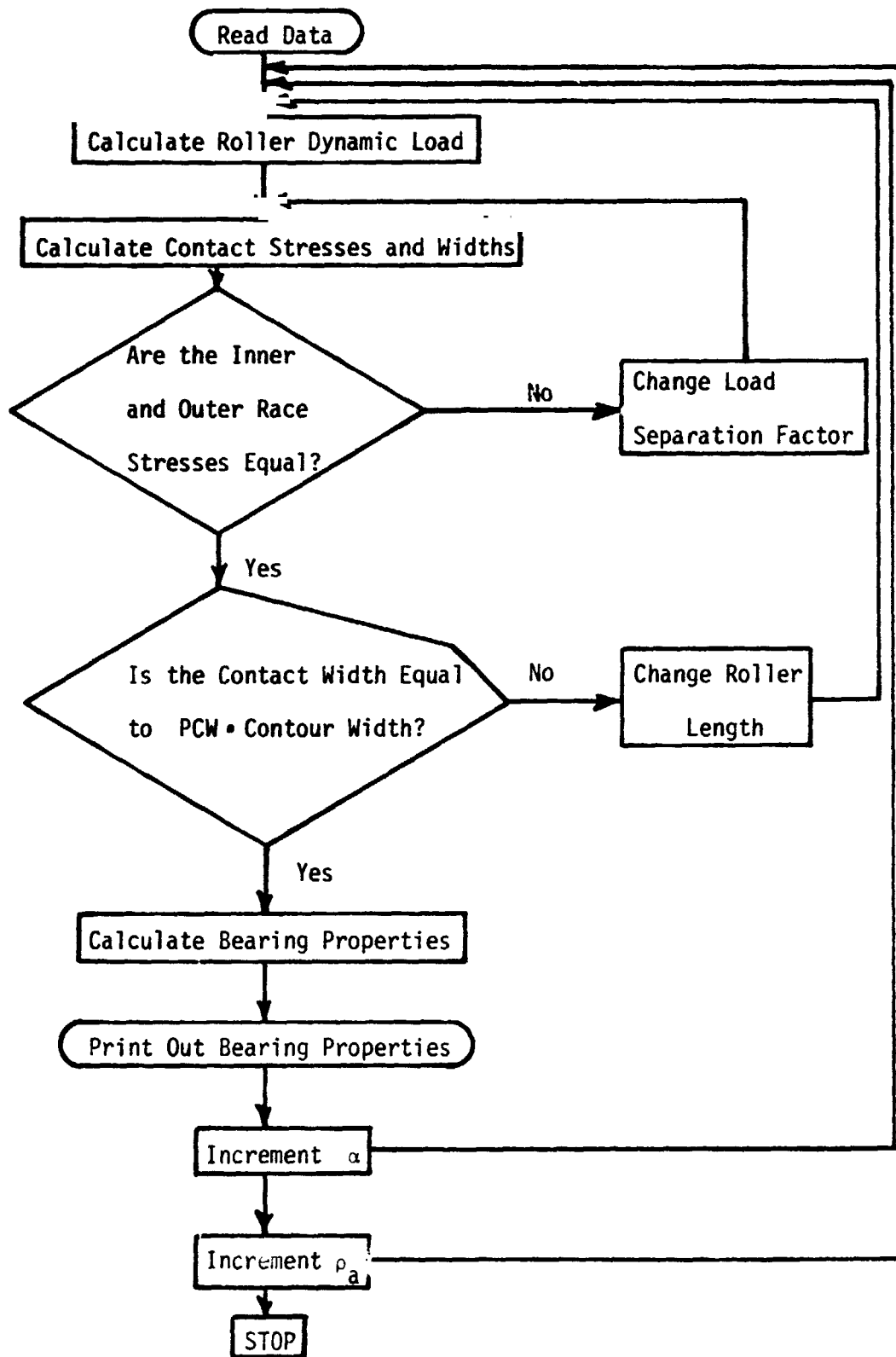


Compound Convex Roller

Figure 31

$\sigma_i$ , by less than 1,000 psi. Although the program puts a limit of 20 iterations on this process, the variable, I, printed out on the same line with Q is the actual number of iterations required for each design. For the examples studied, this value was in the range of 2 to 5 iterations.

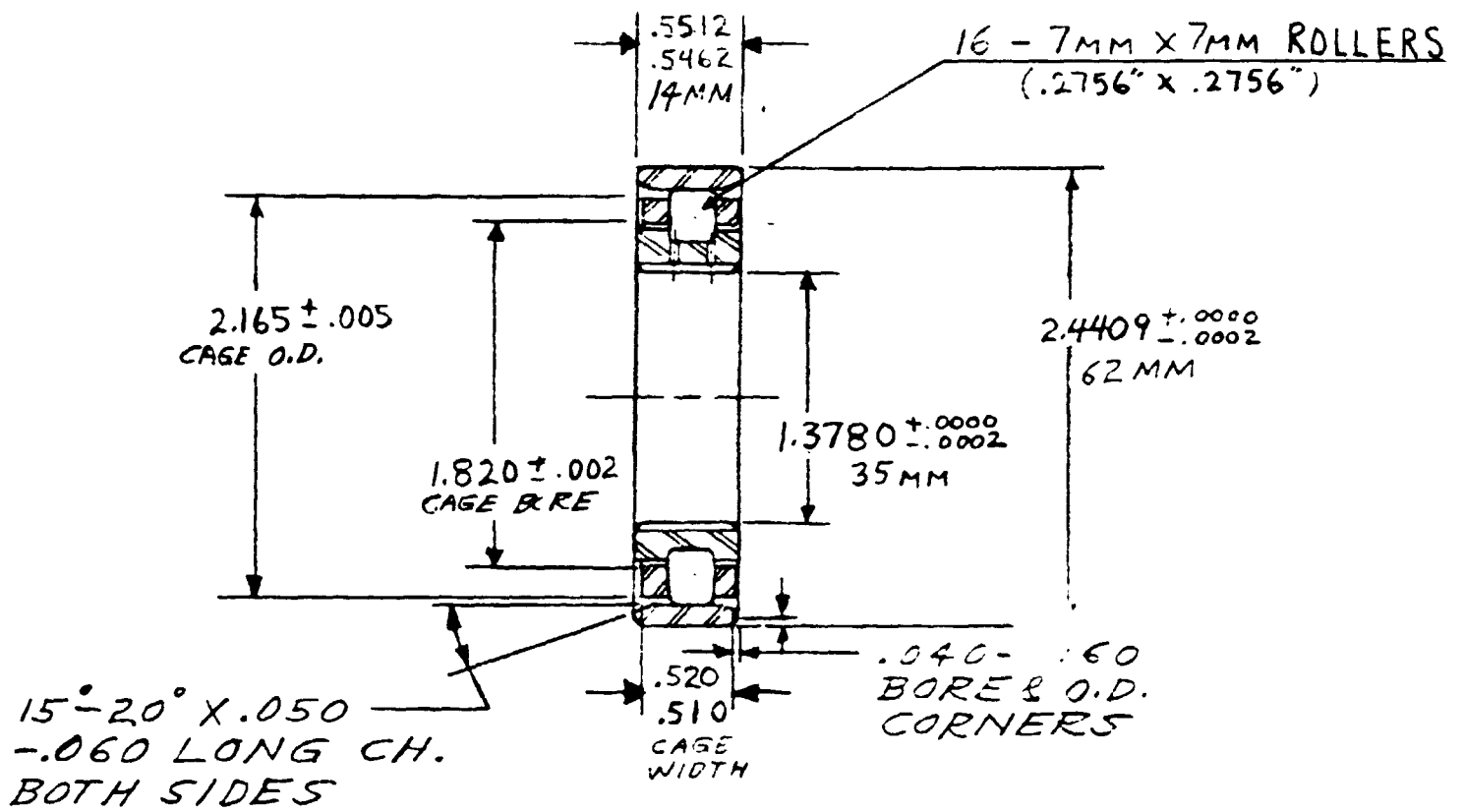
Given the success of this iteration, the program automatically proportions rollers which have nearly equal stresses at their three contact points. A more efficient use of roller material is thus assured. The program includes a new variable, PCW, which is the fraction of the contoured band over which the Hertzian contact pressure acts. Thus for a value of PCW equal to 0.5, one half of the contoured band widths support contact pressure and the roller contact point can shift an amount equal to one quarter of this width in the axial direction while maintaining full Hertzian contact. If PCW equaled unity, then the full length of the roller would support contact pressure and no lateral motion would be possible without changing the manner of load support. The smaller PCW is, the more roller width is present to cause dynamic loading without providing load supporting area. Thus a second iteration is included in the program which changes the roller length by a finite difference Newton Raphson iteration to attain the desired loaded fraction of the two outer bands of the roller. The difference between the actual and the desired loaded lengths in the contoured regions is controlled to be less than one percent of the roller radius. The number of iterations required to do this is printed out as J on the same line that the roller length and the  $\lambda/d$  ratio are printed out. The combination of these two iterations produce rollers which have equal contact stresses and which use as much of their length in actual contact as specified by PCW. Thus excess roller material can be eliminated without sacrificing the roller capacity. Figure 32 is a flow chart for these programs.



Compound Roller Design Flow Chart

Figure 32

REPRODUCIBILITY OF THE ORIGINAL PAGE IS POOR



Reference 35 MM Bearing

Figure 33

These programs look at a series of different radii of transverse curvature of the roller,  $\rho_a$ , as well as a series of different half cone angles,  $\alpha$ , to sweep the design space for each bearing geometry. The examples of this report assume that PCW is 0.5 for all designs. Thus one-half of the contoured regions are loaded.

The programs for the first four geometries make the same assumption about the radii of transverse curvature of the races as the programs for the single curvature rollers do, since the contacting geometries are the same. For the two straight roller geometries the race curvature is varied as the roller curvature is in the other programs. Finally in the last two designs, the convex race curvature is given a radius equal to one half the concave radius of roller transverse curvature. This is done arbitrarily to balance the restoring torque and contact stress properties of the bearing although any radius less than the roller transverse radius would produce a stable bearing.

Working copies of these programs are on file at the NASA Lewis Research Center in the Fluid Systems Component Division.

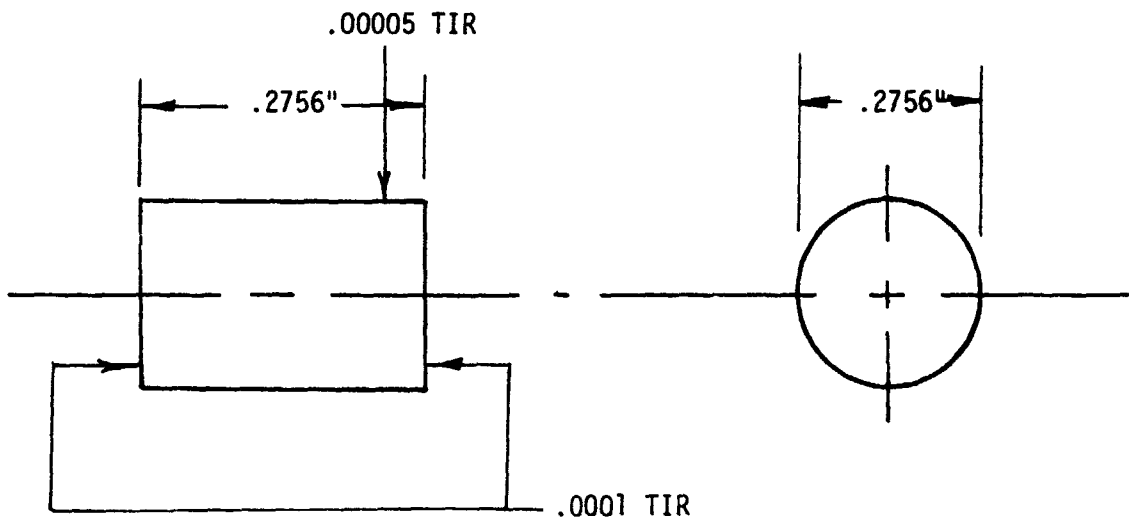
### Design Examples

To compare bearings with corrective geometry, a turbine roller bearing's size and expected operating conditions are used as the design input. The bearing selected is the 35 mm bore bearing shown in Figure 33 operating at 60,000 RPM or  $2.1 \times 10^6$  D'. There are 16 rollers in the bearing which has an approximate dynamic capacity of 1500 pounds at a shaft speed of 500 RPM. Taking one tenth of this capacity as the operating load of the bearing and assuming that about one-third of this load is seen by a single roller, an external roller load of 50 pounds was selected. The standard bearing has

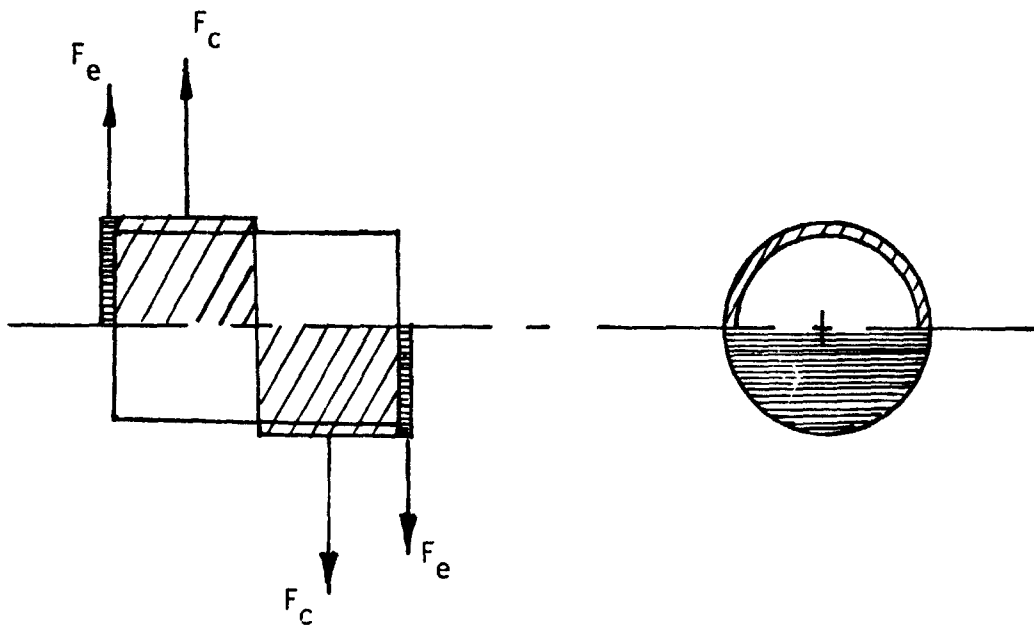
rollers with diameters and lengths of 7 mm or 0.2756 inches. It also has a crown radius of 25 inches. For these parameters, the standard roller would see Hertzian contact stresses of 160,000 psi on the inner race and 220,000 psi on the outer race, which is high. However, our primary interest in this example is to have a reference to match the corrective geometry performance against. These proportions and properties serve that purpose.

The restoring geometry acts kinematically to correct for inaccuracies in race and roller manufacture as well as thermal expansions and slight shaft misalignments. A stable geometry and a slight taper should be sufficient to overcome these difficulties. However, the restoring torque is a measure of the degree of kinematic stabilization of the respective geometries. Furthermore, these are not the only disturbances which cause roller skewing. Dynamic roller imbalance is another. The restoring torque developed by the stable geometries when the roller is displaced from its true rolling position can also balance this disturbance and act to prevent forced skewing.

To model an extreme value of the required restoring torque, standard roller tolerances were applied to the roller to produce the maximum possible roller dynamic imbalance allowed by the manufacturing tolerances. Figure 34 shows a roller with this imbalance. The imbalance is caused basically by an allowable radial variation of 0.0005 inches total indicator reading and an allowable end surface variation from a true radial plane of 0.0001 inches total indicator reading. Figure 34b shows a model of this roller imbalance which can serve as an upper bound. For each of the two imbalances, two equal and opposite imbalances are added to produce a couple. The radial variation could at worst produce two half shells .00005 inches thick which extend for one half the length of the roller. This imbalance would be:



a) Roller Tolerances



b) Imbalance Model

Maximum Roller Imbalance

Figure 34

$$T_c = F_e \frac{\ell}{2} = \frac{W}{g} (\pi r_a) (.00005) \left(\frac{\ell}{2}\right) \left[\frac{2 r_a}{\pi}\right] \omega_a^2 \left(\frac{\ell}{2}\right) \quad (108)$$

or

$$T_c = \frac{.00005}{2} \left(\frac{W}{g}\right) \ell^2 r_a^2 \omega_a^2 \quad (109)$$

The second imbalance caused by two equal and opposite masses is due to the end perpendicularity tolerance. This could at worst produce two half disc end caps each .0001 inches thick. This imbalance would be:

$$T_e = F_e \ell = \frac{W}{g} \left(\frac{\pi r_a^2}{4}\right) (.0001) \left[\frac{4 r_a}{3 \pi}\right] \omega_a^2 \ell \quad (110)$$

or

$$T_e = \frac{.0001}{3} \left(\frac{W}{g}\right) \ell r_a^3 \omega_a^2 \quad (111)$$

an upper bound on the maximum possible imbalance is thus:

$$T = T_c + T_e \quad (112)$$

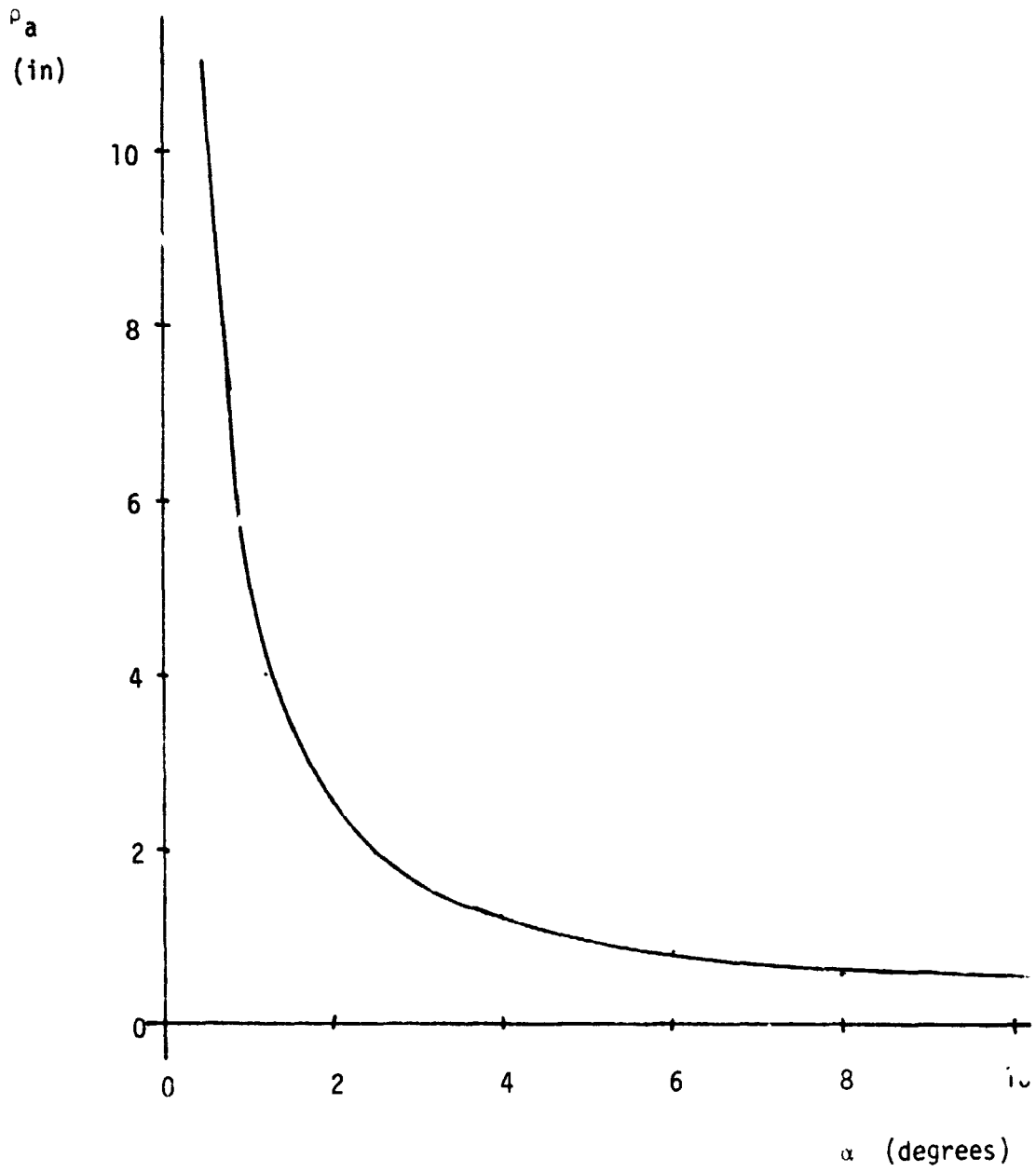
For the 35 mm bearing considered, a shaft speed of 60,000 RPM produces a roller speed of 180,000 RPM. For steel rollers 17 mm by 17 mm which spin at this speed the dynamic imbalance torque is:

$$T = .0063 + .0094 = .0157 \text{ lb-in}$$

Thus a restoring torque per inch of 15.7 pounds or more would offset this imbalance with an axial roller travel of 0.001 inches or less.

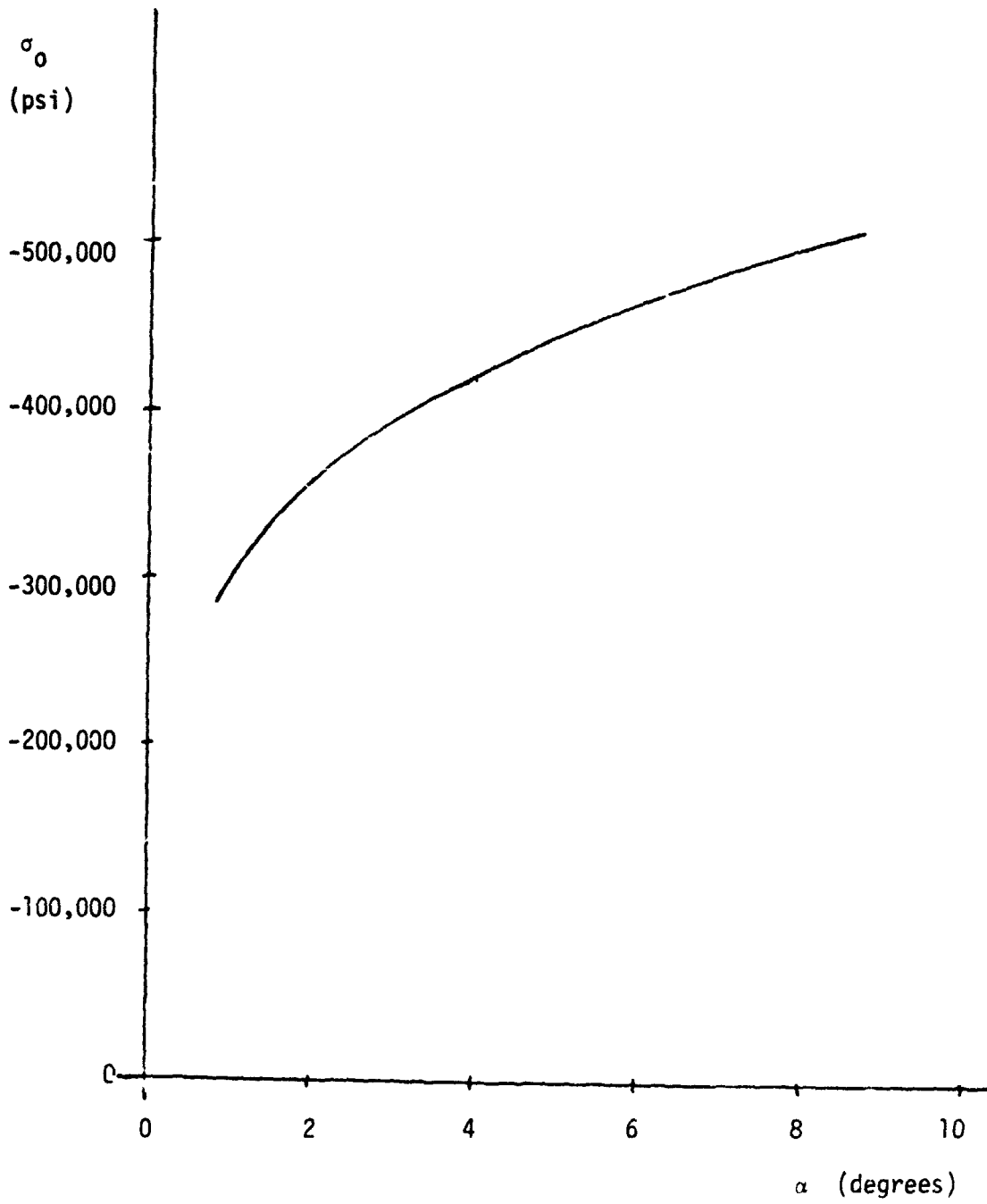
For a load spread factor of 0.625 the simple convex roller bearing design programs were run for values of the half cone angle from one-half of a degree up to eight degrees. Figure 35 is a graph of the roller transverse curvature as a function of half cone angle for these designs. Note that this radius becomes very small for a crown radius even at these low half cone angles.

For the convex-convex-neutral geometry of Figure 10, high contact stresses at the outer race are encountered as shown in Figure 36. In order to keep



Roller Transverse Curvature  
vs. Half Cone Angle

Figure 35



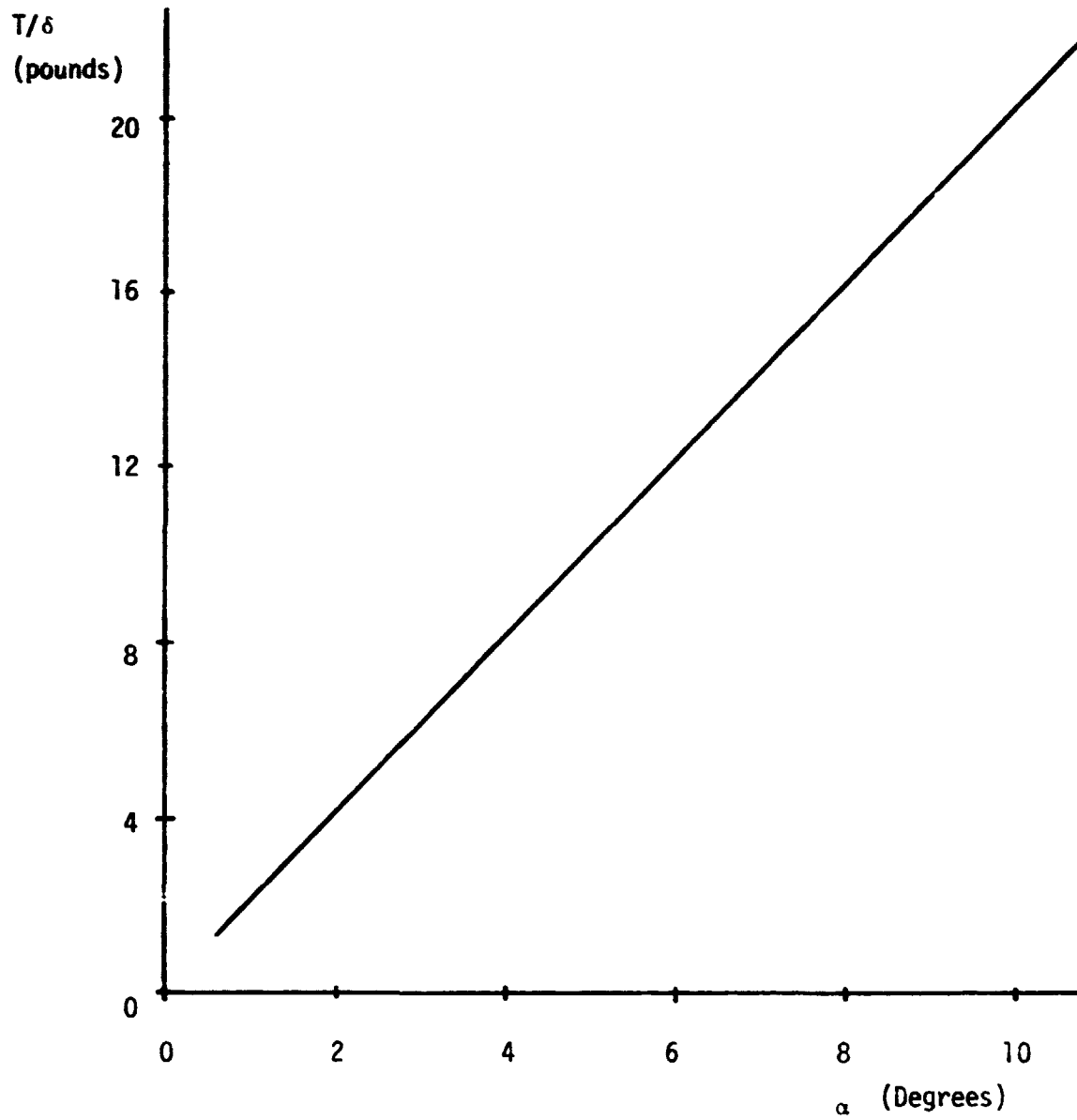
Convex - Convex - Neutral  
Outer Contact Pressure

Figure 36

the contact stress low, a small value of  $\alpha$  must be chosen. This results in a low restoring torque as shown in Figure 37. In fact, this design geometry appears to be the least attractive of the twelve cases considered.

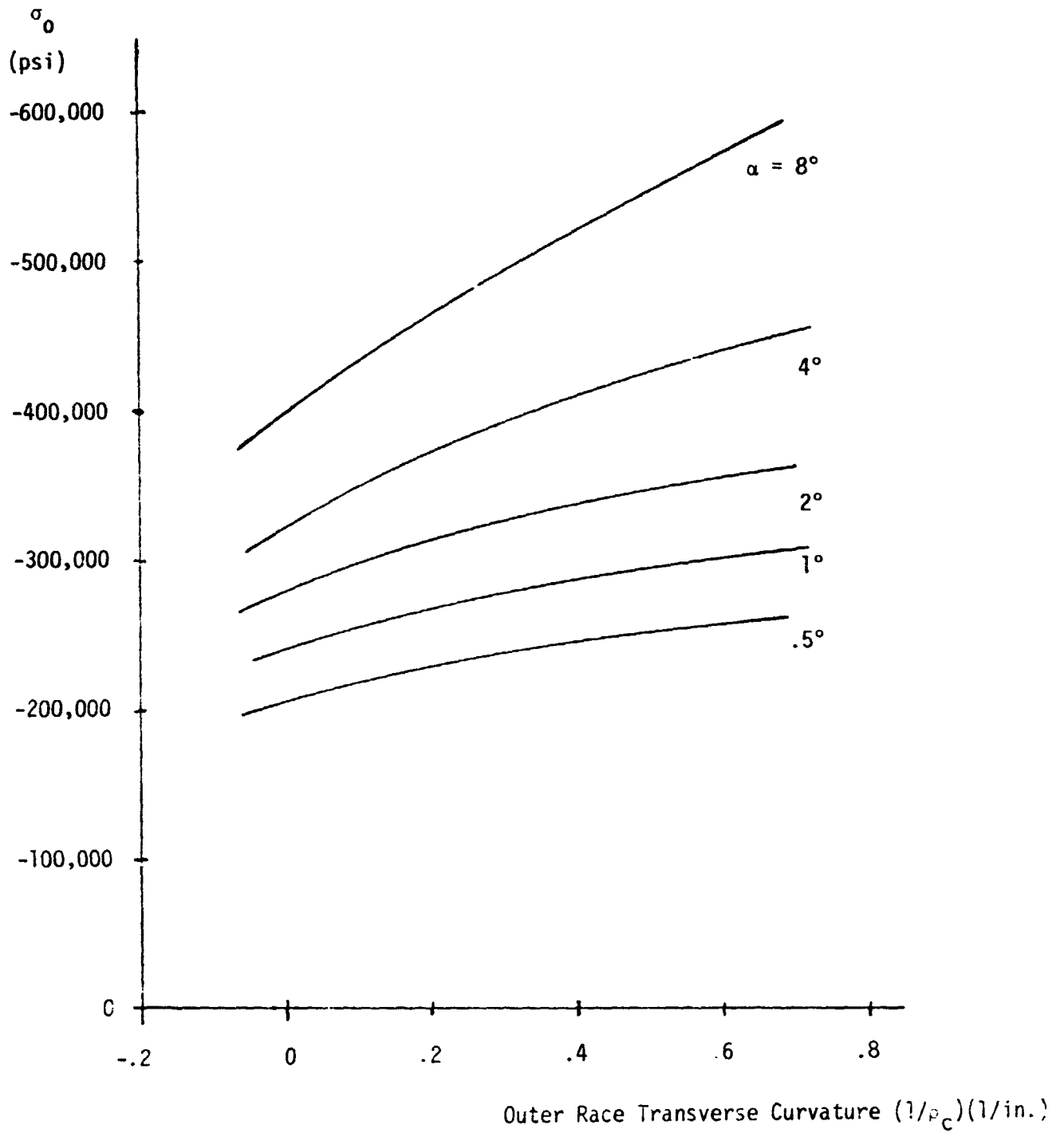
Figures 38 and 39 are graphs of the outer race contact pressure and the restoring torque per inch of axial displacement for the three design geometries of Figures 11, 12 and 13. In these three geometries, the convex roller contacts an outer race which has a transverse curvature which is convex, straight and concave respectively. The two graphs are contour plots of the properties drawn with respect to the outer race curvature,  $1/r_c$ , and the half cone angle,  $\alpha$ . Obviously, the designs are continuous from one design to the other with the intercepting point of zero restoring torque corresponding to the equality of relation 93. Although the restoring torques rise considerably from the first example, an attendant rise in the outer race contact stress tends to offset this gain. One of the best designs of this class of single transverse curvature roller designs would be the bearing with a convex outer race with a radius of transverse curvature equal to that of the roller and a half cone angle of one-half a degree. This design would have a maximum contact pressure of 241,000 psi and a restoring torque of 12.25 pound-inches/inch. The design is shown in Figure 40 four times actual size. This design has a roller with a 9.9 inch crown radius. Unfortunately it does not quite have the desired restoring torque and has a ten percent higher outer race contact stress. In all these bearings the interference is significantly smaller than the Hertzian contact deformations which are less than one thousandth of an inch in all cases. Thus the sign of the clearance is meaningless and no additional loading will occur due to a one-quarter of a degree shaft misalignment for these designs.

Eight different designs are possible with compound rollers. These are the eight geometries shown in Figures 14 through 17. The design programs for



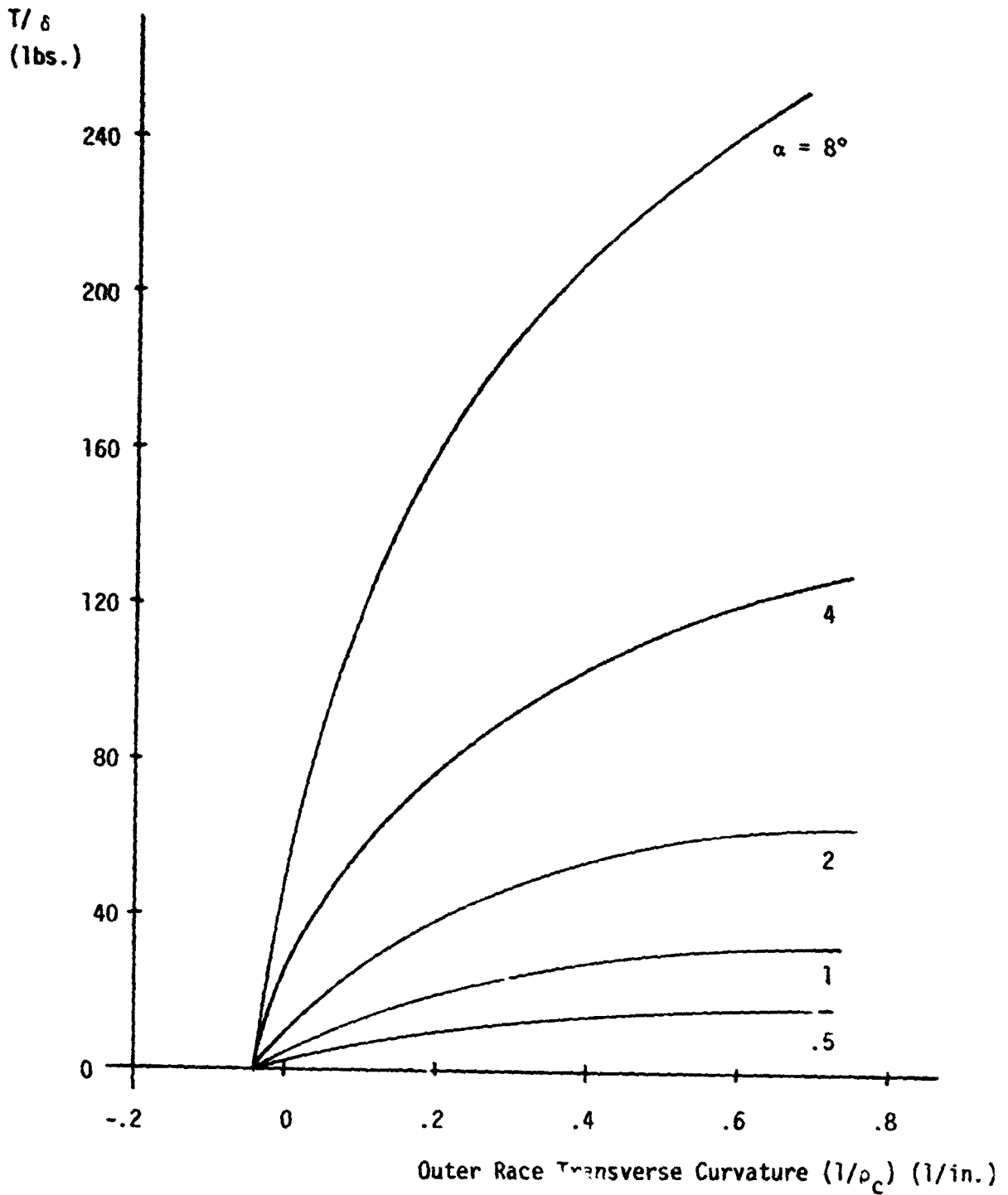
Convex-Convex-Neutral  
Restoring Torque per inch

Figure 37



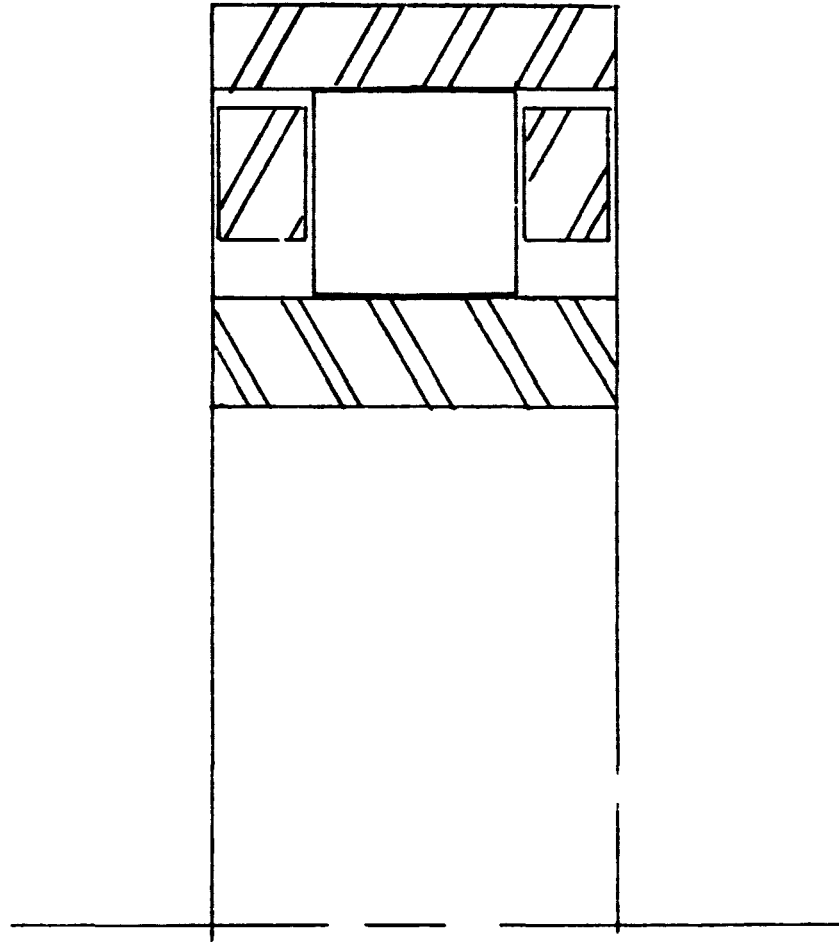
Outer Race Contact Pressure  
for Simple Roller Designs  
with Contoured Outer Races

Figure 38



Restoring Torque per inch  
of Axial Displacement for  
Simple Roller Designs  
with Contoured Outer Races

Figure 39



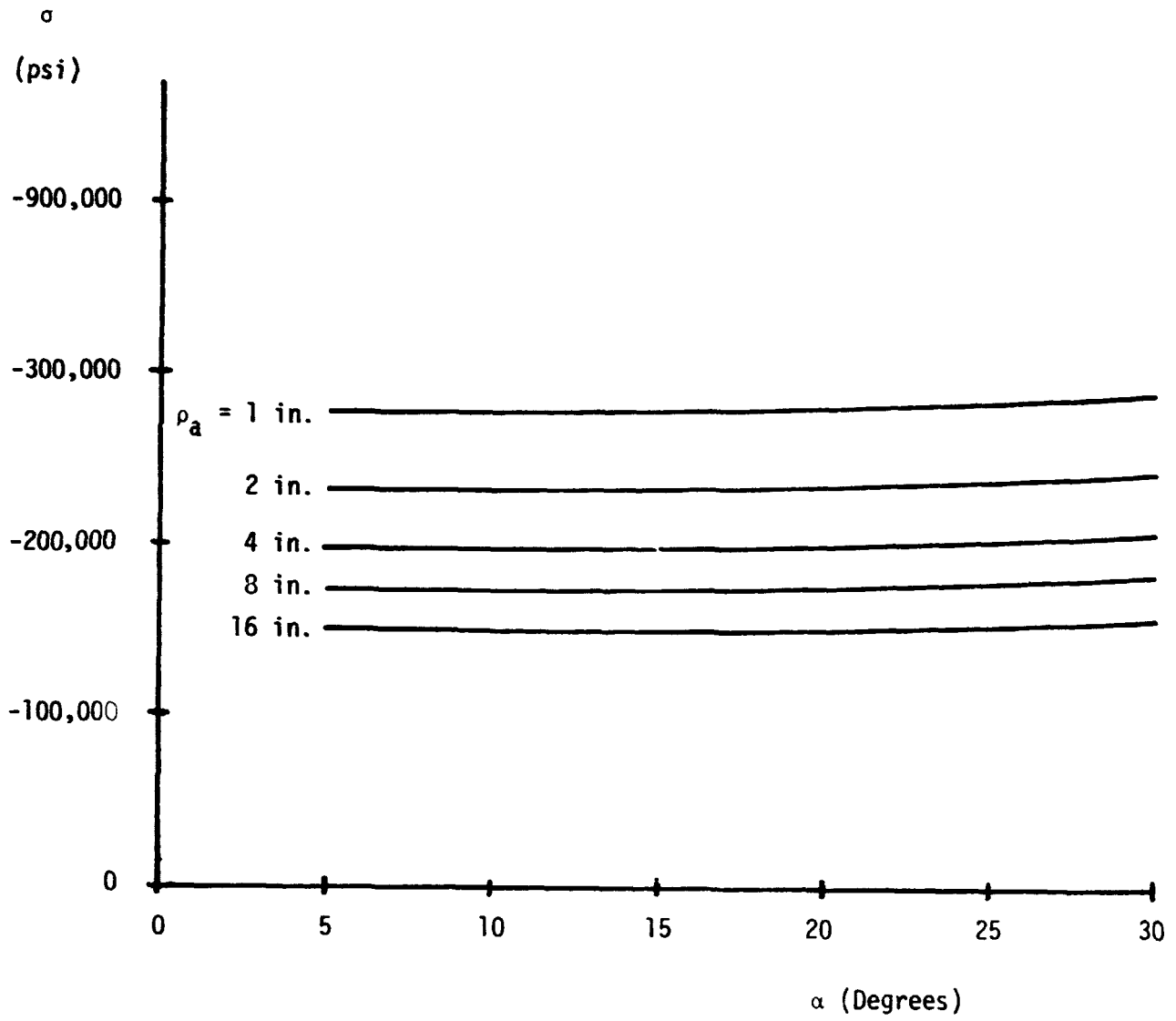
Designed Convex - Neutral - Convex Bearing  
Four Times Actual Size

Figure 40

these compound roller geometries were run for a Hertzian contact width to contour width of 0.5, for roller transverse radii from one inch up to sixteen inches and for half cone angles from five degrees up to thirty degrees. Figures 41 through 56 are contour plots of the contact stresses and the restoring torques per inch of axial displacement for these eight design geometries. The limit lines on Figures 45 to 48, and 51, 52, 55 and 56 identify designs which cannot be built, since half cone angles and radii of transverse curvature greater than at these limit lines cause the roller drop to exceed the roller radius.

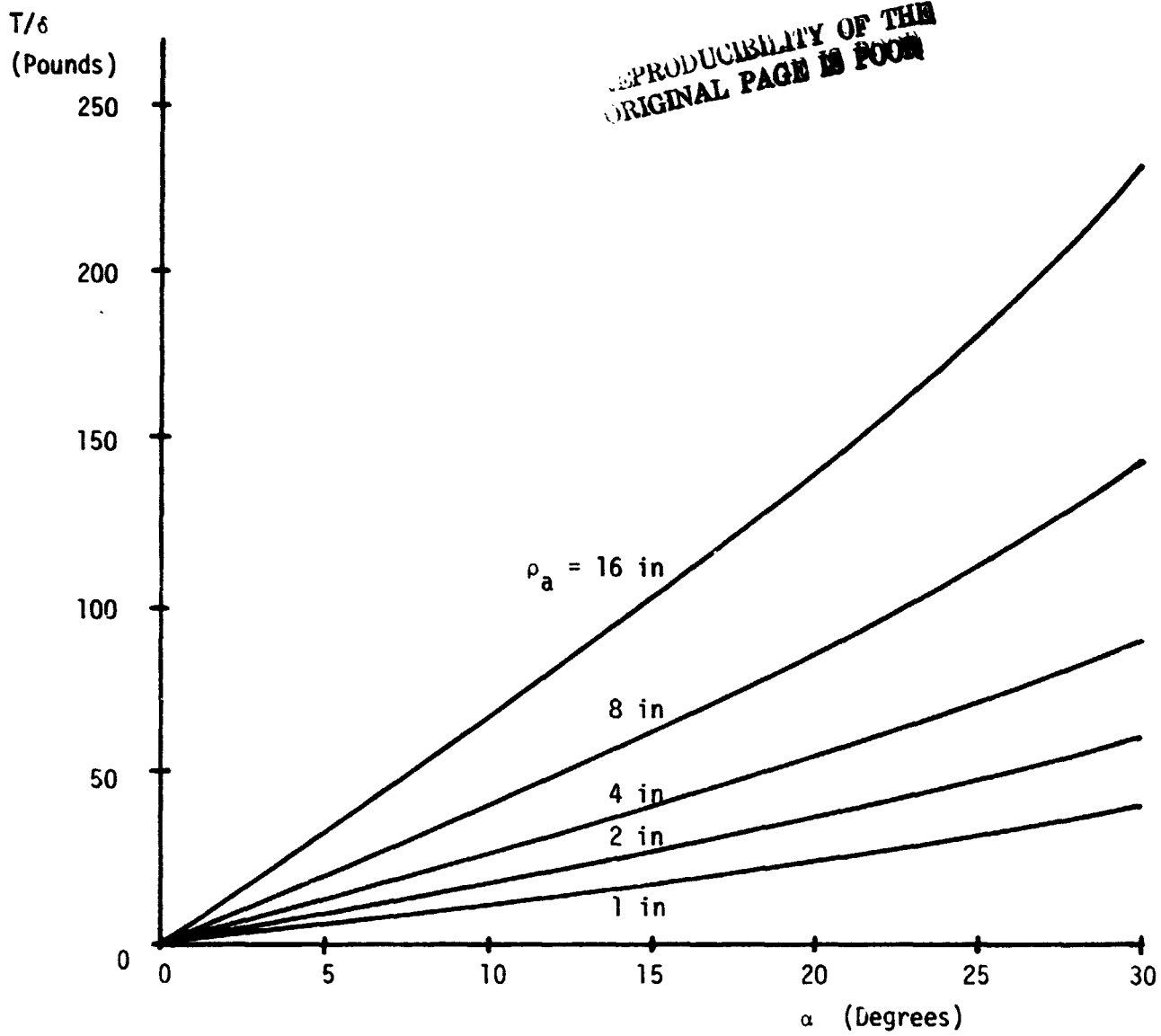
Several basic trends can be noticed in these graphs. The geometries with the contoured race as the inner race and the outer race straight have contact stress values about 100,000 psi less than those for the outer race contoured geometry cases. The restoring torques for the contoured inner race bearings are less than one half those of the corresponding contoured outer race bearings which have the same transverse curvature. Finally both the stress capacity and the restoring torque improve as the transverse curvature of the roller decreases from convex to straight to concave. Thus the best designs are those with concave rollers. This is because the contact points shift more rapidly with axial roller motion as the transverse roller curvature decreases.

Two designs are selected to illustrate the properties of internal and external race correction. Each has a concave roller and a convex transverse radius on its contoured race. Figure 57 is a four times enlargement of the concave-convex-neutral design. In this design the half cone angle is thirty degrees and the roller's radius of transverse curvature is eight inches while that of the inner race is four inches. The load spread factor is 0.708 and the  $\lambda/d$  ratio is 1.73. The resulting contact stress is 180,000 psi while the restoring torque per inch of axial displacement is 2,600 pound-inches per inch.



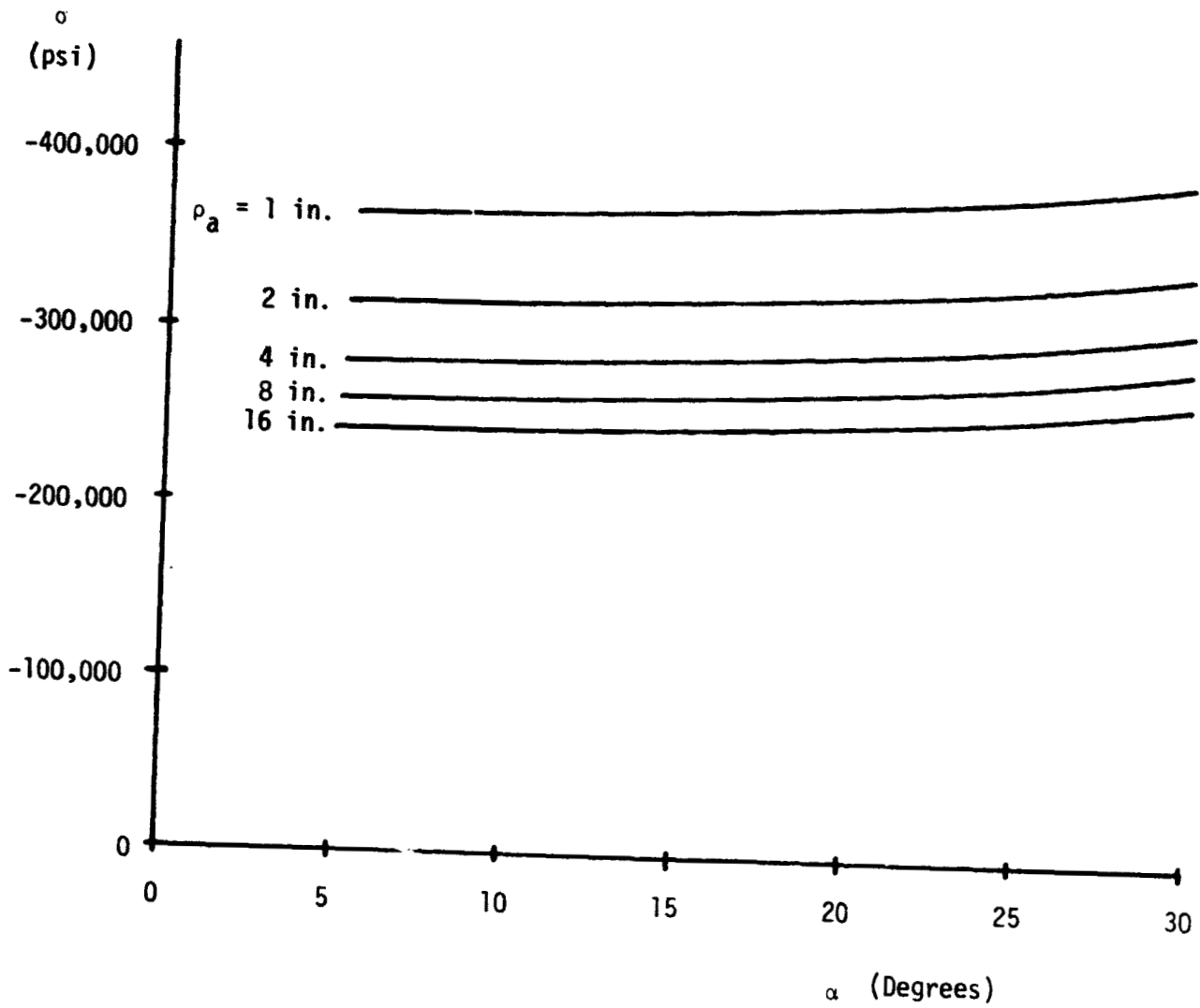
Contact Pressure Contour Graph  
For Convex - Convex - Neutral Bearing

Figure 41



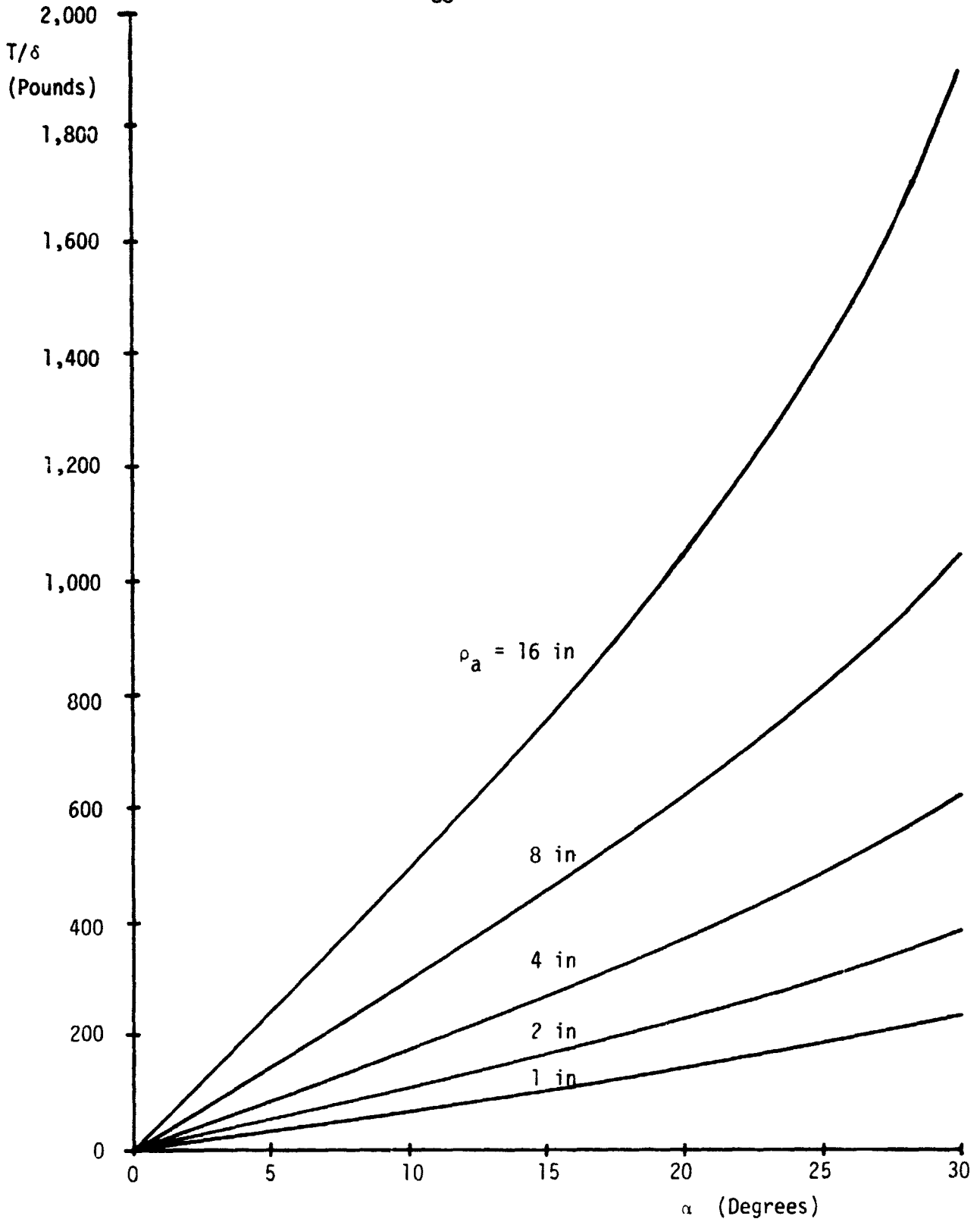
Restoring Torque Per Inch Contour Graph  
For Convex - Convex - Neutral Bearing

Figure 42



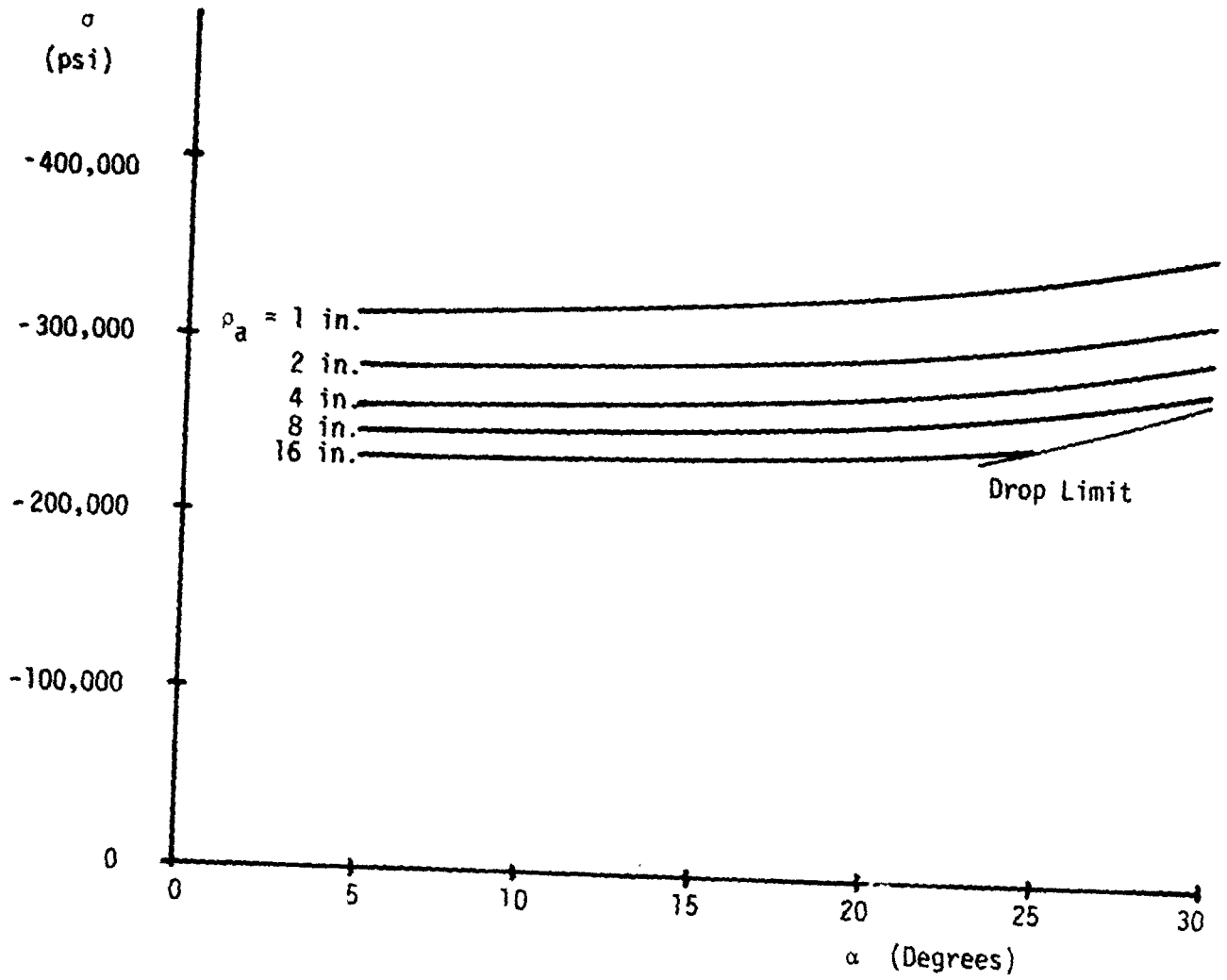
Contact Pressure Contour Graph  
For Convex - Neutral - Convex Bearing

Figure 43



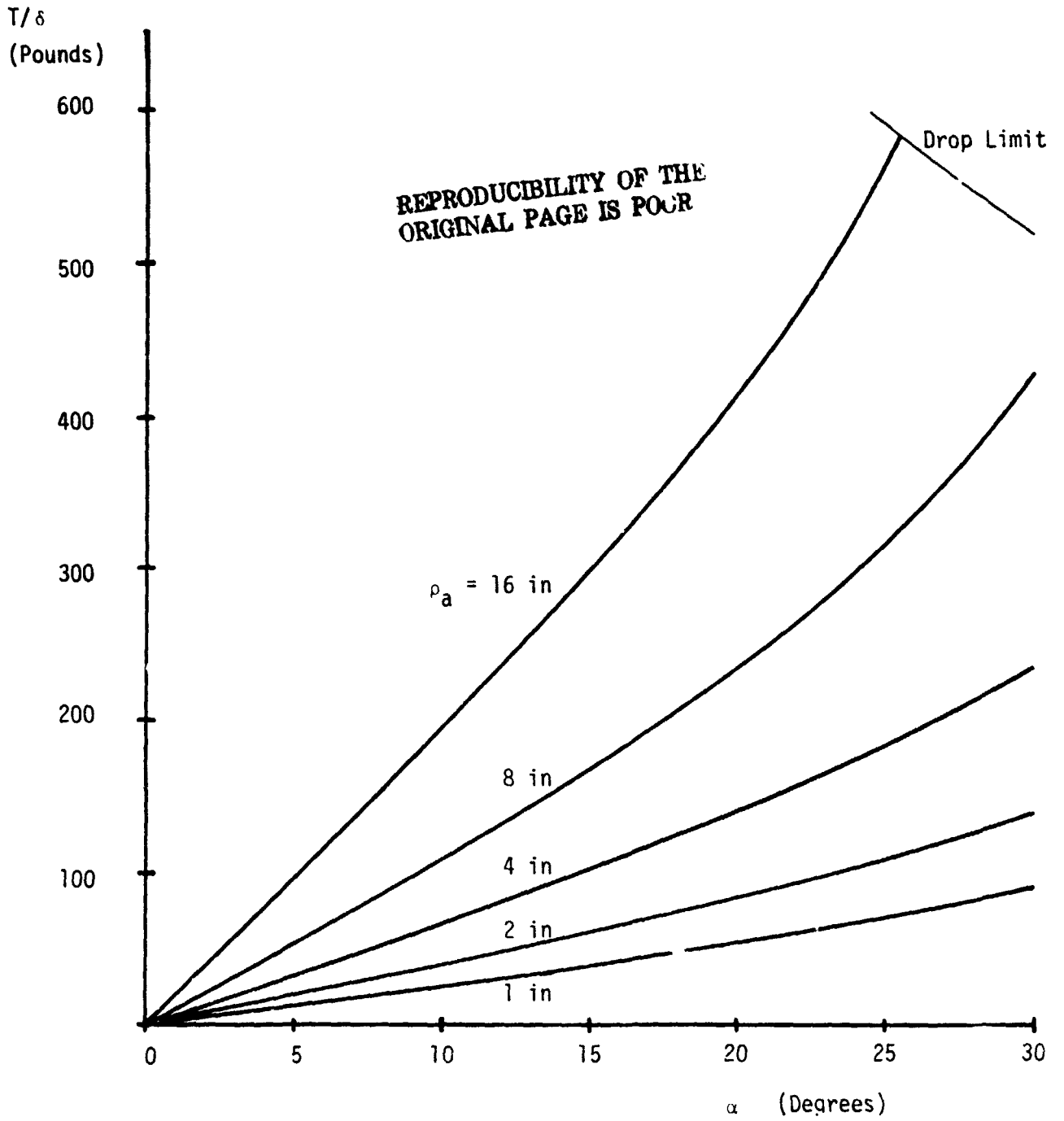
Restoring Torque Per Inch Contour Graph  
For Convex - Neutral - Convex Bearing

Figure 44



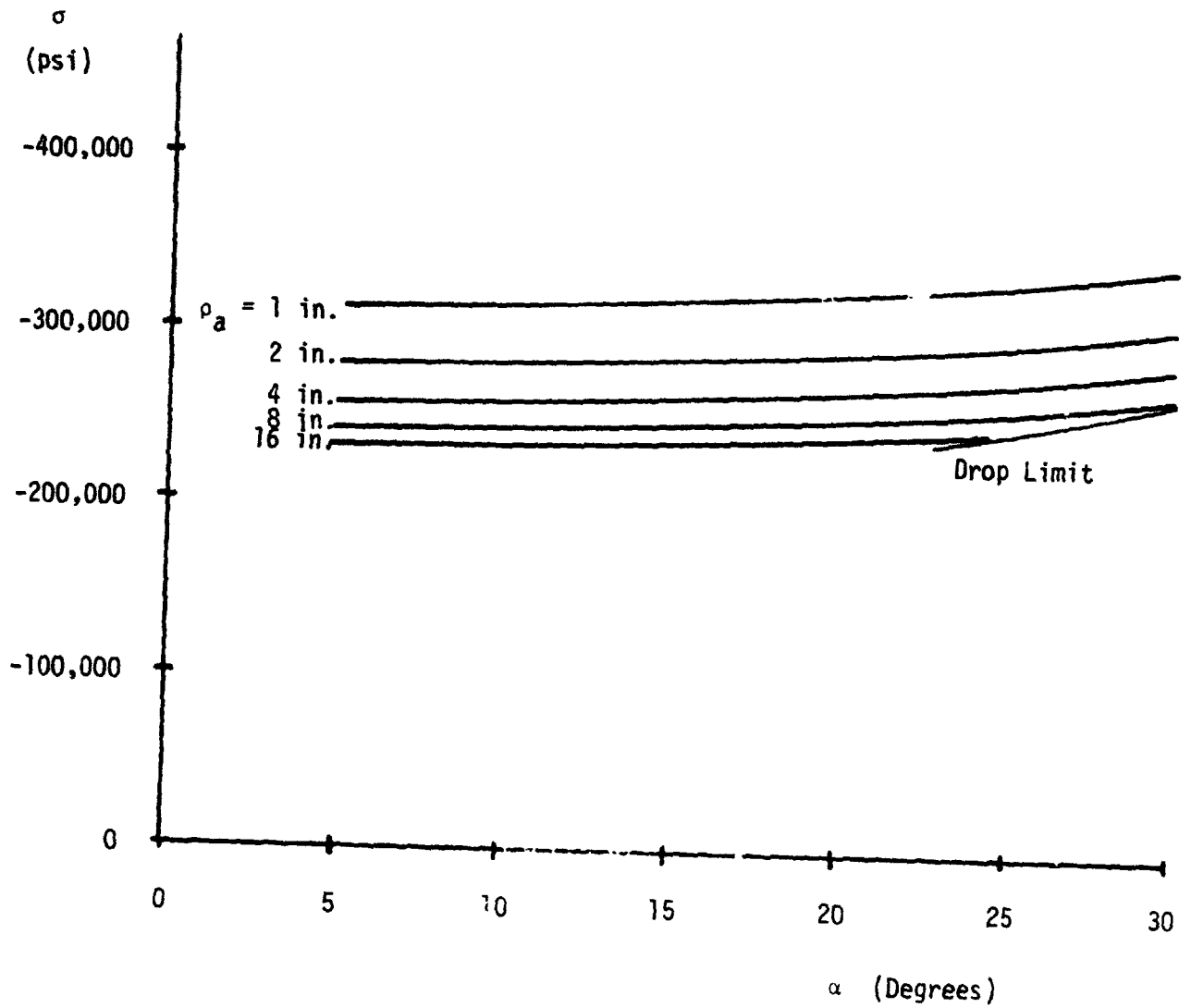
Contact Pressure Contour Graph  
For Convex - Netural - Straight Bearing

Figure 45



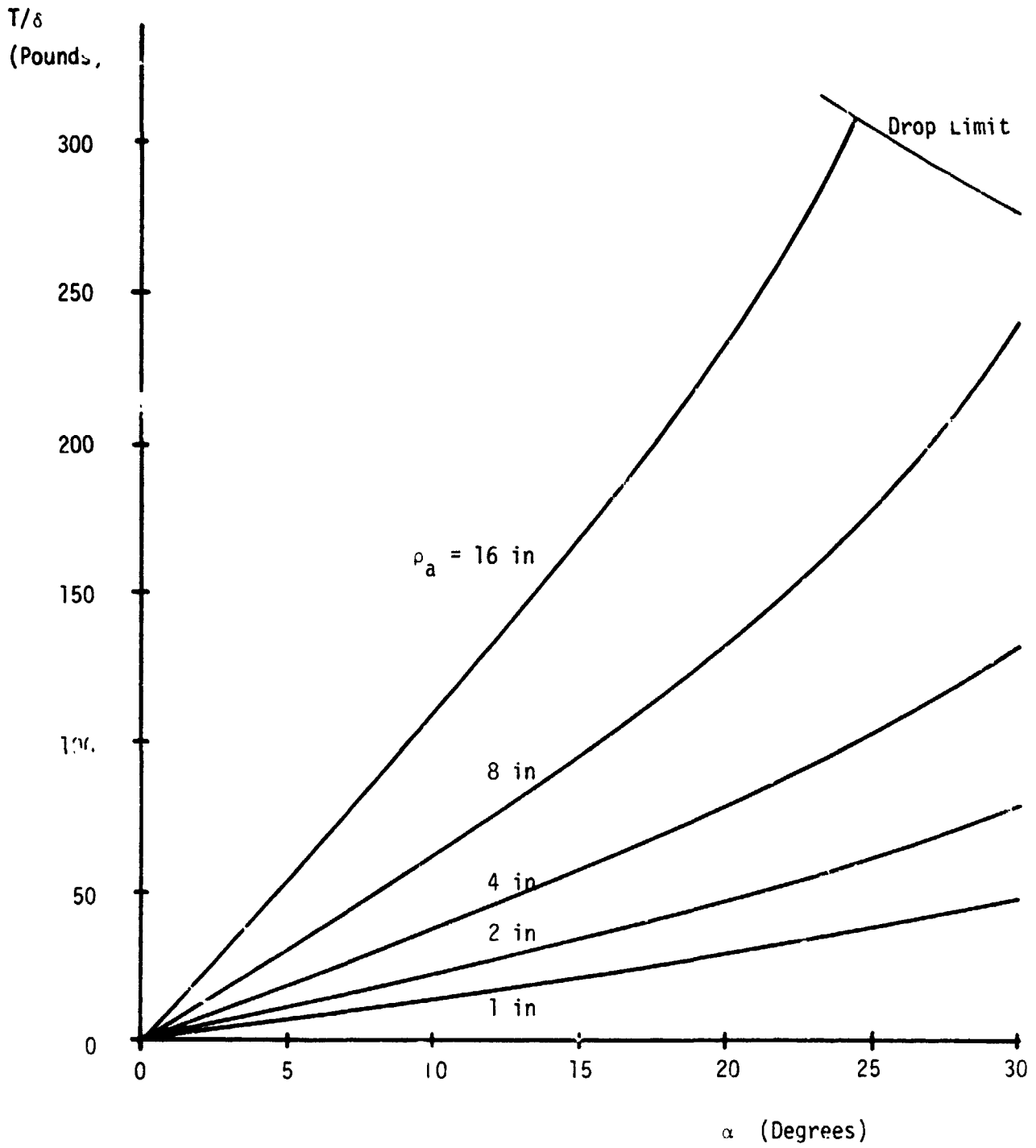
Restoring Torque Per Inch Contour Graph  
For Convex - Neutral - Straight Bearing

Figure 46



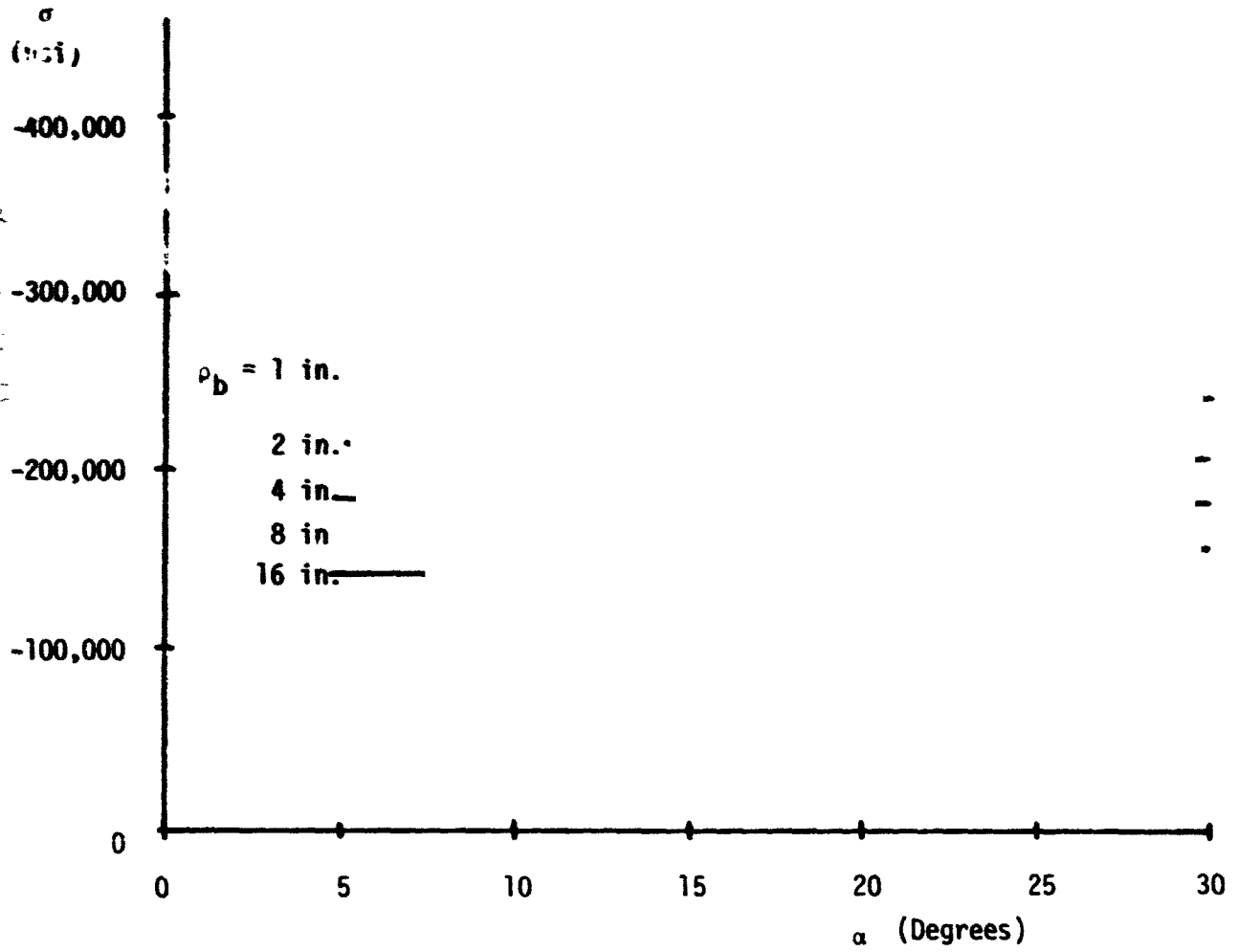
Contact Pressure Contour Graph  
 For Convex - Neutral - Concave Bearing

Figure 47



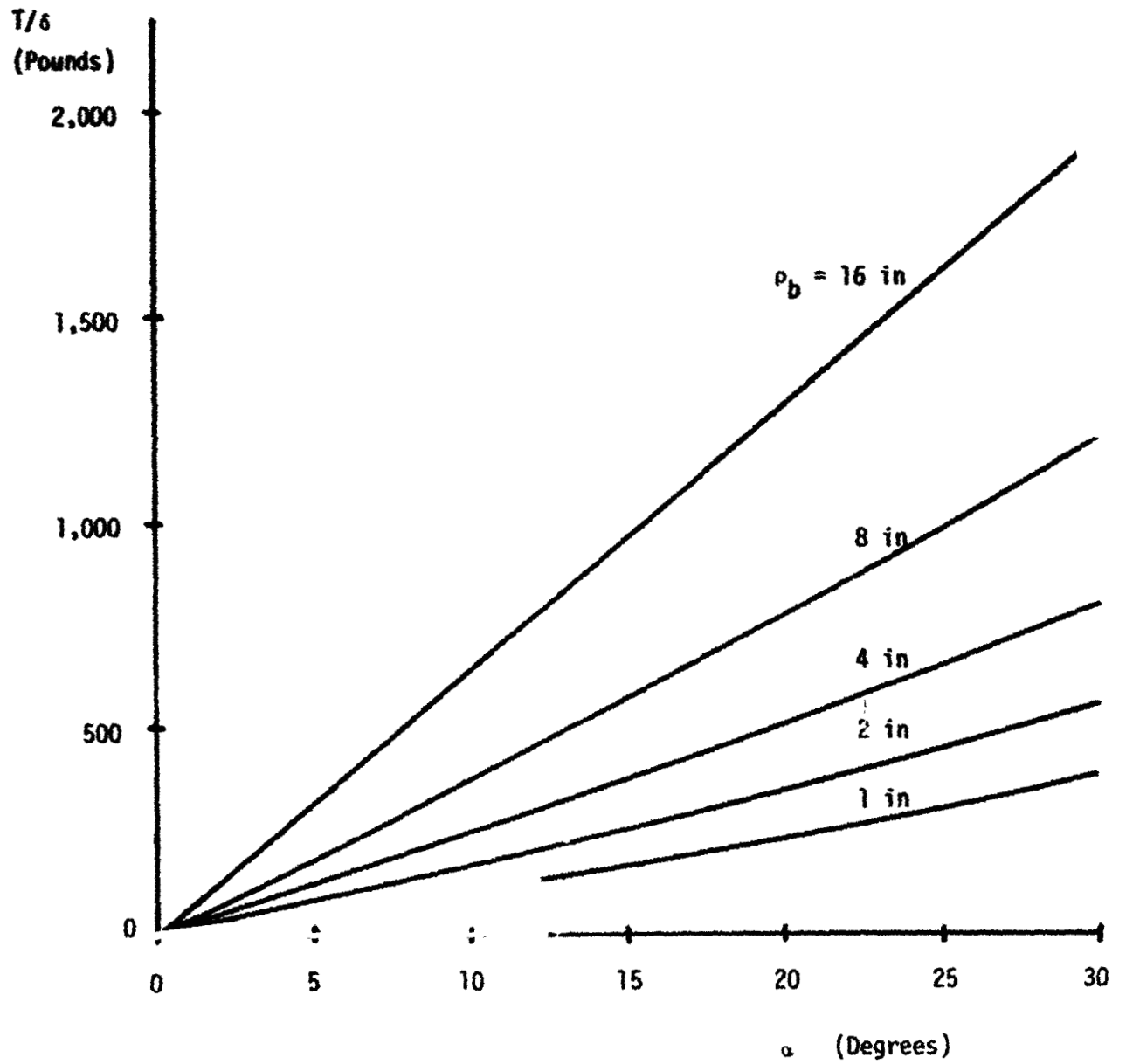
Restoring Torque Per Inch Contour Graph  
For Convex - Neutral - Concave Bearing

Figure 48



Contact Pressure Contour Graph  
 For Straight - Convex - Neutral Bearing

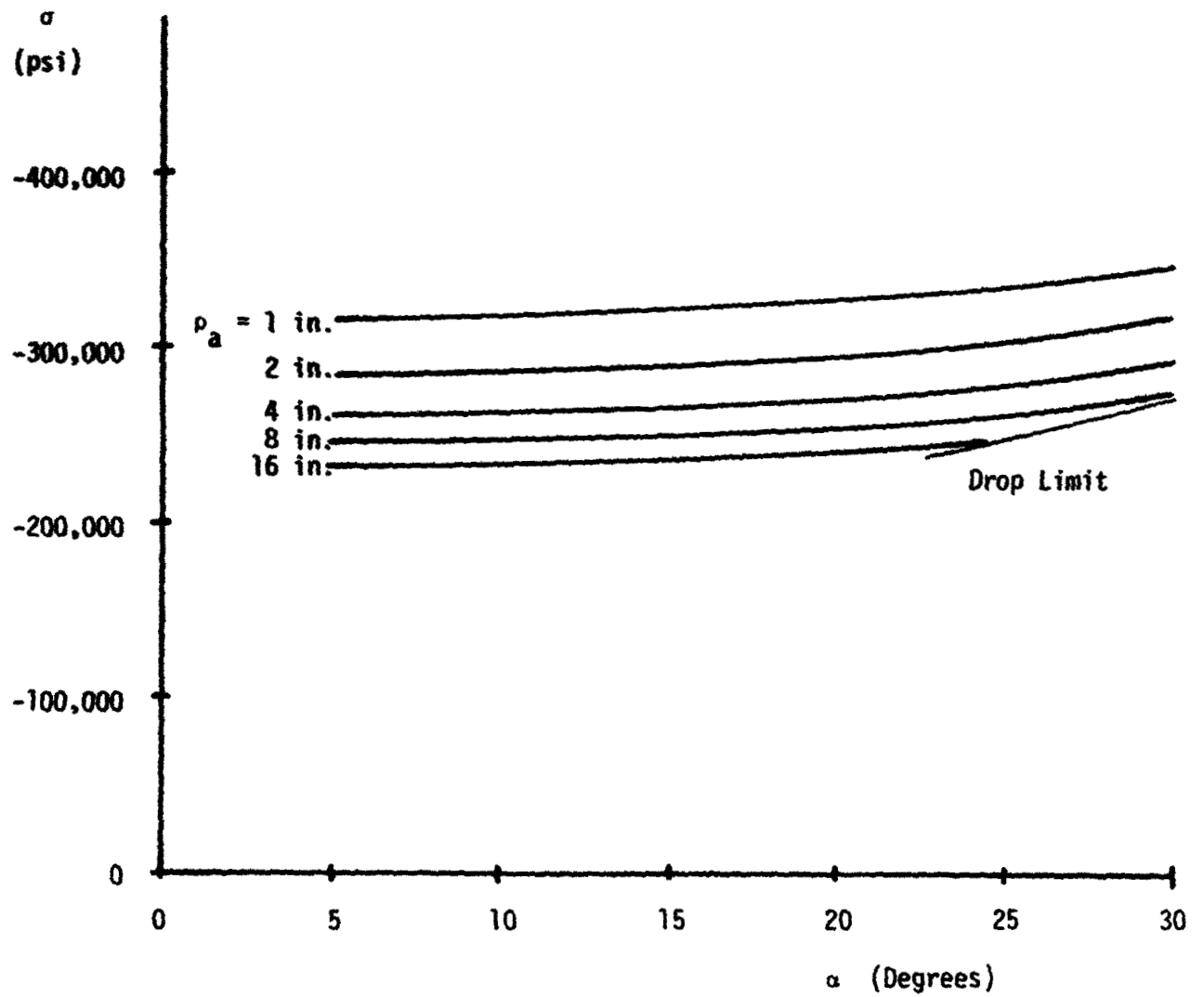
Figure 49



Restoring Torque Per Inch Contour Graph  
For Straight - Convex - Neutral Bearing

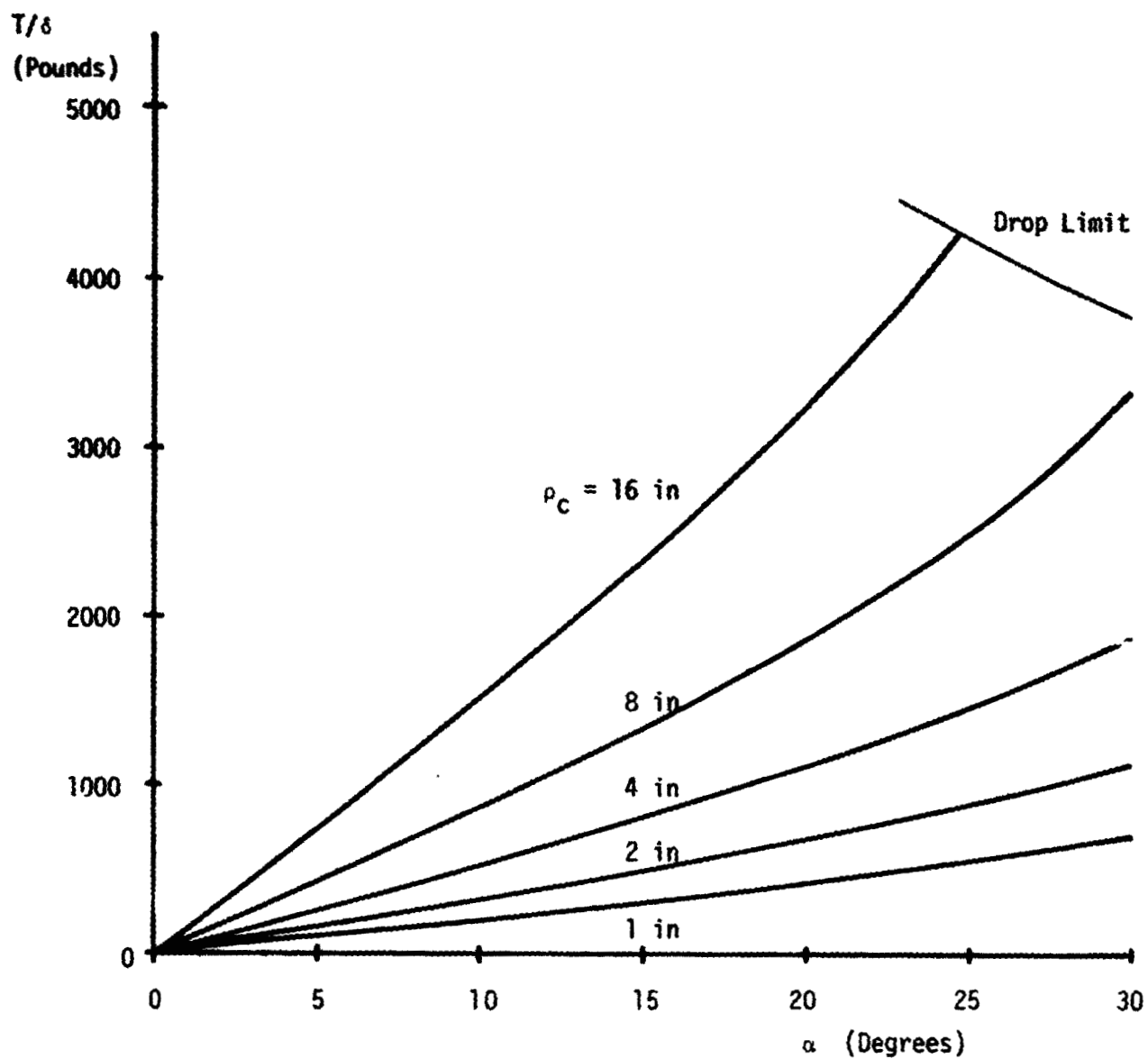
Figure 50

REPRODUCIBILITY OF THE  
ORIGINAL PAGE IS POOR



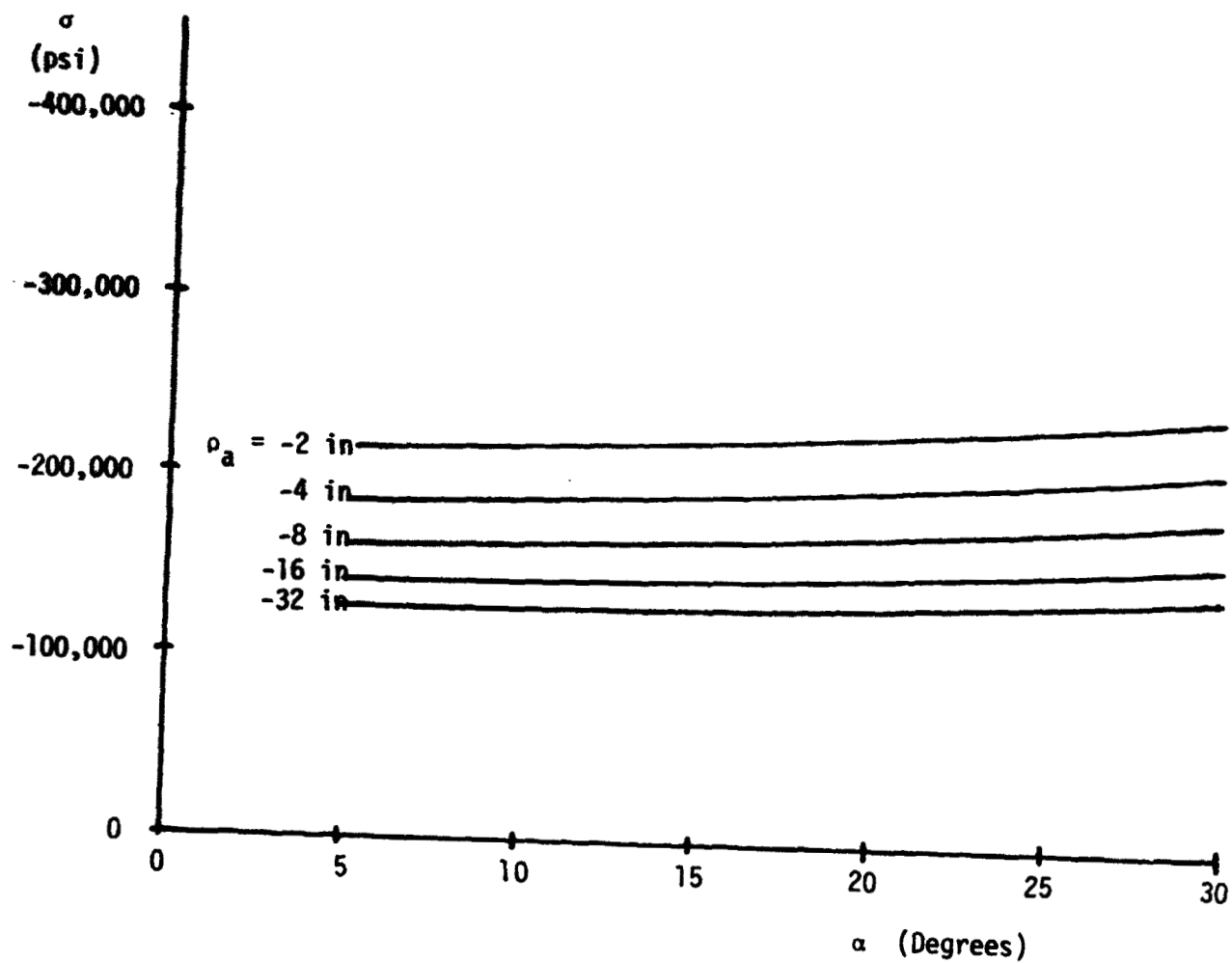
Contact Pressure Contour Graph  
For Straight - Neutral - Convex Bearing

Figure 51



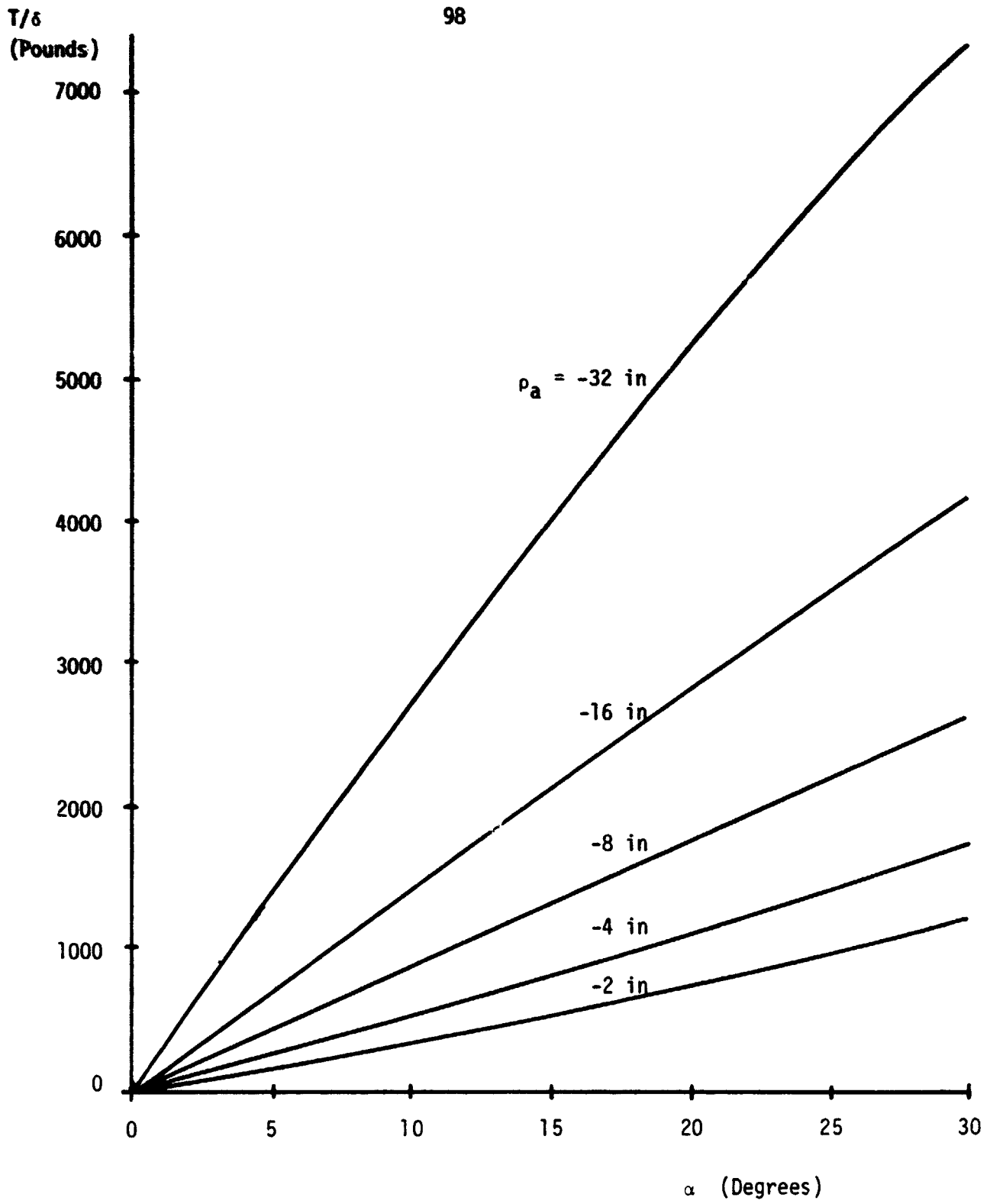
Restoring Torque Per Inch Contour Graph  
For Straight - Neutral - Convex Bearing

Figure 52



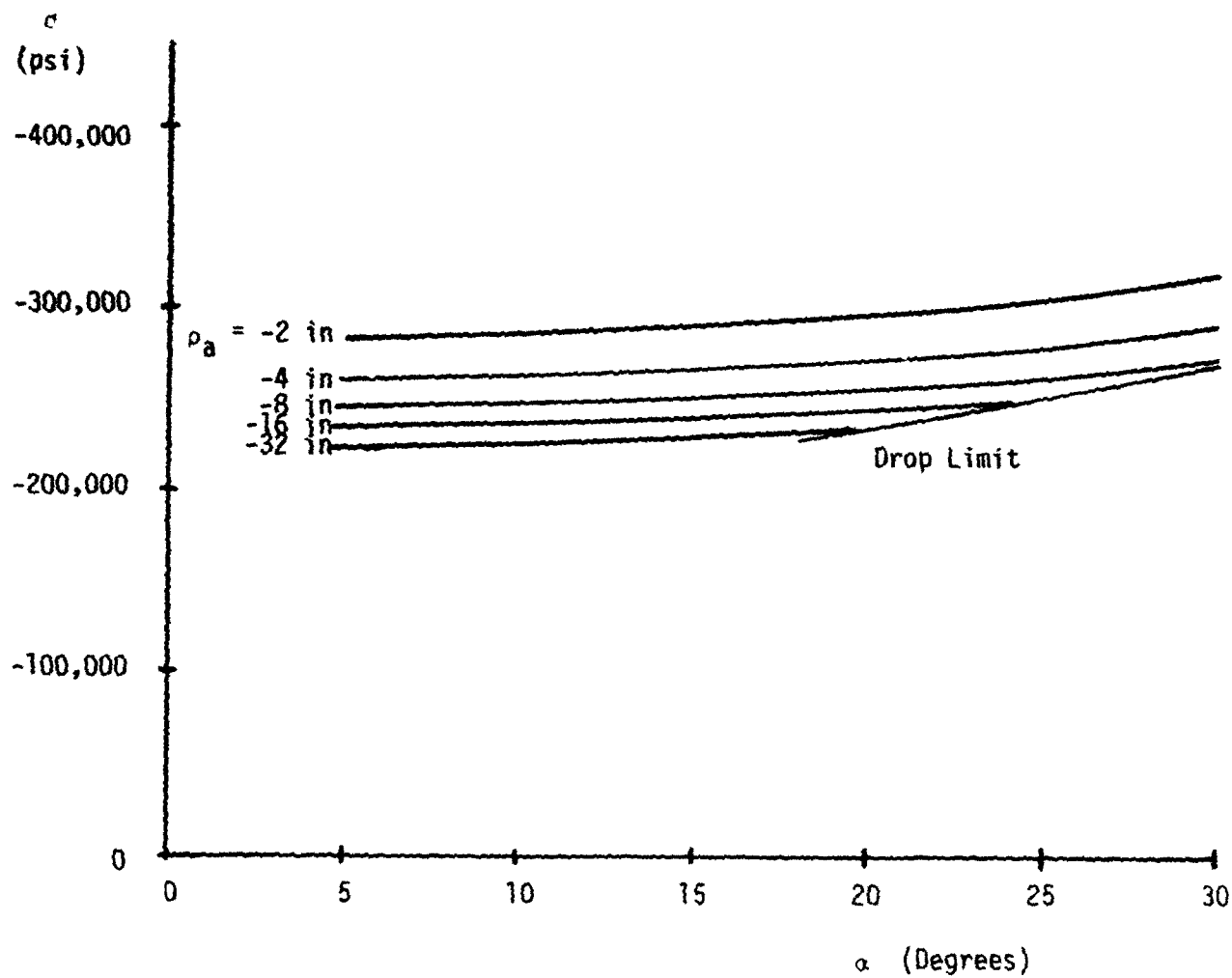
Contact Pressure Contour Graph  
For Concave - Convex - Neutral Bearing

Figure 53



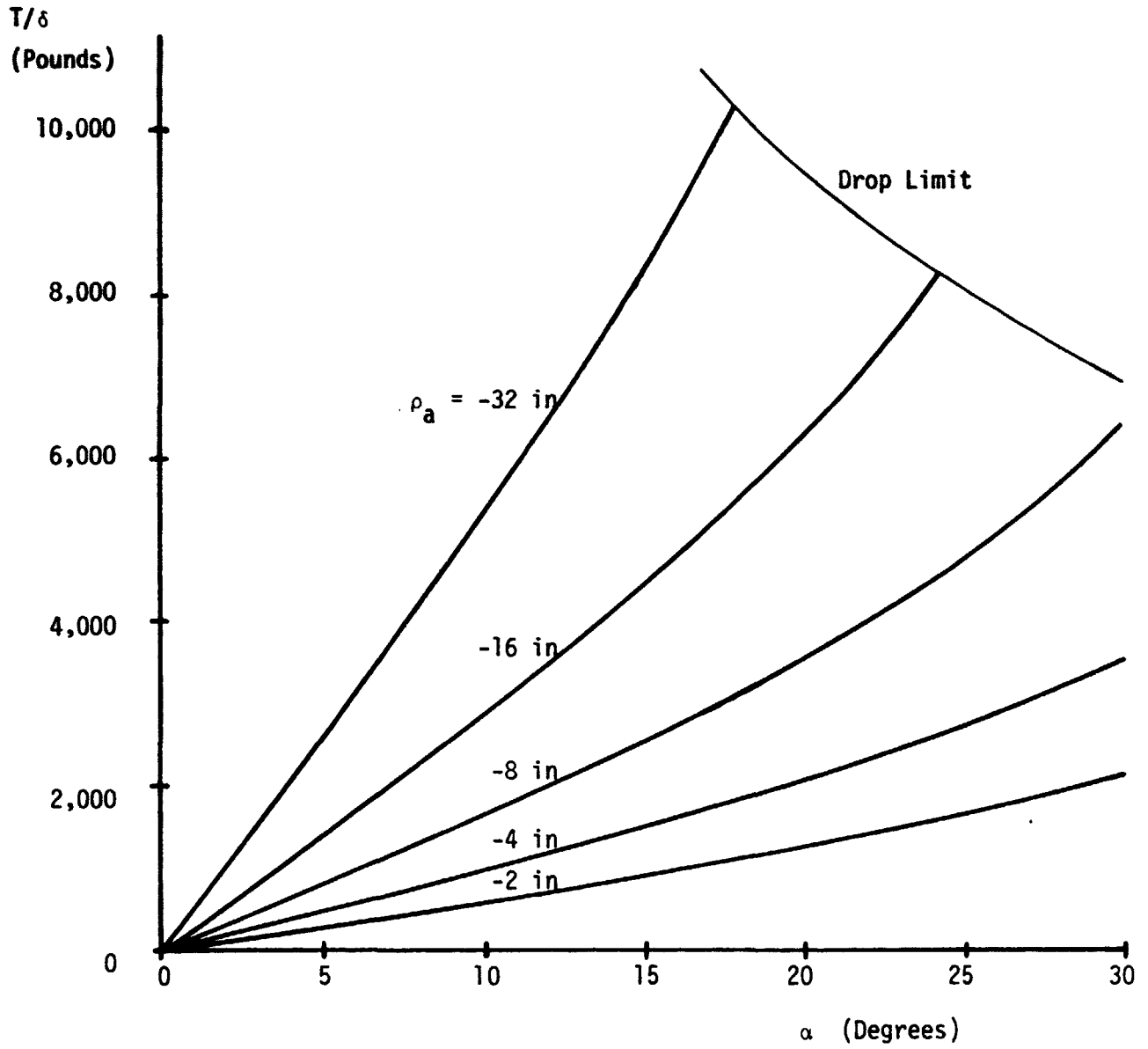
Restoring Torque Per Inch Contour Graph  
For Concave - Convex - Neutral Bearing

Figure 54



Contact Pressure Contour Graph  
 For Concave - Neutral - Convex Bearing

Figure 55



Restoring Torque Per Inch Contour Graph  
For Concave - Neutral - Convex Bearing

Figure 56

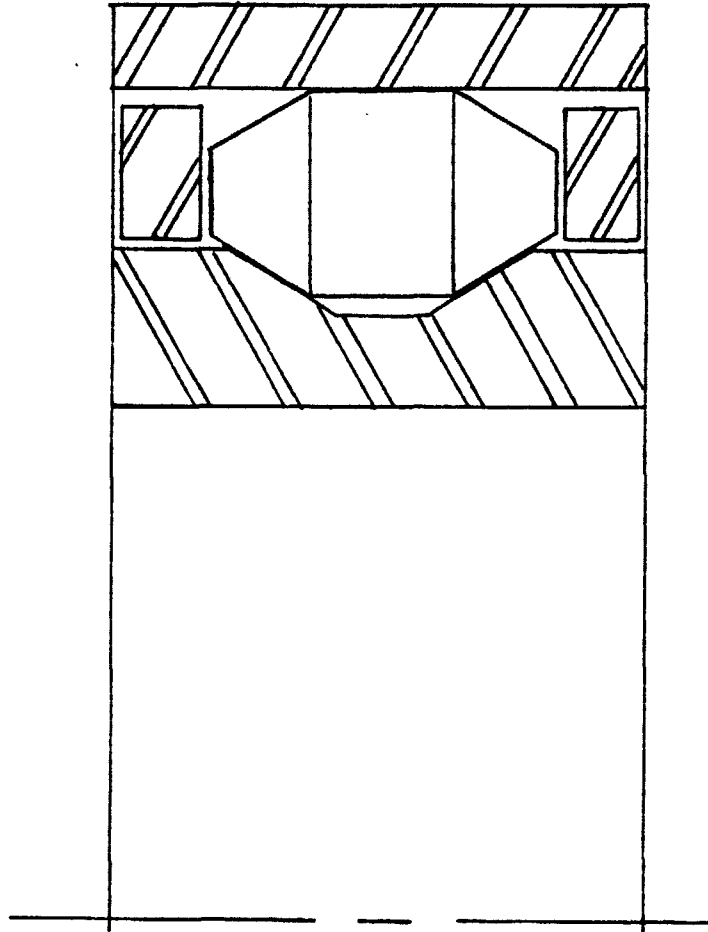
This appears to be one of the best designs of those investigated. The contact stress is reduced twenty percent from that of the target bearing while the restoring torque is over 100 times the anticipated required value.

The second design is shown in Figure 58. This is the concave-neutral-convex design with corrective geometry on the outer race. This design has a load spread factor of 0.53 and a length to diameter ratio of 2.25. It has a half cone angle of twenty degrees and a sixteen inch radius of transverse curvature of the roller. The outer race's contour geometry has an eight inch transverse radius. For this bearing, the contact stress is 243,000 psi while the restoring torque is 6140 pound inches per inch.

### Discussions of Results and Conclusions

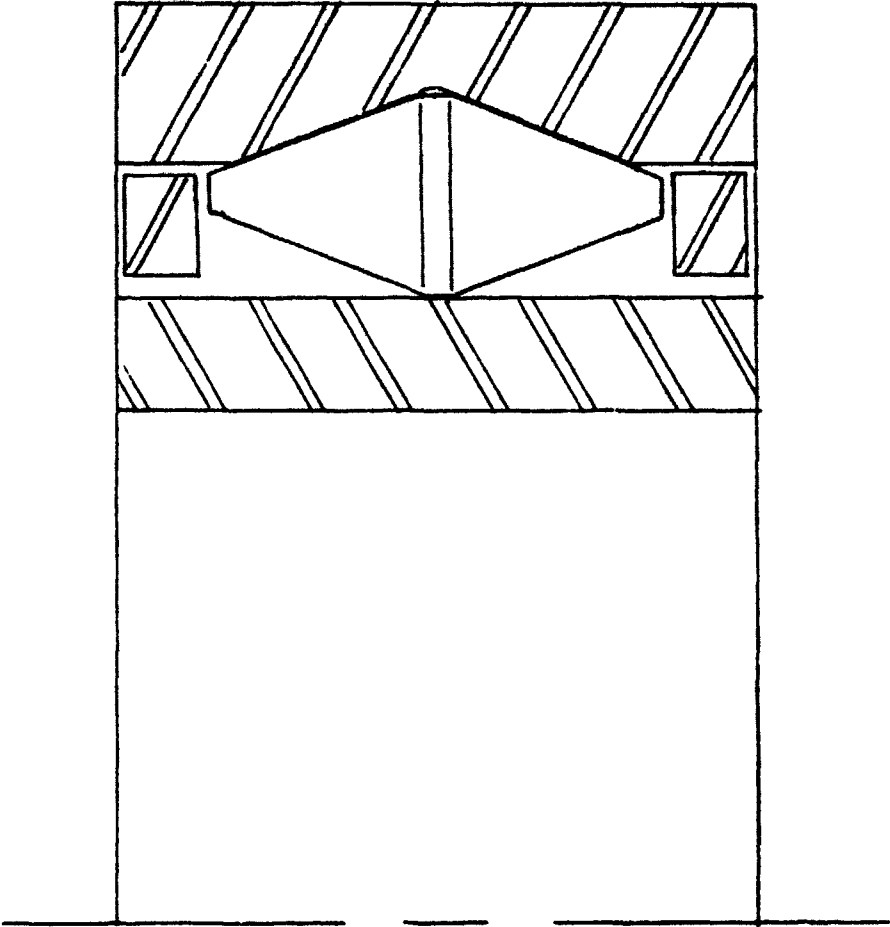
In this work a theory of kinematic stabilization of rolling cylinders is extended and applied to the design of cylindrical roller bearings. The theory was originally developed to predict and prevent axial motion of free rolling external cylinders. The direct cause of this axial motion is a skewing of the rolling elements. The kinematic stabilization mechanism puts a reverse skew into the rolling elements to walk them back in the axial sense. This reverse skew is directly applicable to skew correction in high speed roller bearings.

The theory is extended from external-external roller contact to include internal-external roller contact as well. This complete table of restoring geometries is combined with the restraint that one race must be free to move axially and the desire to minimize the resistance in the bearing to slight shaft slopes. The result is a series of four bearings with single transverse curvature of the roller and eight bearings with three bands of curvature symmetric about the roller center plane. These bearing geometries are tabulated



Compound Roller Design  
Concave - Convex - Neutral Geometry  
Four Times Actual Size

Figure 57



Compound Roller Design  
Concave - Neutral - Convex  
Four Times Actual Size

Figure 58

in table 4 and illustrated in Figures 10 through 17.

Models are generated for the restoring torque per unit axial displacement, the roller contact pressures and contact areas and the bearing sensitivity to shaft misalignment. Roller shape variables are also modeled.

Two design programs are appended to this report - one for the single transverse curvature roller bearings and one for the compound transverse curvature roller bearings. Each geometry has its own program but the basic operation is that of two programs.

The first set of design programs determines the roller crown radius from the slope angle to make the roller slope zero at its center. They sweep a range of potential designs for various slope angles and load separation factors. The second set of design programs proportions the load separation factor to make the contact stresses equal and proportions the roller length to use a given fraction of the contour width for the contact stress. These programs then sweep a range of potential slope angles and radii of transverse roller curvature to obtain a sequence of designs.

These programs are used to investigate a series of designs and three are selected for presentation in the report. Of the three, the design for the compound transverse curvature roller with a concave contoured roller and a convex inner race appears to be the best. This design is illustrated in Figure 57. As analyzed in this report this bearing should provide more than ample skew stabilization while actually reducing the contact stresses incurred in operation at  $2.1 \times 10^6$  DN. This design shows sufficient promise to warrant physical construction and high speed testing.

In future considerations of these bearings, it should be noted that the bearing complexity and modeling of this report represent a first look at the

application of the kinematic restoring mechanism to roller bearing design. Refinements are possible in both the bearing geometry and the modeling. Compound curvature should be extended to include multiple radii of transverse curvature for the roller and correcting race. The model for the contact stress of the center band of the compound roller should be improved to estimate the edge loading and required crowning of this portion of the roller. Finally, the contact point travel must not be ignored in increasing PCW to make the loaded fraction of the roller higher and in combining several radii of transverse curvature in the same contour. Even without these improvements, the design programs should provide interesting alternatives to present high speed roller bearings.

## BIBLIOGRAPHY

1. Palmgren, A. Ball and Roller Bearing Engineering. SKF Industries, Burbank, 1959.
2. Harris, T. A. Rolling Bearing Analysis. John Wiley, 1966, pp. 95-109.
3. Swift, H.W. "Cambers for Belt Pulleys", Proc. Instn. Mech. Engrs. Vol. 122, 1932, pp. 627-671.
4. Woodbury, R.S. History of the Grinding Machine. M.I.T. Press, 1959.
5. Virabov, R.V. "Influence of Shaft Misalignment on Friction-Drive Tractive Properties", Russian Engr. Journal Vol. 53, No. 7, 1973, pp. 20-24.
6. Savage, M. and Loewenthal, S.H., "Kinematic Stability of Roller Pairs in Free-Rolling Contact", NASA Technical Note D-8169, 1976.
7. Korrenn, H. "The Axial Load-Carrying Capacity of Radial Cylindrical Roller Bearings", Journal of Lub. Tech., Vol. 92, No. 1, 1970, pp. 129-137.
8. Liu, J.Y., "The Effect of Misalignment on the Life of High Speed Cylindrical Roller Bearings", Journal of Lub. Tech., Vol. 93, No. 1, 1971, pp. 60-67.
9. Milenkovic, V., "The Generalized Problem of Lateral Guidance Stability in Wheeled Vehicle", ASME Paper 70-TRAN-17, 1970.
10. Wickens, A. H. "The Dynamics of Railway Vehicles on Straight Track: Fundamental Considerations of Lateral Stability", Proc. Instn. Mech. Engrs., Vol. 180, pt. 3f, 1965--1966, pp. 29-44.
11. Cooperrider, N.K., "The Hunting Behavior of Conventional Railway Trucks", Journal Engr. for Ind., Vol. 95, No. 3, 1972, pp. 752-762.
12. Hewko, L.O., "Contact Traction and Creep of Lubricated Cylindrical Rolling Elements at Very High Surface Speeds", A.S.L.E. Transactions, Vol. 12, 1969, pp. 151-161.
13. Seeley, F.B. and Smith, J.O., Advanced Mechanics of Materials, John Wiley, 2nd ed., 1952, pp. 342-362.
14. Cameron, A., Principles of Lubrication, John Wiley, 1st ed., 1966, pp. 195- 200.

**Nomenclature****Variables**

<b>a</b>	half contact width in transverse direction in inches
<b>b</b>	half contact width in circumferential direction in inches
<b>C</b>	transverse curvature center distance in inches
<b>CLR</b>	radial bearing clearance in inches
<b>d</b>	roller diameter in inches
<b>E</b>	elastic modulus in pounds per square inch
<b>F</b>	dynamic roller imbalance force in pounds
<b>f</b>	friction coefficient
<b>g</b>	acceleration due to gravity in inches per second
<b>h</b>	roller drop in inches
<b>K</b>	tractive coefficient in seconds per inch
<b>ℓ</b>	roller length in inches
<b>N</b>	shaft speed in revolutions per minute
<b>O</b>	center of transverse rotation
<b>P</b>	radial bearing force in pounds
<b>PCW</b>	percent width that is stressed
<b>Q</b>	load separation factor
<b>R</b>	radius to center of transverse curvature in inches
<b>r</b>	rolling radius in inches
<b>T</b>	restoring torque in pound inches or dynamic imbalance torque in pound inches
<b>t</b>	center cylinder width in inches
<b>U</b>	slip velocity in inches per second
<b>V</b>	total velocity in inches per second
<b>w</b>	weight density in pounds per cubic inch

$z$	axial roller direction
$\alpha$	half cone angle in degrees
$\gamma$	shaft slope angle in degrees
$\delta$	axial shift of roller in inches or Hertzian compression in inches
$\delta_r$	reduction in roller rolling radius in inches
$\rho$	radius of transverse curvature in inches
$\mu$	Poisson's ratio
$\sigma$	contact pressure in pounds per square inch
$\omega$	angular velocity in radians per second

#### Superscripts

*	nominal value at condition of true rolling
---	--

#### Subscripts

a	roller
b	inner race
c	outer race and cup imbalance
d	external rolling cylinder
e	external rolling cylinder and end imbalance
F	frame
i	inside
0	nominal rolling value
o	outside or radial force initial value
s	cage
1,2	right and left sides of roller

1 Report No. NASA CR135082	2 Government Accession No.	3 Recipient's Catalog No.	
4 Title and Subtitle  Roller Bearing Geometry Design		5 Report Date October 5, 1976	
		6 Performing Organization Code	
7 Author(s)  Michael Savage and Bruce H. H. Pinkston		8 Performing Organization Report No.	
		10 Work Unit No.	
9 Performing Organization Name and Address  Mechanical Design Department  Case Western Reserve University		11 Contract or Grant No. Grant MSG 3077	
		13 Type of Report and Period Covered Contractor Report	
12 Sponsoring Agency Name and Address  National Aeronautics and Space Administration Washington, D.C. 20546		14 Sponsoring Agency Code	
		15 Supplementary Notes Final Report. Project Manager, David E. Brews, U.S. Army Air Mobility R & D Laboratory Lewis Research Center, Cleveland, Ohio.	
16 Abstract The rollers in a high speed roller bearing tend to skew relative to the races. In this work a theory of kinematic stabilization of rolling cylinders is extended and applied to the design of cylindrical roller bearings. The kinematic stabilization mechanism puts a reverse skew into the rolling elements by changing the roller taper. Twelve basic bearing modification designs are identified and modeled in this report. Four of these have single transverse convex curvature in their rollers while eight have rollers which have compound transverse curvature made up of a central cylindrical band surrounded by symmetric bands with slope and transverse curvature. The bearing designs are modeled for restoring torque per unit axial displacement, contact stress capacity and contact area including dynamic loading, misalignment sensitivity and roller proportion. Design programs are available which size the single transverse curvature roller designs for a series of roller slopes and load separations and which design the compound roller bearings for a series of slopes and transverse radii of curvature. The compound rollers are proportioned to have equal contact stresses and minimum size. Designed examples are also given.			
17 Key Words (Suggested by Author(s)) Roller bearings, design, kinematics, roller skew, restoring torque, misalignment		18 Distribution Statement Unclassified - unlimited	
19 Security Classif. (of this report) Unclassified	20 Security Classif. (of this page) Unclassified	21 No. of Pages 119	22 Price*

\* For sale by the National Technical Information Service, Springfield, Virginia 22161